Ari Saarinen

# EMFi-actuator: vibro-acoustical consideration

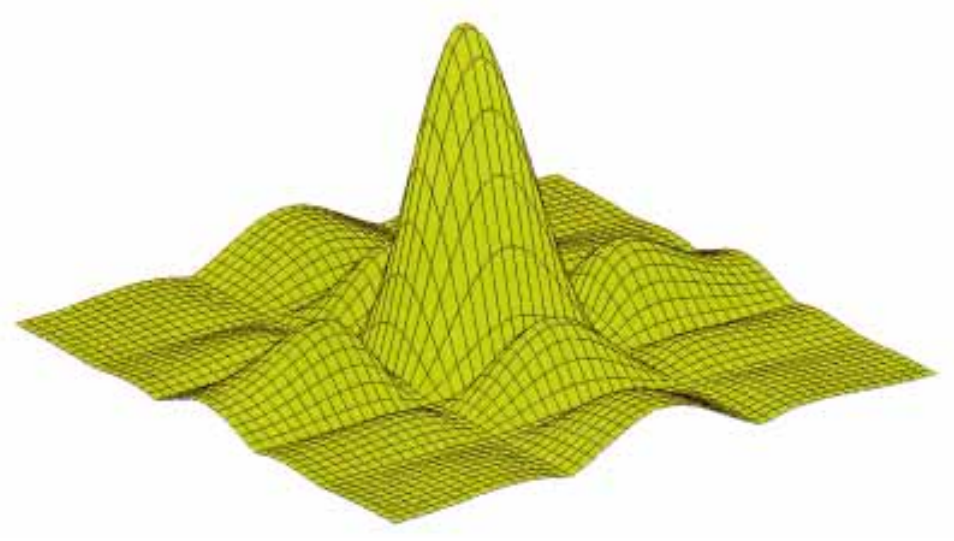

TECHNICAL RESEARCH CENTRE OF FINLAND ESPOO 1999

VTT PUBLICATIONS 405

# EMFi-actuator: vibro-acoustical consideration

Ari Saarinen
VTT Building Technology

TECHNICAL RESEARCH CENTRE OF FINLAND
ESPOO 1999

ISBN 951–38–5554–6 (soft back ed.)
ISSN 1235–0621 (soft back ed.)

ISBN 951–38–5555–4 (URL: http://www.inf.vtt.fi/pdf/)
ISSN 1455–0849 (URL: http://www.inf.vtt.fi/pdf/)



JULKAISIJA – UTGIVARE – PUBLISHER

Valtion teknillinen tutkimuskeskus (VTT), Vuorimiehentie 5, PL 2000, 02044 VTT
puh. vaihde (09) 4561, faksi (09) 456 4374

Statens tekniska forskningscentral (VTT), Bergsmansvägen 5, PB 2000, 02044 VTT
tel. växel (09) 4561, fax (09) 456 4374

Technical Research Centre of Finland (VTT), Vuorimiehentie 5, P.O.Box 2000, FIN–02044 VTT, Finland
phone internat. + 358 9 4561, fax + 358 9 456 4374

VTT Rakennustekniikka, Rakennusfysiikka, talo- ja palotekniikka, Lämpömiehenkuja 3, PL 1804, 02044 VTT
puh. vaihde (09) 4561, faksi (09) 455 2408

VTT Byggnadsteknik, Byggnadsfysik, hus- och brandteknik, Värmemansgränden 3, PB 1804, 02044 VTT
tel. växel (09) 4561, fax (09) 455 2408

VTT Building Technology, Building Physics, Building Services and Fire Technology,
Lämpömiehenkuja 3, P.O.Box 1804, FIN–02044 VTT, Finland
phone internat. + 358 9 4561, fax + 358 9 455 2408

Technical editing Kerttu Tirronen

Libella Painopalvelu Oy, Espoo 1999

Saarinen, Ari. EMFi-actuator: vibro-acoustical consideration. Espoo 1999. Technical Research Centre of Finland, VTT Publications 405. 109 p. + app. 30 p.

**Keywords** EMFi-actuator, actuators, vibration, acoustic properties, modelling, evaluation, vibro-acoustical properties, sound production, measurement

# Abstract

In this paper, the vibro-acoustical properties of the EMFi-actuator are studied. The examination is carried out by modelling the operation of the actuator and by comparing the modelling results to the corresponding measured values in case they are available. The modelling is based on an analytical approach. The equations used are derived in the Appendices. Consideration on the properties of the vibration is divided into three parts: the basic vibration of the film, vibration of the film in the time domain and vibration of the functional elements of the actuator. The sound production properties of the actuator have been examined in the free acoustic field and in cases with boundaries near the source. The effect of the different vibration distributions of the actuator film and impedance loading on the emitted sound has been studied. Also the radiation pattern of the actuator is modelled and compared to the measured results.

The general vibro-acoustical functioning of the EMFi-actuator is stated in the impedance-oriented form by evaluating the loading impedance of the vibrating film based on its boundary conditions. The basic vibration functioning of the actuator film in the frequency domain is predicted by using a linear second-order ordinary differential equation with constant coefficients. In the time domain the non-linear effects of the spring force and electric forces acting on the actuator film are considered. The recoil effect of the actuator is studied with a normal-mode method of dynamic analysis. It is found that the response of the supporting structure may decrease about a decade without influencing the response of the actuator film.

The use of the arithmetic average value of the vibration deflection of the EMFi-actuator in the prediction of sound power or sound pressure in the acoustic far field at low frequencies is compared to the frequency or spatially dependent

vibration of the actuator film. The value of the arithmetic average of vibration is valid even when the outward impedance of the film is not taken into consideration. The large dipole type actuators are more effective sound radiators than monopole sources. The effect of the thickness of the absorbent material under the dipole actuator, the radiation pattern and the effect of the boundary conditions of the vibrating cell on the radiating sound power are considered. The measured and predicted values of radiation patterns are very similar in every angle. The rigidly supported boundary of the actuator cell enables the actuator panel to radiate much more sound power with all the different even modes than it is possible with a simply supported boundary condition. The basic problems concerning the operation of an EMFi-actuator are related to its ineffective low frequency sound production and the distortion caused by non-linear vibration. It is possible to increase the sound power radiation properties of the monopole or dipole type functional modes of the actuator by making the deflection of the membrane larger (using smaller tension), by using larger membrane areas or by using two interacting actuators. The dimensions of the actuator element cell affect the power the single vibration mode is able to radiate into the acoustic far field. When the film cells of the actuator panels are simply supported, the larger dimensions compared to those of the present actuator type produce more sound power at odd and even modes.

The confidence intervals of a normal distribution used in the evaluation of the reliability of the sound power measurements have been obtained by calculating combined standard deviation values from standard deviation values of single frequency bands given in the standards. It is shown that it is possible to find an upper limit for the confidence interval.

The main results of this work are the means to increase the radiated sound power of the actuator element without increasing concurrently the distortion of the radiator. These resources are based on the functioning mode of the actuator (monopole, dipole), boundary conditions of the actuator element or cells of the actuator element, the larger actuator areas, interaction of actuators and the dimensions of the actuator element cells. Another result of this study is the potentiality to evaluate the A-weighted standard deviation of the sound power of the equipment to be measured from the measurement results without specifying the type of emitted sound radiated by the equipment.

# Preface

This study is mainly related to two research projects at VTT (Technical Research Centre of Finland) concerning active noise control (ANC) based on EMFi-transducer technology: The Finnish enterprise AKTIVA (Active Sound Control) is financed by Tekes (National Technology Agency of Finland) and some Finnish companies. The European Union project FACTS (Brite-EuRam III, Film Actuators and Active Noise Control for Comfort in Transportation Systems) is financed by EU and some supranational consolidated corporations. VTT acts as the responsible partner in this project.

The objectives of AKTIVA are to yield basic know-how of active noise control in Finland. Special concern is given to the active noise attenuation of ventilation equipment, to improve the sound insulation of light-weight walls and to control the sound field of three-dimensional rooms in an ANC way. The technical objectives of the FACTS project are, correspondingly, to investigate, design and develop two prototypes for active noise control systems; a hybrid multiple-input multiple-output ANC system to reduce noise in cabins, and a light-weight panel on which actively controlled EMFi-transducers are fixed to increase the transmission loss of the panel against stochastic noise. The main application sites are transportation systems like cars, ships and trains. Both of these projects were divided into separate part entities, such as sound field modelling, testing, structure modelling, system adjustment etc. This paper considers the sound field modelling. The reaching of the goals of the projects depends largely on the performance of EMFi-transducers, because they are used in different applications as anti-noise sources and sensors. Intermediate results of this study were reported in the Technical and Board of management meetings at Tampere, Finland, Turin, Italy and Lyon, France.

This report was prepared as a part of my postgraduate studies in applied physics at the University of Helsinki, Department of Physics, to be submitted as thesis for the degree of Licentiate in Philosophy. Professor Folke Stenman of the Department of Physics has supervised the studies and I wish to express my gratitude for his support during the course of my studies. Dr. Seppo Uosukainen from the VTT Building Technology, another supervisor, has given many

valuable comments to the content of this work which contribution I appreciate deeply.

I have had stimulating discussions, besides with the persons mentioned, also with Mr. Hannu Nykänen, a project leader of AKTIVA and FACTS and a significant contributor to the existing ANC enterprises in Finland; Dr. Jukka Linjama, Mr. Marko Antila, Mr. Veli-Jukka Ollikainen who have carried out the measurements referenced in this study; Dr. Jukka Lekkala, Mr. Kari Kirjavainen and, Mrs. Eetta Saarimäki who are the main contributors of the EMFi technology, and Mr. Dominique Bondoux who has done modelling work in FACTS project. I want to thank also Miss Ulla Peltonen for her contribution to the co-ordination of the projects, which also has affected this work favourably. I wish to thank research director Juho Saarimaa, head of the VTT Building Technology, research director Juho Suokas, head of the VTT Automation, group manager Juhani Laine of the air handling technology and acoustics and chief research scientist Juhani Parmanen for the opportunity to carry out my studies at VTT and for affecting the financing of the projects mentioned above.

Finally I express my gratitude to my family for the time given to complete this work.

Suomenlinna, December 1999

Ari Saarinen

e-mail: Ari.Saarinen@vtt.fi

# Contents

# List of symbols

| | |
|---|---|
| $a$ | radius of the disk [m] |
| $a$, $b$ | dimensions of the panel [m] |
| $a_1$ | radius of the air channel for the typical wool material [m] |
| $a_i$ | A-weighting factors [unitless] |
| $a'$, $a''$, $b'$, $b''$ | regression parameters of the porous material [unitless] |
| $b$ | distance between two closely spaced dipole sources [m] |
| $b/2$ | thickness of the absorbent layer [m] |
| $c$, $c_i$ | viscous modal damping coefficient [unitless] |
| $c_0$ | velocity of sound [m/s] |
| $d$ | distance between the stator and the surface of the conductor [m] |
| $d_b$ | distance between the actuator film and the rigid background layer [m] |
| $d_m$ | width of the actuator cell [m] |
| $d_w$ | thickness of the porous background material [m] |
| $d_0$ | thickness of the background material [m] |
| $d_1$, $d_4$ | thickness of the stator material [m] |
| $d_2$, $d_3$ | thickness of the cavity of the actuator cell [m] |
| $dy$ | infinitesimal width of the membrane strip [m] |
| $dx$ | infinitesimal length of the membrane strip or the cylinder part [m] |
| $f$ | frequency [Hz] |
| $f_i$ | natural frequencies of the vibrator [Hz] |
| $f_c$ | cut-off frequency [Hz] |
| $f_{sigq}$, $f_{sigV}$, $f_{sigx}$, $f_c$ | electric forces acting on the actuator film [N/m$^2$] |
| $h$ | thickness of the film [m] |
| $h_s$ | thickness of the stator [m] |

| | |
|---|---|
| $i$ | index (1 ,2, 3,…) [unitless] |
| $j$ | complex symbol [unitless] |
| $k$ | wave number [1/m] |
| $k_0$ | wave number in air [1/m] |
| $k_x$ | wave number to the direction of the *x*- co-ordinate [1/m] |
| $k_{xm}$ | structural wave number to the direction of the *x*- co-ordinate [1/m] |
| $k_{ym}$, $k_{yn}$ | structural wave number to the direction of the *y*- co-ordinate [1/m] |
| $k$ | spring constant [N/m] |
| $k_{01}$, $k_i$ | dynamic stiffness per unit area [N/m$^3$] |
| $k'_m$ | the spring constant influenced by the initial tension of the film per unit area [ N/m$^3$] |
| $k_v$ | dynamic stiffness of rock wool material [N/m$^3$] |
| $l$ | width of the film cell [m] |
| $m$, $n$ | integers [unitless] |
| $m'_f$ | mass of the fluid per unit area [kg/m$^2$] |
| $m_m$ | mass of the film [kg] |
| $m'_m$ | surface density of the film material [kg/m$^2$] |
| $m''_m$ | density of the film material [kg/m$^3$] |
| $m_i$ | surface mass [kg/m$^2$] |
| $m'_e$ | surface density of the actuator element [kg/m$^2$] |
| $m'_s$ | surface density of the stator [kg/m$^2$] |
| $m''_s$ | density of the stator material [kg/m$^3$] |
| $p$ | sound pressure [Pa] |
| $p_0$ | pressure the fluid adjacent to the film exerts on the film cell from the free field side [Pa] |

| | |
|---|---|
| $p_i$ | pressure affecting the vibrator cell from the boundary layer side [Pa] |
| $p_{in}$ | pressure the fluid adjacent to the film exerts on the film cell from the boundary layer side because of acoustic excitation [Pa] |
| $p_m$ | sound pressure of the monopole source [Pa] |
| $p_d$ | sound pressure of the dipole source [Pa] |
| $p_{dd}$ | sound pressure of two closely spaced dipole sources [Pa] |
| $p_{ddhs}$ | sound pressure of the dipole source on absorbent layer [Pa] |
| $q$ | surface charge density of the film [$C/m^2$] |
| $r$ | distance between the source and observation point [m] |
| $r'_m$ | damping factor per unit area [$kg/m^2s$] |
| $r_1$ | flow resistivity of the porous material per unit length [$Nsm^{-4}$] |
| $t$ | time [s] |
| $\Delta t$ | time step [s] |
| $\vec{u}$ | particle velocity [m/s] |
| $u$ | standard uncertainty [unitless] |
| $u_{c1}$ | combined standard deviation for uncorrelated data [unitless] |
| $u_{c2}$ | combined standard deviation for correlated data [unitless] |
| $u_m$ | velocity amplitude of the vibrating panel [m/s] |
| $u_{rm}$ | radial component of the particle velocity of the monopole source [m/s] |
| $u_{rd}$ | radial component of the particle velocity of the dipole source [m/s] |
| $u_{rdd}$ | radial component of the particle velocity of two closely spaced dipole sources [m/s] |
| $u_{rddhs}$ | radial component of the particle velocity of the dipole source on absorbent layer [m/s] |

| | |
|---|---|
| $u_\omega$ | surface velocity distribution of simply or rigidly supported plate [m/s] |
| $w$, $w_i$ | transverse displacement of the vibrator cell or element [m] |
| $\Delta w$ | displacement step [m] |
| $\dot{w}$ | velocity of the vibrator cell [m/s] |
| $\Delta \dot{w}$ | velocity step [m/s] |
| $\ddot{w}$ | acceleration of the vibrator cell [m/s$^2$] |
| $\Delta \ddot{w}$ | acceleration step [m/s$^2$] |
| $x$, $y$, $z$ | cartesian co-ordinates [m] |
| $A$ | area of the actuator element [m$^2$] |
| $D$ | length of the actuator element [m] |
| $E$ | normalized frequency parameter [unitless] |
| $E_x$ | Young's constant [N/m$^2$] |
| $F$ | force [N] |
| $\Delta F_1$ | change in the resultant force [N] |
| $F_{el}$ | total electric force per unit area [N/m$^2$] |
| $\Delta F_{el}$ | change in the total electric force per unit area [N/m$^2$] |
| $F_k$ | spring force [N] |
| $F_\omega$ | net force exerted by the disk on adjacent fluid [N] |
| $I_{rm}$ | intensity of the monopole source [W/m$^2$] |
| $I_{rd}$ | intensity of the dipole source [W/m$^2$] |
| $I_{rdd}$ | intensity of two closely spaced dipole sources [W/m$^2$] |
| $I_{rddhs}$ | intensity of the dipole source on absorbent layer [W/m$^2$] |
| $K$ | dynamic stiffness of the air cavity [N/m$^3$] |
| $K$ | confidence interval of a normal distribution [unitless] |
| $L$ | width of the actuator element [m] |
| $L_y$ | length of the film strip [m] |

| | |
|---|---|
| $L_{Wm}$ | radiated sound power level of the monopole source [dB] |
| $L_{Wd}$ | radiated sound power level of the dipole source [dB] |
| $M$ | mass [kg] |
| $N$ | number of film strips on the actuator element [unitless] |
| $N$ | number of observations [unitless] |
| $P$ | total force per unit area exerting on the vibrator cell [$N/m^2$] |
| $P_{ax}$ | axial pressure amplitude [Pa] |
| $Q_0$ | strength of the constant velocity sound source [$m^3/s$] |
| $R_{rad}$ | resistance term of the radiation impedance [$kg/m^2s$] |
| $R_{rm}$ | radiation resistance of the monopole source [$kg/m^2s$] |
| $R_{rd}$ | radiation resistance of the dipole source [$kg/m^2s$] |
| $S$ | surface area of the film cell [$m^2$] |
| $SPL_m$ | sound pressure level of the monopole source [dB] |
| $SPL_d$ | sound pressure level of the dipole source [dB] |
| $T$ | force caused by the initial tension of the film strip [N] |
| $T_N$ | force caused by the initial tension of the film strip in z-direction [N] |
| $T_T$ | force caused by the initial tension of the film strip in x-direction [N] |
| $U_0$ | average vibration velocity amplitude of the actuator film [m/s] |
| $V_{sig}$ | signal voltage [V] |
| $X_{rad}$ | reactance term of the radiation impedance [$kg/m^2s$] |
| $Z_a$ | characteristic acoustic impedance of the porous material [$kg/m^2s$] |
| $Z_b$ | boundary layer side acoustic impedance [$kg/m^2s$] |
| $Z_f$ | free field side acoustic impedance [$kg/m^2s$] |
| $Z_i$ | acoustic impedance [$kg/m^2s$] |

| | |
|---|---|
| $Z_r$ | radiation impedance [kg/m$^2$s] |
| $Z_v$ | acoustic impedance of the time harmonic vibrator [kg/m$^2$s] |
| $Z_0$ | characteristic impedance of air [kg/m$^2$s] |
| **C** | damping matrice [unitless] |
| **F** | force matrice [N] |
| **K** | stiffness matrice [N/m$^3$] |
| **M** | mass matrice [kg] |
| $\alpha$ | angle between the reflected wave and normal to the plane [rad] |
| $\alpha'$, $\alpha''$, $\beta'$, $\beta''$ | regression parameters of the porous material [unitless] |
| $\beta$ | phase of the time harmonic vibrator [rad] |
| $\varepsilon$ | dissipation constant of the film material [unitless] |
| $\varepsilon_0$ | permittivity of the vacuum [$N^{-1}m^{-2}$ $C^2$] |
| $\varepsilon_r$ | dielectric constant of the film material [unitless] |
| $\varsigma$ | phase between the incident and reflecting wave [rad] |
| $\eta$ | viscosity of air in normal conditions [kg/ms] |
| $\xi$ | deflection of the membrane [m] |
| $\xi_0$ | average deflection of the actuator film [m] |
| $\theta$, $\phi$ | angles [rad] |
| $\rho_0$ | density of the fluid [kg/m$^3$] |
| $\sigma$ | initial tension of the film [N/m$^2$] |
| $\sigma_M$ | reference standard deviation [unitless] |
| $\sigma_p$ | standard deviation of production [unitless] |
| $\sigma_r$ | standard deviation of reproducibility of the measurement method [unitless] |
| $\sigma_T$ | total standard deviation [unitless] |
| $\nu$ | Poisson constant [unitless] |
| $\omega$ | angular frequency [1/s] |

| | |
|---|---|
| $\Gamma$ | reflection coefficient [unitless] |
| $T_a$ | complex wavenumber of plane sound wave in the bulk porous material [1/m] |
| $T_{ay}$ | complex wavenumber of plane sound wave in the bulk porous material (related to the propagation direction of the wave) [1/m] |
| $\Xi$ | flow resistance of stator material [kg/ms] |
| $\Phi_m$ | velocity potential of the monopole source [$m^2/s$] |
| $\Phi_d$ | velocity potential of the dipole source [$m^2/s$] |
| $\Phi_{dd}$ | velocity potential of two closely spaced dipole sources [$m^2/s$] |
| $\Phi_{ddhs}$ | velocity potential of the dipole source on absorbent layer [$m^2/s$] |
| $\Pi_m$ | radiated sound power of the monopole source [W] |
| $\Pi_d$ | radiated sound power of the dipole source [W] |
| $\Pi_{mm}$ | radiated sound power of two monopole sources [W] |
| $\Pi_{dd}$ | radiated sound power of two dipole sources in the same phase [W] |
| $\Pi_{dd-}$ | radiated sound power of two dipole sources in opposite phase [W] |
| $\Pi_{ddhs}$ | radiated sound power of the dipole source on absorbent layer [W] |
| $\Pi_{ssp}$ | radiated sound power of simply supported panel [W] |
| $\Pi_{rsp}$ | radiated sound power of rigidly supported panel [W] |
| * | complex conjugate [unitless] |
| $J_1$ | Bessel function of first kind [unitless] |
| $\hat{n}$ | normal of the plane [unitless] |

# 1. Introduction

This study deals with the vibro-acoustical operation of the EMFi-actuator [1, 2]. An application area where the EMFi-actuator appears very promising is active noise control (ANC) [3, 4, 5, 6, 7]. In ANC applications the sound radiation properties of the sound sources are very important; especially the ability to produce enough undistorted sound at low frequencies which is the most important frequency range in ANC. The functioning of the sound source and its interaction with surrounding fluid influence the created acoustical impact.

ElectroMechanical Film (EMFi) is an acoustic actuator and sensor material made of polypropylene [1, 8, 9]. It is thin, cellular, biaxially oriented and coated with electrically conductive layers, exploiting the capability to store a permanent charge to form an electret material. It exhibits electro-mechanical properties generating an electric charge on the electrodes when distorted by mechanical or acoustical energy or converting electrical energy into mechanical or acoustic energy. The film is very thin (typically < 100 μm) and elastic which makes it possible to manufacture actuators of almost any shape and size.

EMFi-transducers (combined detectors and actuators) are used as anti-noise sources in ANC-applications. Transducers with small thickness are desired, for example as active wall linings, which will allow the reverberation time of rooms to be adjusted by coherent electroacoustic means [10]. In this application, the wall surface is covered by a planar array of actuators with detectors in front; the detectors pick up the incident sound and feed the actuators in order to realize prescribed acoustic impedance. Electret transmitters can be built very flat. The commercial types are, however, almost exclusively tweeters (high frequency radiators) because of their limited vibration amplitudes. Active acoustic systems mainly apply to low frequency sound. It may be problematic to operate the electret loudspeakers with sufficient high amplitudes to produce enough sound at low frequencies. Assuming, for example, the minimum frequency of 50 Hz and a sound pressure level of 80 dB at this frequency, the amplitude of vibration in air should be 2 μm.

The active cancellation of the sound field by appropriately driven secondary sources has been proposed long ago [3]. The practical realization, with a reasonable amount of electroacoustic and electronic equipment, is, however,

possible only under certain simplifying conditions such as quasiperiodic or almost stationary noise, one-dimensional wave propagation, noise sources concentrated in a small volume of space, or a small volume to be protected against noise from a known source. The perfect cancellation of real sound fields in a room produced by exterior and interior noise sources would require spatially distributed secondary sources of at least as equal complexity as the original sources, a corresponding detector network, and highly sophisticated electronic control units [11]. ANC noise is suppressed by adding a sound wave which has the same shape but opposite phase. The phase reversal is not always simple in practise because the sound field varies both in time and space. A sound reduction of 10 dB requires a phase deviation smaller than 18 degrees or an amplitude deviation smaller than 32%. Correspondingly, a reduction of 40 dB requires values of 0.6 degrees and 1%, respectively [12]. Typically, ANC works better at low frequencies. Passive noise control shows correspondingly poor performance at low frequencies. To be effective, the passive devices have to be large and heavy, and they require dimensions comparable to the wavelength of a controllable acoustic wave. Commercial applications of ANC are found in the one-dimensional noise problem of ventilation ducts and exhausts, in the three-dimensional noise problems of cabin noise (cars, aircraft) and in small devices like headsets.

Sound waves are generated by the vibration of any solid body in contact with the fluid medium (there are also other emergence mechanisms). Energy originally not acoustic is being changed into acoustic energy at the source, to be radiated outward and causing losses at the source. To get a vibrating surface to radiate sound effectively, it must, not only be capable of compressing or changing the density of the fluid with which it is in contact, but it must do so in such a manner that it produces significant density changes in fluid remote from the surface. If local disturbances of particle position due to surface vibration occur sufficiently slowly, the adjacent region of the fluid may be able to accommodate to the changes by virtually incompressible motion. The ability to adjust incompressibility depends upon the spatial distribution of the disturbance. The acceleration normal to the surface, and the spatial distribution of that acceleration, influence the effectiveness of fluid compression significantly and, hence, sound radiation.

To give an exact description of the physical phenomenon concerning sound production of the actuator element, it is necessary to solve the complete vibro-acoustical problem: one differential equation for the structure displacement, one for the acoustic pressure and a condition to ensure the continuity of both the normal velocities of the structure and the field near it. The characteristics of the source determine the frequency and directional properties of the generated sound field. Decreasing the dimensions of the transducer for the reproduction of lower frequencies is physically limited. For good sound reproduction at low frequencies large diaphragm excursions are needed, resulting often in distortion. The pressure field radiated by a real acoustic source may be rather complicated.

Theoretically, it is quite impossible to evaluate the detailed form of a radiation field in terms of amplitude and phase, although computer-based numerical techniques is beginning to expand the possibilities [13, 14, 15, 16, 17, 18, 19, 20, 21, 22, 23, 24, 25, 26]. In many cases, it is only required to estimate the total sound power radiated by the radiator, together with some indication of its frequency distribution. Then analytical methods of the evaluation are more conveniently applied.

The following study is based on the experience achieved by comparing the modelling results to the measurement results of the EMFi-actuator. The study includes both vibrational and acoustical aspects. The main objective is to consider the parameters which afford the most effective radiation properties for the actuator. This means increased sound power with as low distortion levels as possible. Both baffled and unbaffled actuator elements are dealed with, and the functional modes of the EMFi-actuator are then monopole and dipole operation. Also some aspects related to the measurements of sound power of actuators are discussed.

The consideration is based on analytical techniques, and thus it is tried to keep as simple as possible describing the physical phenomena yet as accurately as possible. The equations used are derived in the Appendices. Starting points for the derivations are well known equations in the literature. The examination is mainly restricted to low frequency sound because this frequency range is the most important one for ANC applications and also the most problematic one concerning the EMFi-actuator. In the vibration consideration, the study is restricted to the main factors which influence the dynamic behaviour of the

actuator element or the impact the actuator has on its supporting structure. The non-linearities of the actuator are considered only slightly; no proceedings to decrease the distortion are examined. The study of the sound emission is restricted to the far field so that the comparison with the measurement results would be possible. The distortion of the emitted sound is not taken into consideration in this context. Basically, it is possible to calculate that quantity by using the information of the deflection of the film in time domain at certain frequency, and the relation between the deflection and the delivered sound pressure. The distortion components are achieved from the Fourier-transform of the time signal.

# 2. The general vibro-acoustical functioning

EMFi film is foil-like flexible plastic material with a permanent electric charge [1]. In an EMFi-actuator the film is tensioned between and completely surrounded by metallized plastic panels which form both the stator and electrical and mechanical shield. When fed by an electric signal, the membrane vibrates and produces sound. A schematic picture of the EMFi cavity actuator (plastic panel actuator) is presented in Figure 1.

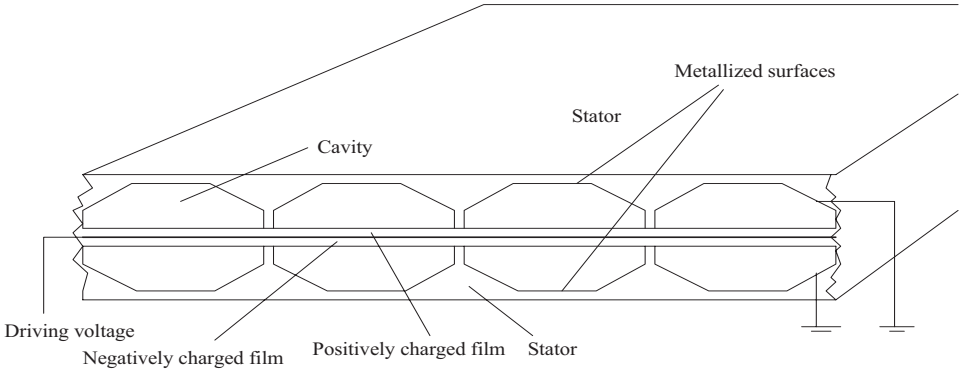


*Figure 1. EMFi plastic panel actuator.*

A unique cell of the actuator element consists of the filmstrip of mass $m_m$ with suitable boundary conditions, cavities and stators (Figures 2 and 3). The quantities of interest are assumed to be independent of the *x* direction and the system is symmetrical in the *y* direction. Because the film material is very elastic, its bending stiffness is minor and it offers thus no resistance to shear. The supporting forces of the stretched membrane are mainly based on its initial tension. If the transverse displacement *w* from equilibrium position is small, this tension $\sigma$ is assumed to be distributed uniformly (constant) throughout the membrane strip when the material on opposite sides of a line segment of length *dx* will tend to be pulled apart with a force $\sigma dx$. The forces exerting the infinitesimal fragment of the actuator cell and its geometry are illustrated in Figure 2.

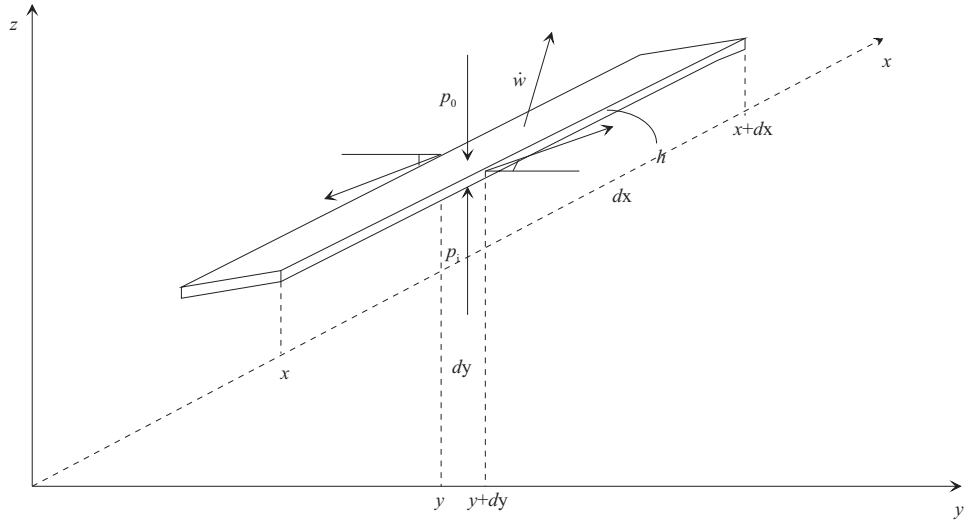


*Figure 2. Infinitesimal fragment of the actuator cell.*

The equation of motion of the vibrator cell by utilizing Taylor series is

$$\sum F = m_m \ddot{w}(y,t)$$

$$\Leftrightarrow m'_m \ddot{w}(y,t)dydx = (p_i - p_o)dydx + \sigma \cdot hdx\sin\theta \Big|_{y+dy} - \sigma \cdot hdx\sin\theta \Big|_{y}$$

$$= Pdydx + \frac{\partial(\sigma \cdot hdx\sin\theta)}{\partial y}dy$$

Because the transverse displacement is assumed to be small

$$w(y,t) << 1 \Rightarrow \sin\theta \approx \tan\theta = \frac{\partial w(y,t)}{\partial y}$$

$$\Rightarrow \frac{\partial^2 w(y,t)}{\partial y^2} = \frac{-P}{\sigma h} + \frac{m'_m}{\sigma h}\ddot{w}(y,t) = \frac{-P}{\sigma h} + \frac{m''_m}{\sigma}\ddot{w}(y,t) \quad (1)$$

where

$p_0$, $p_i$ are the forces per unit area exerting to the vibrator cell from the opposite directions,

$\ddot{w}$ is the acceleration of the film cell,

$h$ is the thickness,

$m''_m$ is the density of the film,

$m'_m$ is the surface density of the film, and

$\theta$ is the angle between the tangent to the membrane strip and the $y$-axis.

The total force $P$ per unit area exerted to the membrane strip can be presented with the aid of the acoustic ($p_{in}$) and electric ($F_{el}$) contributions of the force $p_i$, the free field and the background layer side acoustic impedances $Z_f$ and $Z_b$ respectively, and the vibration velocity $\dot{w}$ of the cell

$$P = p_i - p_o = p_{in} + F_{el} - p_o = \dot{w}Z_b - \dot{w}Z_f + F_{el}$$

The following presumptions have been made when deriving the equation of motion:

- the film is thin and homogeneous
- the stiffness of the film is negligible (totally elastic)
- the film material is free of losses (internal friction is negligible)
- the amplitudes of the vibration are small.

The impedances $Z_b$ and $Z_f$ are possible to be evaluated by considering the boundary conditions of the system. The impedance boundaries of the actuator cell when it is located on a porous lossy material and the background boundary layer is acoustically rigid are illustrated in Figure 3.

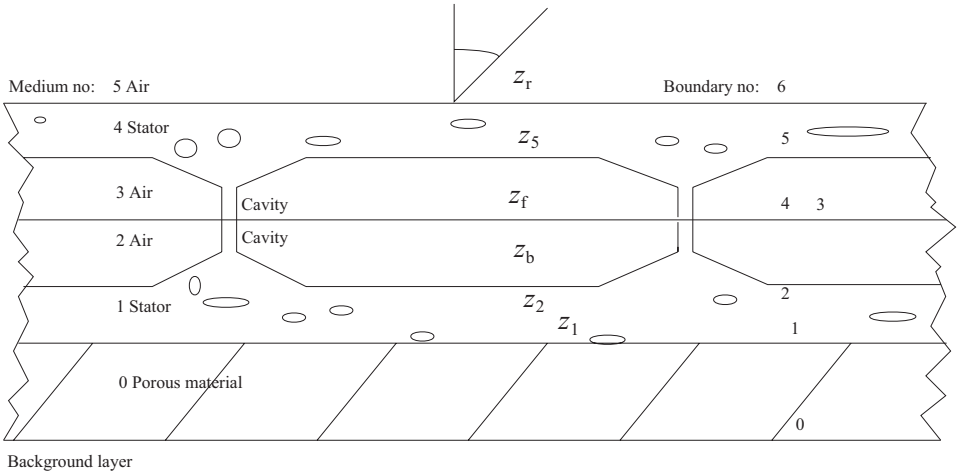


*Figure 3. Impedance boundaries.*

The impedances $Z_f$ and $Z_5$ from the location of the actuator film and from the outer boundary layer of the cavity to the direction of the free acoustic field are

$$Z_f = \rho_0 c_0 \frac{k_0}{\Gamma_{ay}} \frac{\left(1+\frac{\rho_0 c_0 k_0}{Z_5 \Gamma_{ay}}\right) e^{i\Gamma_{ay} d_3} + \left(1-\frac{\rho_0 c_0 k_0}{Z_5 \Gamma_{ay}}\right) e^{-i\Gamma_{ay} d_3}}{\left(1+\frac{\rho_0 c_0 k_0}{Z_5 \Gamma_{ay}}\right) e^{i\Gamma_{ay} d_3} - \left(1-\frac{\rho_0 c_0 k_0}{Z_5 \Gamma_{ay}}\right) e^{-i\Gamma_{ay} d_3}} \tag{2}$$

$$Z_5 = Z_a \frac{\Gamma_a}{\Gamma_{ay}} \frac{\left(1+\frac{Z_a \Gamma_a}{Z_r \Gamma_{ay}}\right) e^{i\Gamma_{ay} d_4} + \left(1-\frac{Z_a \Gamma_a}{Z_r \Gamma_{ay}}\right) e^{-i\Gamma_{ay} d_4}}{\left(1+\frac{Z_a \Gamma_a}{Z_r \Gamma_{ay}}\right) e^{i\Gamma_{ay} d_4} - \left(1-\frac{Z_a \Gamma_a}{Z_r \Gamma_{ay}}\right) e^{-i\Gamma_{ay} d_4}} \tag{3}$$

The impedances $Z_b$ and $Z_2$ from the location of the actuator film and from the outer boundary layer of the cavity to the direction of the background structure are

$$Z_b = \rho_0 c_0 \frac{k_0}{\Gamma_{ay}} \frac{\left(1+\frac{\rho_0 c_0 k_0}{Z_2 \Gamma_{ay}}\right) e^{i\Gamma_{ay} d_2} + \left(1-\frac{\rho_0 c_0 k_0}{Z_2 \Gamma_{ay}}\right) e^{-i\Gamma_{ay} d_2}}{\left(1+\frac{\rho_0 c_0 k_0}{Z_2 \Gamma_{ay}}\right) e^{i\Gamma_{ay} d_2} - \left(1-\frac{\rho_0 c_0 k_0}{Z_2 \Gamma_{ay}}\right) e^{-i\Gamma_{ay} d_2}} \tag{4}$$

$$Z_2 = Z_a \frac{\Gamma_a}{\Gamma_{ay}} \frac{\left(1+\frac{Z_a \Gamma_a}{Z_1 \Gamma_{ay}}\right) e^{i\Gamma_{ay} d_1} + \left(1-\frac{Z_a \Gamma_a}{Z_1 \Gamma_{ay}}\right) e^{-i\Gamma_{ay} d_1}}{\left(1+\frac{Z_a \Gamma_a}{Z_1 \Gamma_{ay}}\right) e^{i\Gamma_{ay} d_1} - \left(1-\frac{Z_a \Gamma_a}{Z_1 \Gamma_{ay}}\right) e^{-i\Gamma_{ay} d_1}} \tag{5}$$

$$Z_1 = -iZ_a \cot\left(\Gamma_a d_0\right) \qquad \Gamma_{ay}{}^2 = \Gamma_a{}^2 - k_x{}^2 \qquad \text{and} \qquad k_x = k_0 \sin\phi \tag{6}$$

The quantities

| | |
|---|---|
| $k_0$, $\Gamma_a$, $\Gamma_{ay}$ | are the wavenumbers in air and in the relevant bulk porous material respectively, |
| $\rho_0$ | is the density of the air, |
| $c_0$ | is the velocity of the sound, |
| $Z_a$ | is the characteristic acoustic impedance of the relevant porous material (stator material or porous material above the background layer), |
| $Z_r$ | is the radiation impedance, and |
| $d_2$, $d_3$, $d_1$, $d_4$, $d_0$ | are the depths of the cavity, stator material and the background material respectively. |

The general equations for the propagation constant and characteristic impedance are [27, 28, 29]

$$\Gamma_a = k_0\left[a' E^{-\alpha'} + i(1 + a'' E^{-\alpha''})\right] \quad \text{and}$$

$$Z_a = Z_0\left[1 + b' E^{-\beta'} - ib'' E^{-\beta''}\right] \tag{7}$$

where

| | |
|---|---|
| $a'$, $a''$, $b'$, $b''$, $\alpha'$, $\alpha''$, $\beta'$, $\beta''$ | are the regression parameters of the relevant porous material (based on the measurements), |
| $E = (\rho_0 f)/ r_1$ | is the normalized frequency parameter (dimensionless), |
| $r_1$ | is the flow resistivity of the relevant porous bulk material, |
| $Z_0 = \rho_0 c_0$ | is the characteristic impedance of the air, and |
| $f$ | is frequency. |

When the propagsation direction $\phi = 0$, then $k_x = 0$ and $\Gamma_{ay} = \Gamma_a$ and

$$Z_f = Z_0 \frac{-iZ_5 \cot\left(k_0 d_3\right) + Z_0}{Z_5 - iZ_0 \cot\left(k_0 d_3\right)} \quad \text{and}$$

$$Z_5 = Z_a \frac{-iZ_r \cot\left(\Gamma_a d_4\right) + Z_a}{Z_r - iZ_a \cot\left(\Gamma_a d_4\right)} \tag{8}$$

$$Z_b = Z_0 \frac{-iZ_2 \cot\left(k_0 d_2\right) + Z_0}{Z_2 - iZ_0 \cot\left(k_0 d_2\right)} \quad \text{and}$$

$$Z_2 = Z_a \frac{-iZ_1 \cot\left(\Gamma_a d_1\right) + Z_a}{Z_1 - iZ_a \cot\left(\Gamma_a d_1\right)} \tag{9}$$

# 3. Vibration

## 3.1 The basic vibration

The elemental approach to consider the mechanical operation of the actuator cell is based on a lumped model and time harmonic vibration. The vibrator is assumed to be located on a rigid boundary layer (Figure 4) where the dynamic properties of the actuator affect upon the vibration of the membrane. This influence is included to the character of the mechanical impedance of the actuator. The dynamic force which exerts to the actuator cell is caused by the electric interaction between the stator and the actuator film. The spring force resisting the motion is assumed to be proportional to the deflection, the damping force to the velocity (viscous damping), and the mass of the film is taken to be time-wise invariant.

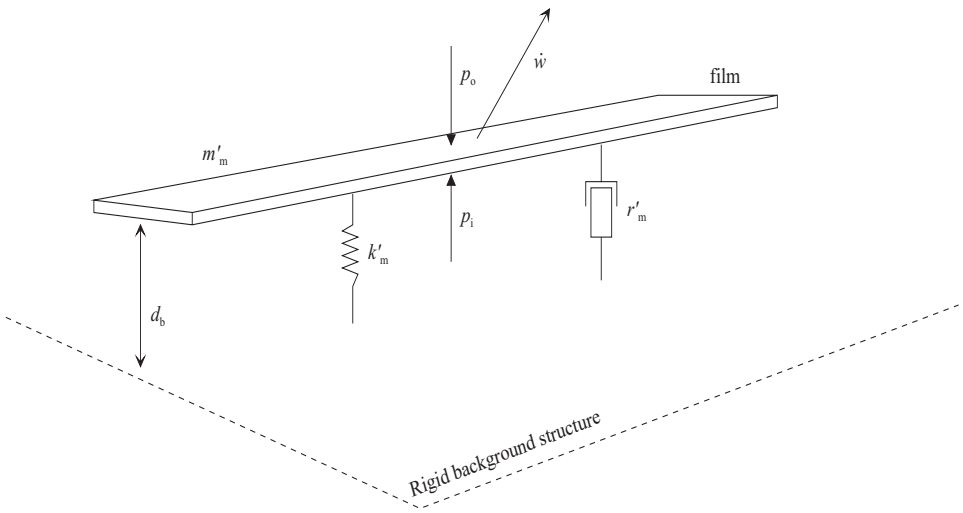


*Figure 4. A lumped model of the actuator cell.*

Consequently, the equation of motion is a linear, second-order ordinary differential equation with constant coefficients

$$m'_m \frac{d\dot{w}(t)}{dt} + r'_m \dot{w}(t) + k'_m \int \dot{w}(t)dt = p_i(t) - p_o(t) \qquad (10)$$

where

$m'_m$, $k'_m$, $r'_m$ are the mass of the actuator film, the spring constant of the film caused by the initial tension and damping factor (flow resistivity), all per unit area, respectively,

$p_i$ is the applied force per unit area which causes the vibration of the film,

$p_o$ is the pressure the fluid adjacent to the film exerts on the actuator cell,

$\dot{w}$ is the velocity of the film, and

$d_b$ is the distance between the film and a rigid boundary layer.

In the region adjacent to the film, the fluid can be considered incompressible and the compliance term associated with radiation impedance $Z_r$ can be assumed to equal zero. Therefore, $Z_r$ has only inertance and resistance terms associated with it. The variable $p_o$ can be expressed

$$p_o(t) = \dot{w}(t)Z_r = \dot{w}(t)\left[R_{rad} + jX_{rad}\right] = \dot{w}(t)\left[R_{rad} + j\omega m'_f\right] = R_{rad}\dot{w}(t) + m'_f \frac{d\dot{w}(t)}{dt} \qquad (11)$$

where

$R_{rad}$, $X_{rad}$ are the real and imaginary parts of the radiation impedance $Z_r$, respectively, and

$m'_f$ is the mass of the fluid per unit area.

Inserting this expression in equation (10) and rearranging the terms yield

$$\left[m'_m + m'_f\right]\frac{d\dot{w}(t)}{dt} + \left[r'_m + R_{rad}\right]\dot{w}(t) + k'_m \int \dot{w}(t)dt = p_i(t) \qquad (12)$$

When the actuator cell is immersed in a fluid, there is an effective mass $m'_f$ added to the mass of the film due to the fluid loading. There is also an added damping term $R_{rad}$, which represents the energy that is taken out of the vibrator and radiated from the vibrator as sound. Both of these phenomena are well known in sound radiation considerations. If the applied force to the actuator cell $p_i$ is time harmonic and depends only on the supplied electric force $F_{el}$, the velocity of the film is also time harmonic and the equation gets the form

$$\left\{\left[r'_m + R_{rad}\right] + j\left[\left[m'_m + m'_f\right]\omega - \frac{k'_m}{\omega}\right]\right\}\dot{w} = F_{el} \quad \text{or} \quad \dot{w} = \frac{F_{el}}{\left|Z_v\right|e^{j\beta}} \tag{13}$$

$$\left|Z_v\right| = \left\{\left[r'_m + R_{rad}\right]^2 + \left[\left[m'_m + m'_f\right]\omega - \frac{k'_m}{\omega}\right]^2\right\}^{1/2}$$

$$\beta = \tan^{-1}\left[\frac{\left[m'_m + m'_f\right]\omega - \frac{k'_m}{\omega}}{r'_m + R_{rad}}\right] \tag{14}$$

Four types of electric forces act on the EMFi-actuator film [30]. Those are

$$f_{sigq} = \frac{qV_{sig}}{2d'}\frac{(2d')^2}{d'^2 - w^2} \qquad f_{sigV} = \frac{qV_{sig}}{2d'}\frac{2d'h(d'^2 + w^2)}{\varepsilon_r(d'^2 - w^2)^2} - f_{sigq} \tag{15}$$

$$f_{sigx} = \frac{q^2 w}{2\varepsilon_0 d'}\left(\frac{d'h/\varepsilon_r}{d'^2 - w^2}\right)^2 \qquad f_c = \frac{2d'\varepsilon_0 V_{sig}^2 w}{(d'^2 - w^2)^2}$$

$$F_{el} = f_{sigq} + f_{sigV} + f_{sigx} + f_c \qquad 2d' = 2d - \frac{\varepsilon_r - 1}{\varepsilon_r}h$$

where

$d$ is the static distance between the stator and the surface of the conductor between the films (see Figure 1),

$q$ is the surface charge density of the film,

$V_{sig}$ is the signal voltage,

$\varepsilon_0$ is permittivity of vacuum, and

$\varepsilon_r$ is the dielectric constant of the film material.

Some of the single electric forces are non-linear. In small deflections the non-linear effects are, however, minor. The vibration velocity and impedance terms dominating the vibration according to equation (13) and (14) are

$$\begin{aligned} \dot{w}_k &= \frac{\omega F_{\mathrm{el}}}{k'_m} & \dot{w}_m &= \frac{F_{el}}{\left(m'_m + m'_f\right)\omega} & \dot{w}_r &= \frac{F_{\mathrm{el}}}{r'_m + R_{rad}} \\ Z_k &= \frac{k'_m}{\omega} & Z_m &= \left(m'_m + m'_f\right)\omega & Z_r &= r'_m + R_{rad} \end{aligned} \tag{16}$$

where the subscripts *k*, *m* and *r* mark stiffness, mass and resistance controlled variables. Figure 5 illustrates the measured vibration velocities of the stator and film of the EMFi-actuator located above the floor on a 20 mm thick mineral wool layer [31, 32]. The excitation of the film is a broad band (20 Hz - 20 kHz) white noise of 23 Volt (rms) signal voltage. The vibration of the film is measured through a hole approximately in the middle of the single cell element. Table 1 consists of the deflection and velocity data in tabular form. The average deflection and velocity of the film are 0.33 μm and 1.33 mm/s, respectively. The deflection of the film is very small in the reference frequency range compared to the distance 160 μm between the symmetric plane of the film and the stator. The vibration velocity of the lumped model vibrator, based on the equations (13) - (16), consisting of equal mechanical parameters such as the measured actuator (see Appendix A), is presented in Figure 6.

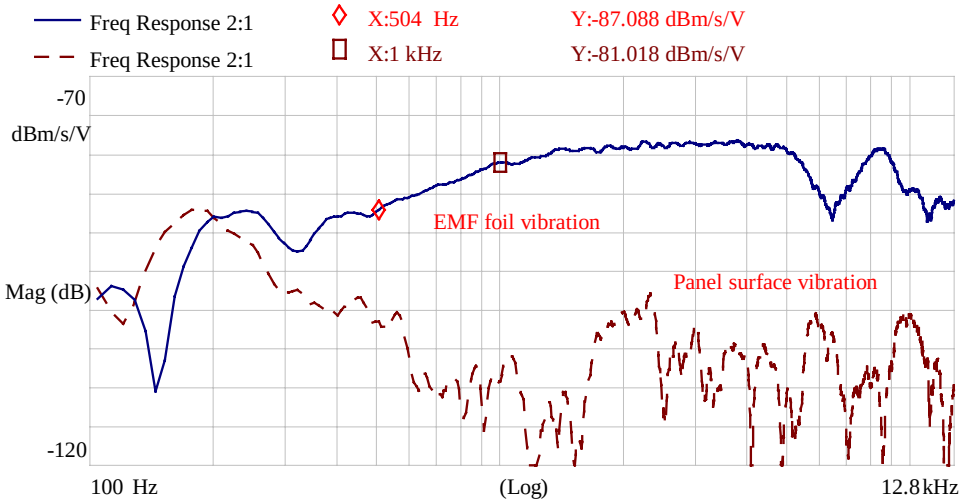


*Figure 5. The surface velocity of EMFi film and stator* [31].

*Table 1. The deflections and velocities of the actuator film.*

| **Frequency/Hz** | 100 | 125 | 160 | 200 | 250 | 315 | 400 | 500 | 630 |
|---|---|---|---|---|---|---|---|---|---|
| **Deflection/µm** | 0.41 | 0.24 | 0.22 | 0.80 | 0.64 | 0.43 | 0.32 | 0.32 | 0.32 |
| **Velocity/mm/s** | 0.26 | 0.17 | 0.26 | 1.0 | 1.0 | 1.2 | 0.8 | 1.0 | 1.26 |
| **Frequency/Hz** | 800 | 1000 | 1250 | 1600 | 2000 | 2500 | 3150 | 4000 | |
| **Deflection/µm** | 0.32 | 0.32 | 0.30 | 0.27 | 0.24 | 0.20 | 0.15 | 0.08 | |
| **Velocity/mm/s** | 1.6 | 2.0 | 2.0 | 2.0 | 2.0 | 2.0 | 2.0 | 2.0 | |

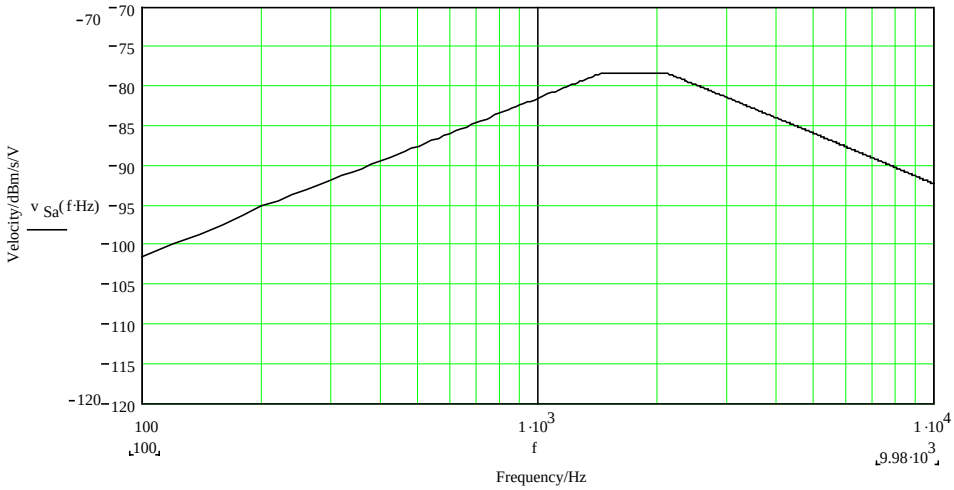


*Figure 6. The vibration velocity of a simple lumped vibrator.*

The basic behaviours of the measured and modelled vibrations are similar, except in the frequency range where the masses of the actuator film and fluid as well as radiation resistance influence the vibration (from 2 kHz to higher frequencies). If these effects are less insignificant than it is supposed in the lumped model, the vibration velocity of the film starts to decrease from higher frequencies than presented in Figure 6. This situation is presented in Figure 7.

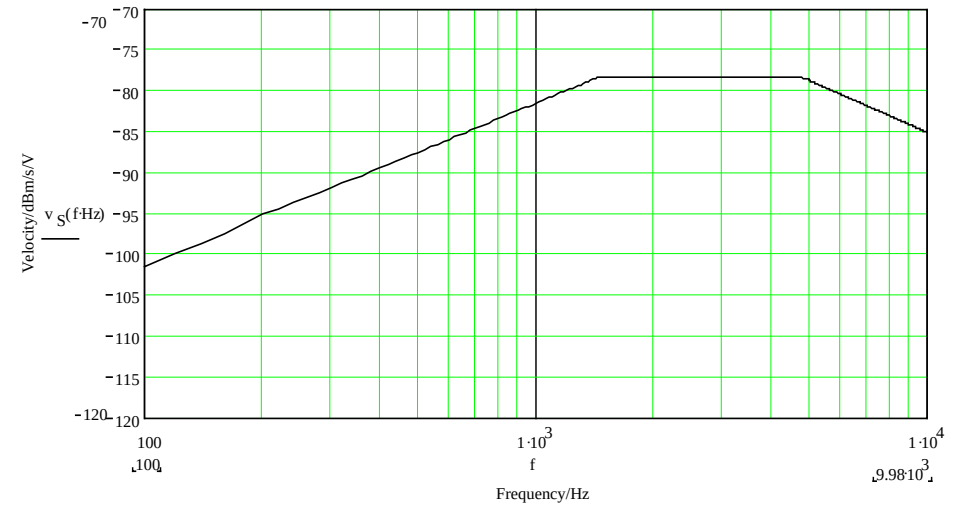


*Figure 7. The vibration velocity of a simple lumped vibrator.*

The operations of the measured and modelled vibrators are now very similar except at low and high frequencies where the resonances appear in the measurement results. The stiffness force caused mainly by the initial tension of the film restricts the vibration velocity of the film at low frequencies. At middle frequencies, where the natural frequency of the film exists (the natural frequencies for actuator film and stator calculated according to linear model are 1750 and 195 Hz, respectively), the response of the film is restricted by the resistance controlled variables (radiation resistance and flow resistivity). At high frequencies, the masses of the film and fluid restrict the velocity of the actuator film, and the displacement falls towards zero. The terms of equation (16) describe the vibration velocity characteristics of the film quite satisfactorily. For example, according to the measurements, the doubled vibration velocity between frequency range 500 Hz to 1 kHz (Table 1) is directly related to radian frequency according to the term $\dot{w}_k$ of equation (16) which gives the same result when the electric force and stiffness are constant. The force which is needed to generate a certain vibration velocity or the mechanical impedance of the film is illustrated in Figure 8.

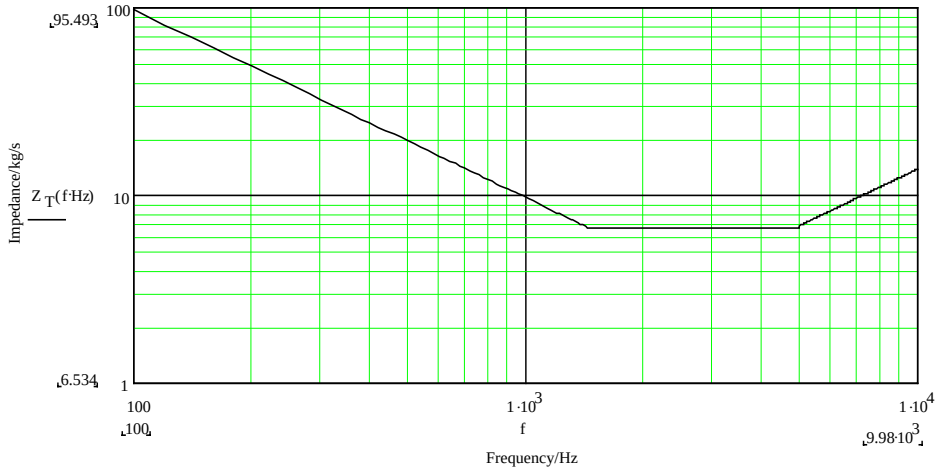


*Figure 8. The impedance of a simple vibrator.*

The deficiencies of the one-degree of freedom lumped element model are:

- the spring (wool layer) is assumed to be massless and operate totally linearly
- the background structure is not necessarily inflexible.

## 3.2 Acting forces

Figure 9 illustrates the electric forces (see equation 15) related to the deflection of the film at 23 V signal voltage. In small deflections (compare to Table 1) the effective total force is basically linearly related to the deflection even if some of the single electric forces are non-linear. In small deflections the non-linear effects are minor.

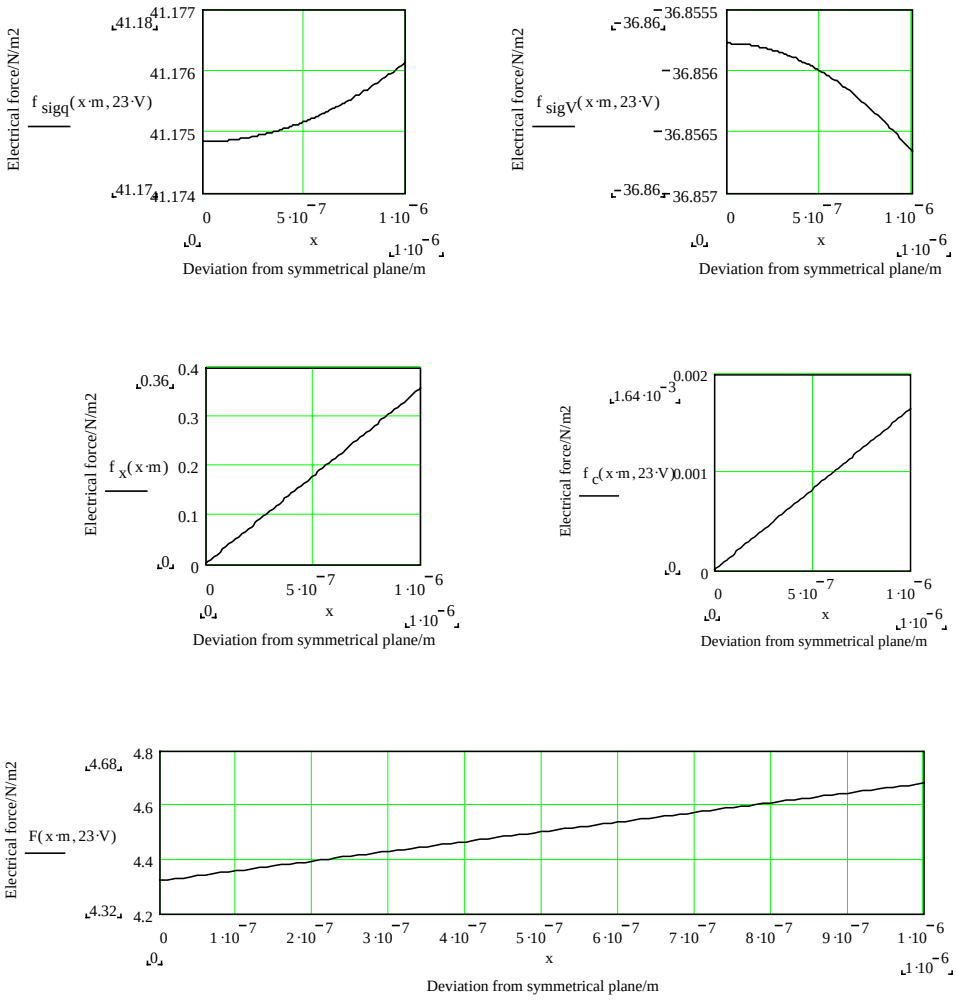


*Figure 9. Electric forces.*

Figure 10 illustrates a linear vertical force (dotted line, see Appendix B) caused by initial tension of the film (30 MPa) and the electric force as function of deflection when the signal voltage is 0 Volt. The influence of the spring force dominates the electric force, and the film is located on its position of equilibrium. At 23 Volt excitation signal (dashed line), the electric force dominates until the deflection of the film reaches 1.2 µm according to Figure 11. The dashed curve is the spring force, and the lowest solid curve is the electric force at excitation signal of 0 Volt. The spring force restricts the deflection of the film and the operation range depends on the excitation voltage.

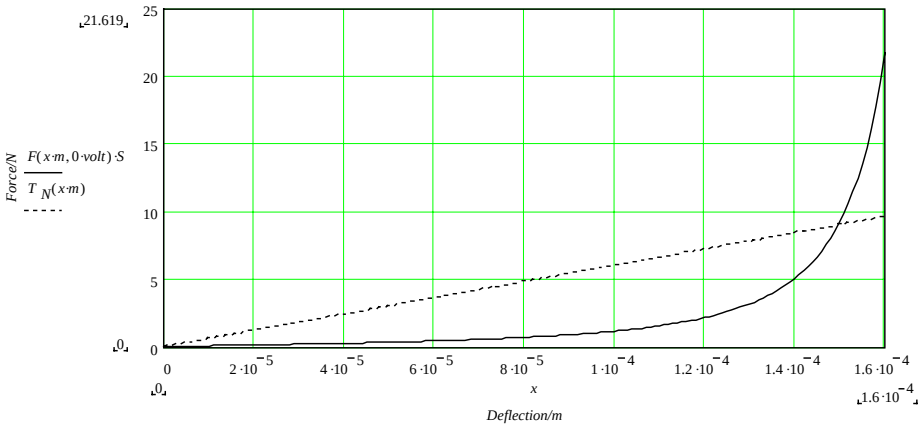


*Figure 10. The spring force and electric force as a function of deflection.*

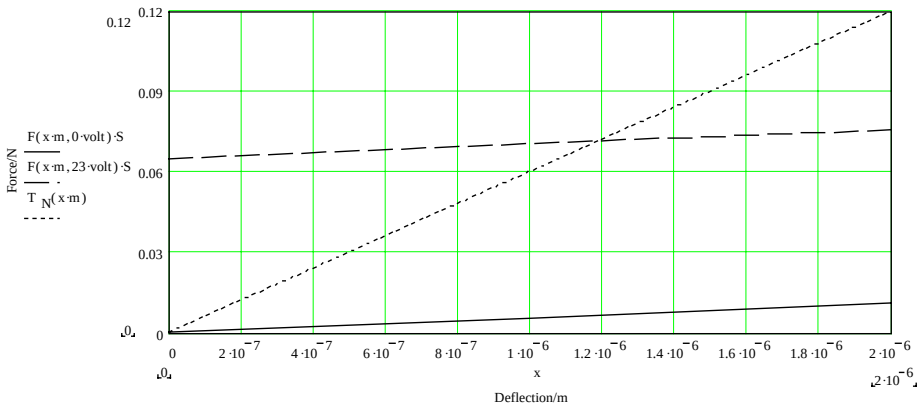


*Figure 11. The spring force and electric force as a function of deflection (mind the scale).*

## 3.3 Vibration in time domain

As the deflection amplitude of the vibrating film increases, the elastic properties of the film material change so that the strain achieves its limit and the material becomes spastic. Spring coefficient cannot remain constant when film displacements approach the original dimensions of the system. In practise, the spring force caused by the initial tension of the film is, after some limit, no more a linear function of deflection, but the spring stiffens approximately according to Figure 12.

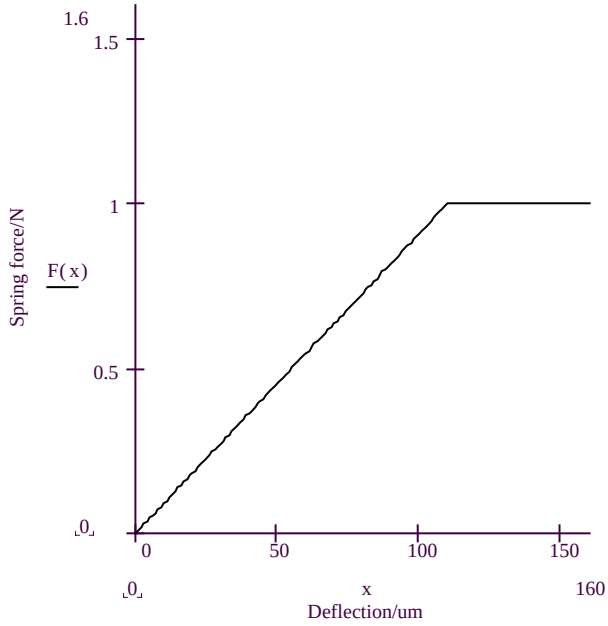


*Figure 12. Non-linear spring force.*

The spring force acting on the film is also a function of frequency. When the frequency is high enough, the force related to the strain of the film material is not in the same phase, and the spring stiffens. If the vibration amplitudes or the frequency are relatively high, the spring force caused by initial tension of the film has to be modelled non-linear. Because of non-linear electric forces acting on the actuator film, the motion of the membrane is not linear either. Therefore, the actuator does not reproduce, for example, time harmonic signal voltage

ideally, but in the frequency domain there are also other frequency components, so called distortion components, with the excitation frequency. When the deflection amplitude of the film increases, the distortion increases usually as well. For such a system, the whole behaviour quite crucially depends upon the various non-linearities present in the coefficients and in the function of the electric force $F_{el}$ (see equation 15). Mathematically, this property is reflected in the requirement that the differential equation describing the behaviour of the system is no more linear but at least one of the coefficients $r'_m$ or $k'_m$ depends on the dependent deflection variable $w$. The system may have more than one equilibrium point which may be stable or unstable. It is also possible that the force producing a given strain does not depend only on that strain itself but also on the previous strains.

In the direct time integration, the equation of motion is solved by integration without any transformation [33, 34]. The properties of the system can vary, or they can also be considered non-linear cases. The method is based on the dynamical balance of the acting forces at each time step of integration. The values of displacement and velocity are used as initial values for the next time step. The basic hypotheses are that the acceleration changes linearly during the time step and the properties of the system (mass, dynamic stiffness and damping) are constant through that time. The incremental equation of motion is [33, 34] (compare to equation 12)

$$m'_m \,\Delta\ddot{w}(t) + r'_m(t)\Delta\dot{w}(t) + k'_m(t)\Delta w(t) = \Delta F_{el}(t) \tag{17}$$

The velocity and deflection are obtained from the linearly changing acceleration (during time step) by integration

$$\begin{aligned} \Delta\dot{w}(t) &= \ddot{w}(t)\Delta t + \Delta\ddot{w}(t)\frac{\Delta t}{2} \\ \Delta w(t) &= \dot{w}(t)\Delta t + \ddot{w}(t)\frac{\Delta t^2}{2} + \Delta\ddot{w}(t)\frac{\Delta t^2}{6} \end{aligned} \tag{18}$$

and by solving from equations above

$$\Delta\ddot{w}(t) = \frac{6}{\Delta t^2}\Delta w(t) - \frac{6}{\Delta t}\dot{w}(t) - 3\ddot{w}(t)$$
$$\Delta\dot{w}(t) = \frac{3}{\Delta t}\Delta w(t) - 3\dot{w}(t) - \frac{\Delta t}{2}\ddot{w}(t) \qquad (19)$$

By inserting these equations in the equation (17), the basic form of the incremental equation of motion is achieved

$$k_1(t)\Delta w(t) = \Delta F_1(t)$$
$$\text{where } k_1(t) = k'_m(t) + \frac{6}{\Delta t^2}m'_m + \frac{3}{\Delta t}r'_m(t)$$
$$\text{and } \Delta F_1(t) = \Delta F_{el}(t) + m'_m\left(\frac{6}{\Delta t}\dot{w}(t) + 3\ddot{w}(t)\right) + r'_m(t)\left(3\dot{w}(t) + \frac{\Delta t}{2}\ddot{w}(t)\right) \qquad (20)$$

where

$r'_m$ is the damping factor,

$k'_m$ is dynamic stiffness,

$m'_m$ is mass,

$\Delta t$ is time step,

$\Delta w(t)$ is displacement step,

$\Delta F(t)$ is change in resultant force,

$\dot{w}(t)$ is velocity, and

$\ddot{w}(t)$ is acceleration.

Figure 13 presents the deflection of the actuator film in the time domain at 500 Hz and 23 V excitation signal. The response of the actuator film for time harmonic excitation signal is non-linear. If the dynamic stiffness and damping factor are constant, the following depictions, Figures 14 and 15, for the maximum deflection and velocity of the actuator film in the time domain for 23 V harmonic excitation at different frequencies are achieved [Appendix C]. The dotted lines in the figures are the measured quantities for comparison reasons. If the damping factor is assumed to be constant, the dynamic stiffness seems to

depend on frequency so that at high frequencies it is constant and at lower frequencies it decreases as the frequency decreases.

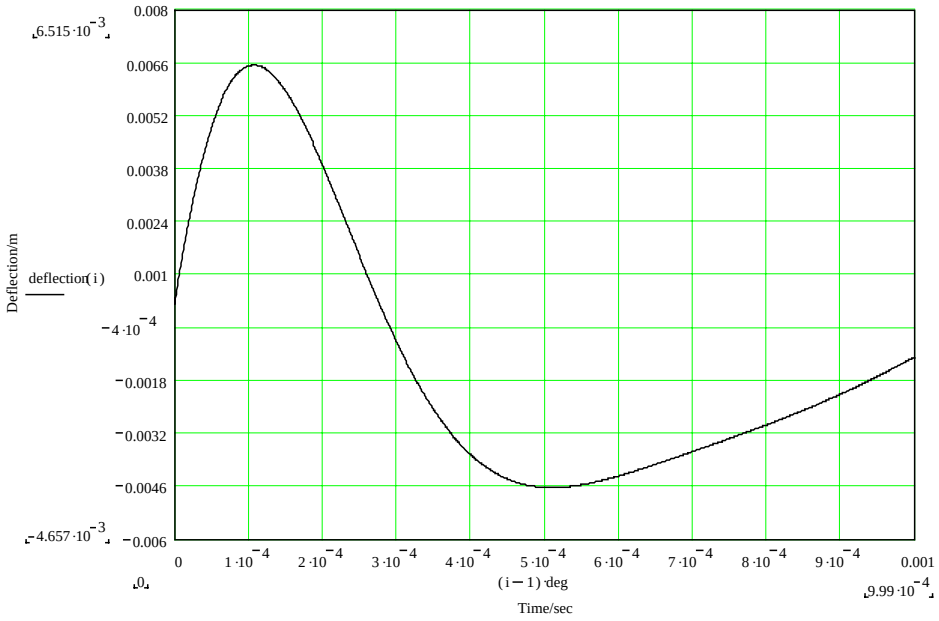


*Figure 13. Deflection of the film in time domain.*

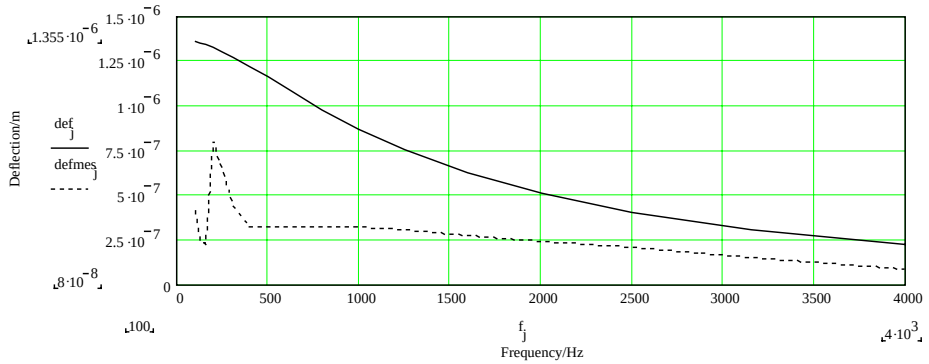


*Figure 14. Deflection of the film.*

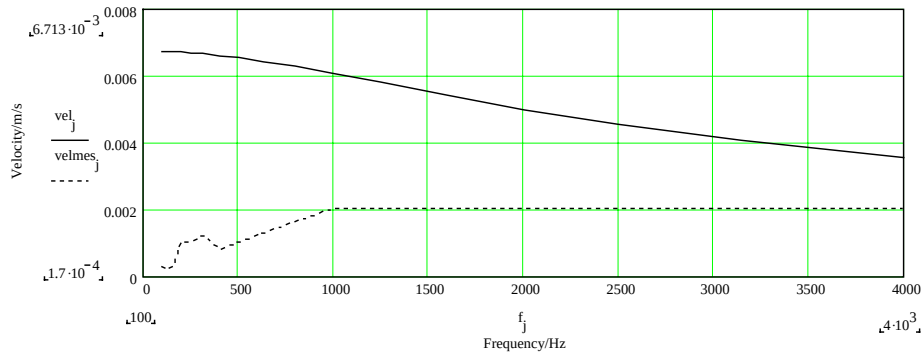


*Figure 15. Velocity of the film.*

## 3.4 Non-recoiling actuator element

The electric forces cause vibration, not only of the actuator film, but also of the stator structure of the EMFi-actuator (Figure 5). This recoil effect may be large enough to endanger the supporting structure of the actuator element vibrating which may generate sound. The element operates optimally when the linear film displacements are large enough (much sound power) while the stator displacements still remain small (non-recoil).

The approach applied to this consideration is based on a normal-mode method of dynamic analysis [34]. The equations of undamped motion of the different mass elements become uncoupled if the principal modes of vibration for a system are used as generalized co-ordinates. In these co-ordinates each equation may be solved as if it pertained to a system with only one-degree of freedom. The displacements of the masses are calculated at their characteristic frequencies in the time domain to get the maximum deflections. The input forces are assumed to be constant compulsion forces, and they stay thus unchangeable when the constructional parameters change.

### 3.4.1 Spatial model

Figure 16 presents a mechanical (spatial) model for the actuator element. The model is composed of a non-suspended actuator, the background structure of which includes damping material and film. The system is encapsulated airtightly on its boundaries. The masses of the stators are combined with a single mass element (they have the same direction of displacement at every instant in a dynamic process). It is assumed that the masses move as rigid bodies so that their masses can be considered to concentrate at single points. The electric forces acting on the actuator film and stators have equal magnitudes but opposite directions.

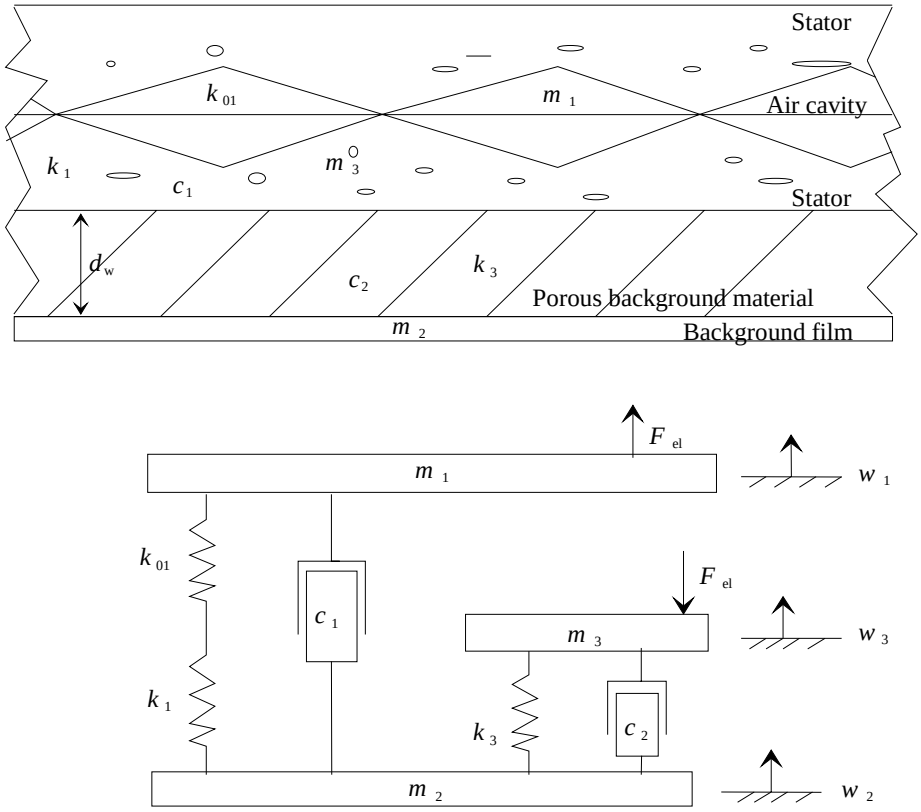


*Figure 16. The spatial model of the actuator element.*

The quantities

$m_1$, $m_2$, $m_3$ are the masses of the actuator film, the combined background film and background material (including 1/3 part of the mass of the porous spring material) and the stator respectively,

$k_{01}$, $k_1$, $k_3$ are the spring constants caused by initial tension of the actuator film, the elasticity of the air (air cavity) and the dynamical stiffness of the porous background material ($k_2$ is the combined effect of $k_{01}$ and $k_1$),

$c_1$ is the common damping coefficient (related to flow resistance) of the stator and background material,

$c_2$ is the damping coefficient, and

$d_w$ the thickness of the porous background material.

Because air flows through the stator material, the air spring has no effect. The stators and background film are supposed to be totally rigid. In reality, both elements have some elasticity.

### 3.4.2 Modal model

The operation of the system is described as a set of vibration modes (natural frequencies with corresponding vibration mode shapes and modal damping factors). The solution describes the various ways in which the actuator element is capable of vibrating naturally or without external forcing or stimulus. Mass (**M**) -, stiffness (**K**) -, damping (**C**) - and force matrices (**F**) for the system illustrated in Figure 16 are the following (the damping coefficients $c$ are assumed to be equal):

$$\mathbf{M}=\begin{bmatrix} m_1 & 0 & 0 \\ 0 & m_2 & 0 \\ 0 & 0 & m_3 \end{bmatrix} \quad \mathbf{K}=\begin{bmatrix} k_2 & -k_2 & -k_1 \\ -k_2 & k_2+k_3 & -k_3 \\ 0 & -k_3 & k_3 \end{bmatrix} \quad \mathbf{C}=\begin{bmatrix} c & 0 & -c \\ 0 & c & -c \\ -c & -c & 2c \end{bmatrix} \quad \mathbf{F}=\mathrm{F}'\cdot\begin{bmatrix} 1 \\ -1 \\ 0 \end{bmatrix} \tag{21}$$

The characteristic values of the system, natural frequencies and characteristic vector matrices are calculated by solving the characteristic equation **H**(f) =

$\mathbf{K} - \omega^2(f)\cdot\mathbf{M}$ [34]. Table 2 includes the calculated values of natural frequencies of various different modifications compared to the basic situation (case 0) and the changes performed to the initial values (if no changes are made, the values are the same as in case 0). Because the system is non-suspended, the first mode is characterized by transfer and its natural frequency is in every case 0 Hz and thus not included in the table. The natural frequencies are very sensitive to the slightest changes in the parameters of the system which is very usual with mechanical constructions.

*Table 2. Natural frequencies and modified mechanical parameters.*

| **Case** | **Natural frequencies (Hz)** | | **Depth (mm)** | **Masses (kg m$^{-2}$)** | | | **Spring constants (kg m$^{-2}$ s$^{-2}$)·10$^6$** | | |
|---|---|---|---|---|---|---|---|---|---|
| | $f_2$ | $f_3$ | $d_w$ | $m_1$ | $m_2$ | $m_3$ | $k_{01}$ | $k_2$ | $k_3$ |
| **0** | 302 | 914 | 50 | 0.042 | 1.01 | 3.96 | 3.3 | 1.3 | 3.0 |
| **1** | 47 | 947 | - | - | 0.34 | - | - | - | 0.03 |
| **2** | 896 | 2110 | - | - | 3,01 | - | - | - | 300 |
| **3** | 237 | 716 | 100 | - | 2.01 | - | - | 0.83 | - |
| **4** | 35 | 729 | 100 | - | 0.68 | - | - | 0.83 | 0.03 |
| **5** | 709 | 1785 | 100 | - | 6.01 | - | - | 0.83 | 300 |
| **6** | 210 | 608 | 150 | - | 3,01 | - | - | 0.60 | - |
| **7** | 30 | 616 | 150 | - | - | - | - | 0.60 | 0.03 |
| **8** | 605 | 1663 | 150 | - | 9,01 | - | - | 0.60 | 300 |
| **9** | 394 | 1117 | 25 | - | 0.51 | - | - | 1.9 | - |
| **10** | 61 | 1188 | 25 | - | 0,18 | - | - | 1.9 | 0.03 |
| **11** | 1070 | 2642 | 25 | - | 1,51 | - | - | 1.9 | 300 |
| **12** | 235 | 513 | 100 | 0.084 | 2.01 | 3.92 | - | 0.83 | - |
| **13** | 238 | 1006 | 100 | 0.021 | 2.01 | 3.98 | - | 0.83 | - |
| **14** | 237 | 716 | 100 | - | 2.005 | - | - | 0.83 | - |
| **15** | 237 | 715 | 100 | - | 2.02 | - | - | 0.83 | - |
| **16** | 274 | 716 | 100 | - | 2.01 | 1.98 | - | 0.83 | - |
| **17** | 216 | 716 | 100 | - | 2.01 | 7.92 | - | 0.83 | - |
| **18** | 141 | 3453 | 12.5 | - | 0,76 | - | 0.033 | 0.033 | 300 |
| **19** | 141 | 412 | 25 | - | 0,51 | - | 0.033 | 0.033 | - |
| **20** | 59 | 159 | 25 | - | 0,18 | - | 0.033 | 0.033 | 0,03 |
| **21** | 141 | 2637 | 25 | - | 1,51 | - | 0.033 | 0.033 | 300 |
| **22** | 366 | 484 | 25 | - | 0,51 | - | 0.33 | 0.31 | - |
| **23** | 140 | 309 | - | - | - | - | 0.033 | 0.033 | - |
| **24** | 139 | 1785 | 100 | - | 6.01 | - | 0.033 | 0.032 | 300 |

The directions and amplitudes of the mass elements vary in different cases. Figure 17 illustrates the main modal forms of some cases. The basic case (first mode, solid line), for example, illustrates the transfer of the structure. At the second mode (dotted line), all mass elements move to the same direction with different relative amplitudes. At the third mode, the actuator film and stators move upwards and the background film downwards.

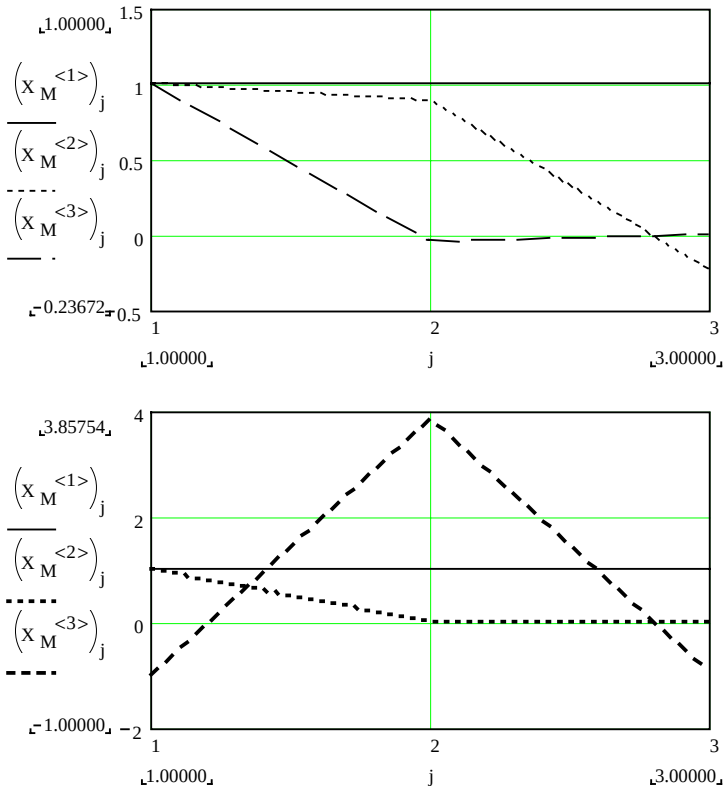


*Figure 17. The main modal forms of the basic case and case 23, respectively.*

### 3.4.3 Response model

Figure 18 presents the steady state responses ($2^{nd}$ mode, $2^{nd}$ natural frequency) of the actuator and background films in time domain (vibration of the mass elements under condition of time harmonic excitation). Table 3 shows the maximum responses of the actuator and background films and the stator for

various natural frequencies of 2nd and 3rd modes. The maximum responses of the mass elements are bolded in the table.

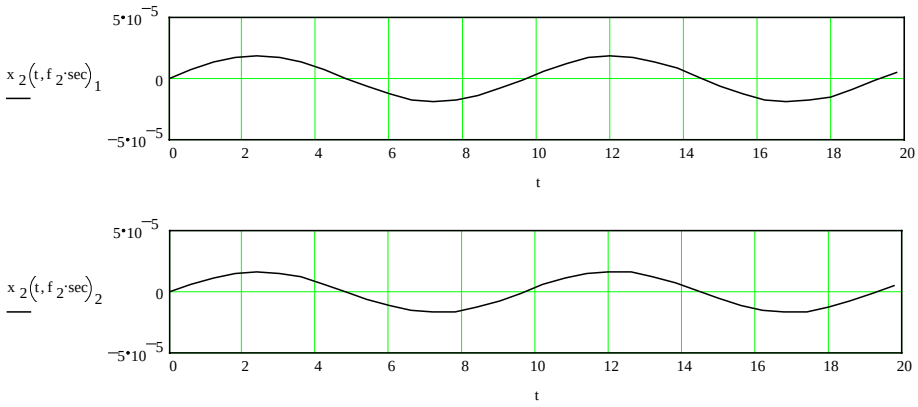


*Figure 18. The steady state responses of the actuator and background films respectively.*

The deflections in the Table 3 are not directly comparable to the measured deflections (Figure 5, Table 1) because of different initial conditions. The deflections of the background film can be made smaller according to Tables 2 and 3 by increasing the thickness or the dynamic stiffness of the background material and by increasing the damping ratio of the natural mode. It is possible to increase the response of the actuator film by decreasing the spring constant caused by the initial tension of the film. This, however, increases the deflection of the background film. The response of the background film may decrease about a decade without influencing the response of the actuator film. The most useful construction alternatives are cases 2, 5 and 8. In general, the responses of the actuator system (actuator and background films and stator) are dependent on each other. The changes in the geometrical and material parameters have a straight influence on the natural frequencies of the system. Parameters are connected to each other and they influence the responses of the different system elements in complex ways. Basically, the situation is an optimization problem of a multi parameter case [35].

*Table 3. The maximum responses of the actuator elements.*

| | | **2nd mode** | | **3rd mode** | |
|---|---|---|---|---|---|
| | | **2nd natural freq.** | **3rd natural freq.** | **2nd natural freq.** | **3rd natural freq.** |
| Basic case | Actuator film | $1{,}9\cdot10^{-5}$ | $3{,}8\cdot10^{-8}$ | $1{,}0\cdot10^{-5}$ | $\mathbf{3{,}7\cdot10^{-4}}$ |
| | Background film | $\mathbf{1{,}7\cdot10^{-5}}$ | $3{,}4\cdot10^{-8}$ | $4{,}7\cdot10^{-7}$ | $1{,}7\cdot10^{-6}$ |
| | Stator | $\mathbf{4{,}5\cdot10^{-6}}$ | $9{,}0\cdot10^{-9}$ | $1{,}1\cdot10^{-8}$ | $4{,}0\cdot10^{-7}$ |
| Case 1 | Actuator film | $2{,}5\cdot10^{-6}$ | $1{,}8\cdot10^{-9}$ | $4{,}5\cdot10^{-7}$ | $\mathbf{3{,}3\cdot10^{-4}}$ |
| | Background film | $2{,}5\cdot10^{-6}$ | $1{,}8\cdot10^{-9}$ | $5{,}6\cdot10^{-8}$ | $\mathbf{4{,}1\cdot10^{-5}}$ |
| | Stator | $\mathbf{2{,}5\cdot10^{-7}}$ | $1{,}8\cdot10^{-10}$ | $1{,}2\cdot10^{-11}$ | $8{,}7\cdot10^{-9}$ |
| Case 2 | Actuator film | $\mathbf{3{,}9\cdot10^{-4}}$ | $1{,}4\cdot10^{-6}$ | $3{,}6\cdot10^{-9}$ | $1{,}2\cdot10^{-7}$ |
| | Background film | $\mathbf{1{,}7\cdot10^{-6}}$ | $5{,}8\cdot10^{-9}$ | $1{,}7\cdot10^{-8}$ | $5{,}4\cdot10^{-7}$ |
| | Stator | $\mathbf{2{,}9\cdot10^{-6}}$ | $1{,}0\cdot10^{-8}$ | $1{,}3\cdot10^{-8}$ | $4{,}1\cdot10^{-7}$ |
| Case 3 | Actuator film | $1{,}1\cdot10^{-5}$ | $1{,}5\cdot10^{-8}$ | $1{,}4\cdot10^{-5}$ | $\mathbf{3{,}5\cdot10^{-4}}$ |
| | Background film | $\mathbf{9{,}4\cdot10^{-6}}$ | $1{,}3\cdot10^{-8}$ | $3{,}2\cdot10^{-7}$ | $7{,}9\cdot10^{-6}$ |
| | Stator | $\mathbf{4{,}8\cdot10^{-6}}$ | $7{,}0\cdot10^{-9}$ | $1{,}3\cdot10^{-8}$ | $3{,}1\cdot10^{-7}$ |
| Case 4 | Actuator film | $1{,}2\cdot10^{-5}$ | $9{,}1\cdot10^{-10}$ | $4{,}4\cdot10^{-7}$ | $\mathbf{1{,}6\cdot10^{-5}}$ |
| | Background film | $\mathbf{1{,}2\cdot10^{-6}}$ | $9{,}0\cdot10^{-10}$ | $2{,}8\cdot10^{-8}$ | $1{,}0\cdot10^{-6}$ |
| | Stator | $\mathbf{2{,}1\cdot10^{-7}}$ | $1{,}6\cdot10^{-10}$ | $1{,}0\cdot10^{-11}$ | $3{,}7\cdot10^{-10}$ |
| Case 5 | Actuator film | $\mathbf{3{,}5\cdot10^{-4}}$ | $1{,}3\cdot10^{-5}$ | $7{,}9\cdot10^{-10}$ | $1{,}6\cdot10^{-9}$ |
| | Background film | $\mathbf{1{,}3\cdot10^{-6}}$ | $4{,}7\cdot10^{-9}$ | $4{,}3\cdot10^{-9}$ | $8{,}6\cdot10^{-9}$ |
| | Stator | $\mathbf{1{,}7\cdot10^{-6}}$ | $6{,}4\cdot10^{-9}$ | $6{,}5\cdot10^{-9}$ | $1{,}3\cdot10^{-8}$ |
| Case 6 | Actuator film | $7{,}8\cdot10^{-6}$ | $9{,}0\cdot10^{-9}$ | $1{,}8\cdot10^{-5}$ | $\mathbf{3{,}2\cdot10^{-4}}$ |
| | Background film | $\mathbf{6{,}9\cdot10^{-6}}$ | $7{,}9\cdot10^{-9}$ | $2{,}6\cdot10^{-7}$ | $4{,}9\cdot10^{-6}$ |
| | Stator | $\mathbf{5{,}3\cdot10^{-6}}$ | $5{,}6\cdot10^{-9}$ | $1{,}4\cdot10^{-8}$ | $2{,}6\cdot10^{-7}$ |
| Case 7 | Actuator film | $7{,}5\cdot10^{-7}$ | $5{,}1\cdot10^{-10}$ | $4{,}6\cdot10^{-7}$ | $\mathbf{3{,}2\cdot10^{-4}}$ |
| | Background film | $7{,}5\cdot10^{-7}$ | $5{,}1\cdot10^{-10}$ | $1{,}9\cdot10^{-8}$ | $\mathbf{1{,}3\cdot10^{-5}}$ |
| | Stator | $\mathbf{2{,}0\cdot10^{-7}}$ | $1{,}4\cdot10^{-10}$ | $9{,}6\cdot10^{-12}$ | $6{,}7\cdot10^{-9}$ |
| Case 8 | Actuator film | $\mathbf{3{,}3\cdot10^{-4}}$ | $1{,}5\cdot10^{-6}$ | $2{,}5\cdot10^{-10}$ | $1{,}6\cdot10^{-8}$ |
| | Background film | $\mathbf{1{,}0\cdot10^{-6}}$ | $4{,}5\cdot10^{-9}$ | $1{,}7\cdot10^{-9}$ | $1{,}1\cdot10^{-7}$ |
| | Stator | $\mathbf{1{,}2\cdot10^{-6}}$ | $5{,}6\cdot10^{-9}$ | $3{,}8\cdot10^{-9}$ | $2{,}4\cdot10^{-7}$ |
| Case 9 | Actuator film | $\mathbf{2{,}6\cdot10^{-5}}$ | $3{,}6\cdot10^{-8}$ | $6{,}2\cdot10^{-6}$ | $8{,}2\cdot10^{-6}$ |
| | Background film | $\mathbf{2{,}3\cdot10^{-5}}$ | $3{,}1\cdot10^{-8}$ | $5{,}8\cdot10^{-7}$ | $7{,}7\cdot10^{-7}$ |
| | Stator | $\mathbf{3{,}2\cdot10^{-6}}$ | $4{,}3\cdot10^{-9}$ | $9{,}1\cdot10^{-9}$ | $1{,}2\cdot10^{-8}$ |
| Case 10 | Actuator film | $\mathbf{5{,}3\cdot10^{-6}}$ | $1{,}2\cdot10^{-9}$ | $4{,}8\cdot10^{-7}$ | $5{,}0\cdot10^{-5}$ |
| | Background film | $\mathbf{5{,}4\cdot10^{-5}}$ | $1{,}2\cdot10^{-9}$ | $1{,}2\cdot10^{-7}$ | $1{,}2\cdot10^{-7}$ |
| | Stator | $\mathbf{3{,}0\cdot10^{-7}}$ | $6{,}0\cdot10^{-11}$ | $1{,}6\cdot10^{-11}$ | $1{,}6\cdot10^{-9}$ |
| Case 11 | Actuator film | $\mathbf{1{,}7\cdot10^{-4}}$ | $8{,}8\cdot10^{-7}$ | $3{,}2\cdot10^{-9}$ | $1{,}7\cdot10^{-7}$ |
| | Background film | $6{,}4\cdot10^{-7}$ | $3{,}3\cdot10^{-9}$ | $1{,}6\cdot10^{-8}$ | $\mathbf{8{,}9\cdot10^{-7}}$ |
| | Stator | $\mathbf{1{,}6\cdot10^{-6}}$ | $8{,}1\cdot10^{-9}$ | $6{,}2\cdot10^{-9}$ | $3{,}4\cdot10^{-7}$ |
| Case 12 | Actuator film | $2{,}7\cdot10^{-5}$ | $8{,}4\cdot10^{-8}$ | $1{,}6\cdot10^{-5}$ | $\mathbf{3{,}5\cdot10^{-4}}$ |
| | Background film | $\mathbf{2{,}1\cdot10^{-5}}$ | $6{,}5\cdot10^{-8}$ | $7{,}6\cdot10^{-7}$ | $1{,}8\cdot10^{-5}$ |
| | Stator | $\mathbf{1{,}1\cdot10^{-5}}$ | $3{,}5\cdot10^{-8}$ | $6{,}1\cdot10^{-8}$ | $1{,}4\cdot10^{-6}$ |
| Case 13 | Actuator film | $4{,}8\cdot10^{-6}$ | $1{,}6\cdot10^{-8}$ | $5{,}3\cdot10^{-5}$ | $\mathbf{3{,}9\cdot10^{-5}}$ |
| | Background film | $\mathbf{4{,}5\cdot10^{-6}}$ | $1{,}5\cdot10^{-8}$ | $5{,}6\cdot10^{-7}$ | $4{,}2\cdot10^{-7}$ |
| | Stator | $\mathbf{2{,}4\cdot10^{-6}}$ | $7{,}6\cdot10^{-9}$ | $1{,}1\cdot10^{-8}$ | $8{,}0\cdot10^{-9}$ |
| Case 14 | Actuator film | $1{,}1\cdot10^{-5}$ | $1{,}5\cdot10^{-8}$ | $1{,}4\cdot10^{-5}$ | $\mathbf{3{,}5\cdot10^{-4}}$ |
| | Background film | $\mathbf{9{,}9\cdot10^{-6}}$ | $1{,}3\cdot10^{-8}$ | $3{,}2\cdot10^{-7}$ | $7{,}9\cdot10^{-6}$ |
| | Stator | $\mathbf{5{,}1\cdot10^{-6}}$ | $7{,}0\cdot10^{-9}$ | $1{,}3\cdot10^{-8}$ | $3{,}1\cdot10^{-7}$ |

to be continued

continues

| | | | | | |
|---|---|---|---|---|---|
| Case 15 | Actuator film | $1{,}1\cdot10^{-5}$ | $1{,}5\cdot10^{-8}$ | $1{,}4\cdot10^{-5}$ | $\mathbf{3{,}5\cdot10^{-4}}$ |
| | Background film | $\mathbf{9{,}7\cdot10^{-6}}$ | $1{,}3\cdot10^{-8}$ | $3{,}2\cdot10^{-7}$ | $7{,}9\cdot10^{-6}$ |
| | Stator | $\mathbf{5{,}1\cdot10^{-6}}$ | $6{,}9\cdot10^{-9}$ | $1{,}3\cdot10^{-8}$ | $3{,}1\cdot10^{-7}$ |
| Case 16 | Actuator film | $1{,}0\cdot10^{-5}$ | $1{,}7\cdot10^{-8}$ | $1{,}7\cdot10^{-5}$ | $\mathbf{3{,}5\cdot10^{-4}}$ |
| | Background film | $8{,}6\cdot10^{-6}$ | $1{,}5\cdot10^{-8}$ | $3{,}8\cdot10^{-7}$ | $\mathbf{7{,}9\cdot10^{-5}}$ |
| | Stator | $\mathbf{8{,}9\cdot10^{-6}}$ | $1{,}5\cdot10^{-8}$ | $3{,}1\cdot10^{-8}$ | $6{,}4\cdot10^{-7}$ |
| Case 17 | Actuator film | $1{,}2\cdot10^{-5}$ | $1{,}4\cdot10^{-8}$ | $1{,}3\cdot10^{-5}$ | $\mathbf{3{,}5\cdot10^{-4}}$ |
| | Background film | $\mathbf{1{,}1\cdot10^{-5}}$ | $1{,}3\cdot10^{-8}$ | $2{,}9\cdot10^{-7}$ | $7{,}9\cdot10^{-6}$ |
| | Stator | $\mathbf{2{,}7\cdot10^{-6}}$ | $3{,}3\cdot10^{-9}$ | $5{,}5\cdot10^{-9}$ | $1{,}5\cdot10^{-7}$ |
| Case 18 | Actuator film | $\mathbf{7{,}8\cdot10^{-3}}$ | $3{,}7\cdot10^{-6}$ | $2{,}1\cdot10^{-11}$ | $1{,}4\cdot10^{-8}$ |
| | Background film | $\mathbf{6{,}9\cdot10^{-5}}$ | $3{,}2\cdot10^{-8}$ | $1{,}1\cdot10^{-8}$ | $8{,}7\cdot10^{-6}$ |
| | Stator | $\mathbf{7{,}0\cdot10^{-5}}$ | $3{,}3\cdot10^{-8}$ | $2{,}4\cdot10^{-9}$ | $1{,}7\cdot10^{-6}$ |
| Case 19 | Actuator film | $\mathbf{8{,}0\cdot10^{-3}}$ | $7{,}5\cdot10^{-7}$ | $2{,}7\cdot10^{-11}$ | $2{,}1\cdot10^{-9}$ |
| | Background film | $\mathbf{6{,}1\cdot10^{-5}}$ | $6{,}0\cdot10^{-9}$ | $9{,}3\cdot10^{-9}$ | $7{,}5\cdot10^{-7}$ |
| | Stator | $\mathbf{6{,}2\cdot10^{-5}}$ | $5{,}8\cdot10^{-9}$ | $3{,}6\cdot10^{-9}$ | $2{,}9\cdot10^{-7}$ |
| Case 20 | Actuator film | $6{,}5\cdot10^{-6}$ | $7{,}0\cdot10^{-6}$ | $2{,}9\cdot10^{-5}$ | $\mathbf{7{,}3\cdot10^{-3}}$ |
| | Background film | $5{,}4\cdot10^{-6}$ | $5{,}7\cdot10^{-6}$ | $6{,}8\cdot10^{-6}$ | $\mathbf{6{,}8\cdot10^{-6}}$ |
| | Stator | $3{,}5\cdot10^{-7}$ | $3{,}3\cdot10^{-7}$ | $6{,}2\cdot10^{-8}$ | $\mathbf{1{,}6\cdot10^{-5}}$ |
| Case 21 | Actuator film | $\mathbf{7{,}9\cdot10^{-3}}$ | $4{,}2\cdot10^{-5}$ | $2{,}3\cdot10^{-7}$ | $2{,}1\cdot10^{-5}$ |
| | Background film | $2{,}4\cdot10^{-6}$ | $1{,}3\cdot10^{-8}$ | $1{,}8\cdot10^{-6}$ | $\mathbf{1{,}6\cdot10^{-4}}$ |
| | Stator | $\mathbf{8{,}5\cdot10^{-5}}$ | $4{,}5\cdot10^{-7}$ | $2{,}2\cdot10^{-7}$ | $2{,}0\cdot10^{-5}$ |
| Case 22 | Actuator film | $\mathbf{9{,}3\cdot10^{-4}}$ | $1{,}5\cdot10^{-5}$ | $4{,}8\cdot10^{-5}$ | $6{,}3\cdot10^{-4}$ |
| | Background film | $\mathbf{2{,}6\cdot10^{-4}}$ | $4{,}2\cdot10^{-6}$ | $1{,}3\cdot10^{-5}$ | $1{,}7\cdot10^{-4}$ |
| | Stator | $\mathbf{4{,}3\cdot10^{-5}}$ | $7{,}0\cdot10^{-7}$ | $1{,}1\cdot10^{-6}$ | $1{,}5\cdot10^{-5}$ |
| Case 23 | Actuator film | $\mathbf{8{,}8\cdot10^{-3}}$ | $1{,}0\cdot10^{-4}$ | $4{,}5\cdot10^{-7}$ | $4{,}4\cdot10^{-5}$ |
| | Background film | $1{,}8\cdot10^{-6}$ | $2{,}3\cdot10^{-8}$ | $1{,}8\cdot10^{-6}$ | $\mathbf{1{,}7\cdot10^{-4}}$ |
| | Stator | $\mathbf{8{,}5\cdot10^{-5}}$ | $1{,}1\cdot10^{-6}$ | $4{,}4\cdot10^{-7}$ | $4{,}2\cdot10^{-5}$ |
| Case 24 | Actuator film | $\mathbf{8{,}1\cdot10^{-3}}$ | $1{,}1\cdot10^{-6}$ | $1{,}7\cdot10^{-11}$ | $9{,}2\cdot10^{-10}$ |
| | Background film | $\mathbf{3{,}4\cdot10^{-5}}$ | $4{,}6\cdot10^{-9}$ | $2{,}8\cdot10^{-9}$ | $1{,}5\cdot10^{-7}$ |
| | Stator | $\mathbf{3{,}4\cdot10^{-5}}$ | $4{,}6\cdot10^{-9}$ | $4{,}2\cdot10^{-9}$ | $2{,}3\cdot10^{-7}$ |

# 4. Sound production

The sound field radiated by a vibrator embedded in a fluid can be calculated if the normal velocity of its external boundary is known. When the ambient fluid is gas, such as air, the source response can be, more or less, approximated by its in vacuo one [36]. The loading can be described quite easily, however, by an added mass or by radiation impedance. Thus, in the presence of fluid loading, the applied force encounters the sum of the mechanical impedance of the source and the radiation impedance.

A plane, the linear dimensions of which are very large compared to the wavelength and vibrating with the same amplitude and phase over its entire surface, produces a plane wave propagating perpendicularly to its surface [37]. The distribution of the acoustic field around a vibrating surface with bounded dimensions is more complicated. The radiation properties of this type of an acoustic source will depend on the shape and dimensions of the surface, the distribution of the vibration velocity over its surface, and the interaction between the two sides of the plane. If the dimensions of a sound source are much smaller than the wavelength of the sound being radiated, then the details of the surface motion are not important, and it will radiate exactly the same sound as any other simple source with the same source strength [38].

If the vibrating surface is a rigid body (at a given instant vibration, velocity is constant over the entire surface), the source is called a piston-membrane. Usually, the mode of vibration is more complicated than that of a piston, and it depends on the manner of fixing the membrane, its elastic properties and the frequency of vibrations. If the membrane is located in a free acoustic space, the fields on both sides interfere with each other, producing a certain resultant field. If the membrane is located in free space, but the radiation of one of its sides is entirely attenuated by means of an insulating box, then only one side of the membrane radiates, but the radiation may propagate over the entire space.

In the present chapter, the above mentioned consideration is applied to the operation of the EMFi-actuator. The examination of the sound emission is restricted to the far field and the medium is supposed to be homogenous, isotropic and at rest. The medium is also assumed to be thermally non-conductive fluid and to obey the linear stress-strain laws (Hooke’s laws). The

acoustic pressure generated outside the source is assumed to be small enough so that the first-order equations of sound are valid in the region outside the source [39]. A Sommerfield condition (or any equivalent condition) is assumed for the sound pressure field. This means that the boundary condition at infinity enables no reflection so that only the outgoing waves exist.

## 4.1 Actuator in free acoustic field

The radiation resistances of the plane monopole and dipole sources at low frequencies, respectively, are [Appendixes D and E]

$$R_{rm} = \frac{\pi \rho_0 \omega^2 a^4}{2c_0} \quad \text{and} \quad R_{rd} = \frac{2\pi \rho_0 \omega^4 a^6}{27 {c_0}^3} \tag{22}$$

where

$\rho_0$ is the density of the air,

$\omega$ is the angular frequency, and

$c_0$ is the velocity of the sound.

The rectangular radiator element is accounted as a circular membrane of radius $a$. The radius is approximated from the area of the element $a = (DL/\pi)^{½}$ where $D$ and $L$ are the dimensions of the rectangular membrane. Radiation resistances are dependent on the frequency of excitation, the properties of the actuator structure and the medium into which the sound is radiated. The sound power, radiated by an actuator panel vibrating with a spatial mean square value of velocity $U_0$, is by the definition related to the radiation resistance $R_{\text{rad}}$ [40]. The radiated sound powers of the monopole and dipole sources at low frequencies, respectively, are

$$\Pi_m = \frac{1}{2} {U_0}^2 R_{rm} \qquad \Pi_d = \frac{1}{2} {U_0}^2 R_{rd} \tag{23}$$

The monopole source is assumed to be functioning as an encapsulated disk, and the dipole source as a free vibrating disk. Sound pressure amplitudes at low frequencies and on axis one meter from the source are correspondingly

$$P_{axm} = \frac{1}{4} \rho_0 c_0 U_0 k a^2 \qquad P_{axd} = \frac{1}{6} \rho_0 c_0 U_0 k^2 a^3 \tag{24}$$

### 4.1.1 Constant velocity distribution

The velocity amplitude of vibration $U_0$, normal to the radiator surface, is related to the deflection of the membrane, $U_0 = \omega\xi_{0e}$, where $\xi_{0e}$ is an average deflection of the membrane. At 23 Volt signal voltage the average deflection is calculated from the values in Table 1. The emitted sound power levels of monopole and dipole sources into the far field at low frequencies, when the velocity distribution of the actuator film is assumed to be constant (piston source) [see Appendix A], are presented in Figure 19.

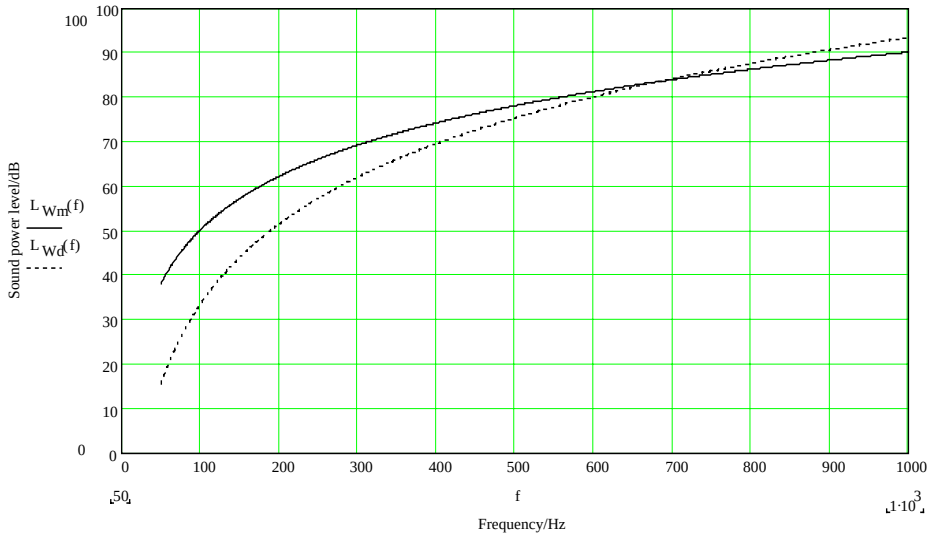


*Figure 19. Sound power levels of monopole and dipole sources at low frequencies.*

The frequency when the sources radiate sound equally effectively is 680 Hz. At higher frequencies the dipole source (dotted line) emits more sound power than the monopole source. In frequencies less than 300 Hz, the radiated sound powers of both sources diminish intensively. The decrement in the radiated power is more significant for the dipole source. The sound pressure levels of monopole and dipole sources at low frequencies at the distance of one meter from the sources on their axis are presented in Figure 20.

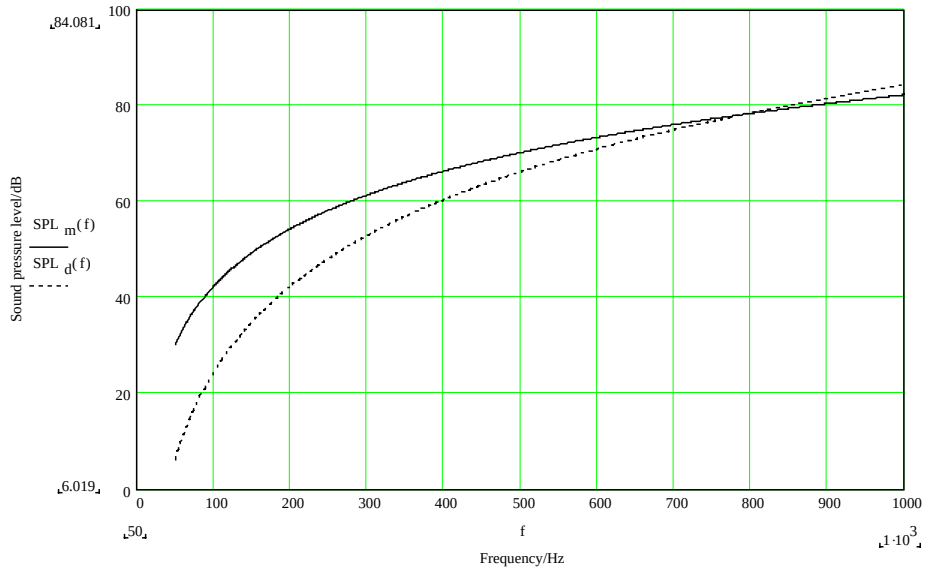


*Figure 20. Sound pressure levels of monopole and dipole sources.*

At high frequencies the dipole source produces more sound pressure into the far field than the monopole source. This occurs when the frequency exceeds 800 Hz. The frequency change is related to the area of the dipole actuator so that when the area increases, the frequency decreases. This is natural because, in the case of a dipole source, the effect of an acoustical short circuit also decreases when the area increases. The large dipole actuators emit thus more sound power (and produce higher pressure levels) into the far field than the monopole sources.

### 4.1.2 Frequency dependent velocity distribution

In reality the vibration velocity of the actuator film is dependent on the frequency according to Figure 5 and Table 1. By using this data and the assumptions made in chapter 4.1.1 concerning the spatial vibration distribution on the membrane, the sound power levels of monopole and dipole sources are as presented in Figure 21. The solid lines in the figure present the curves of Figure 19, respectively, for comparison reasons. It is evident, according to Figure 21, that the arithmetic average of the vibration deflection can replace the frequency dependent vibration of the actuator film satisfactorily in the frequency domain most of the time when evaluating the radiated sound power of the monopole and dipole actuators.

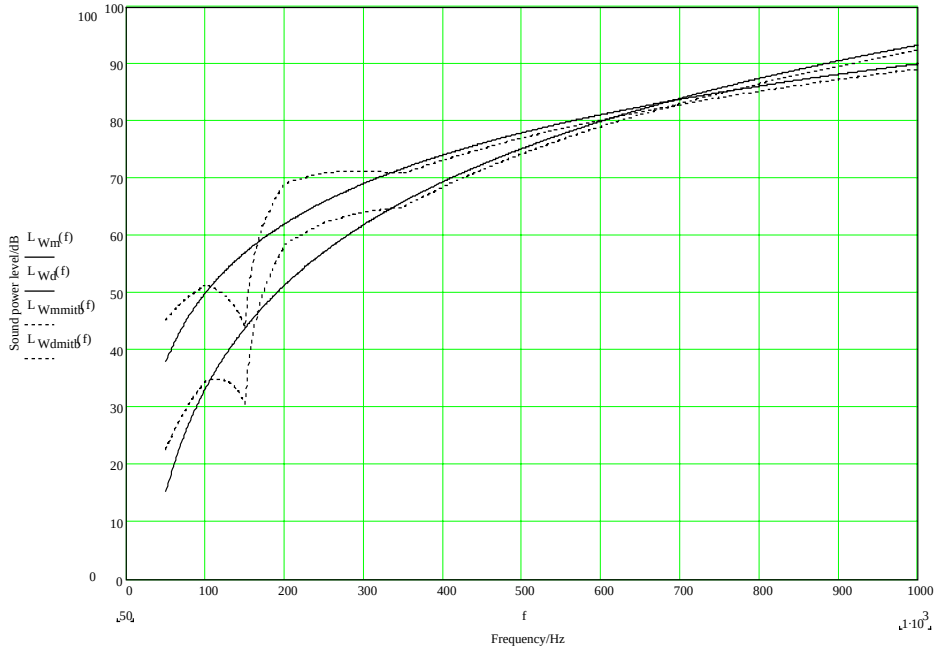


*Figure 21. Sound power levels of monopole and dipole sources.*

### 4.1.3 Sinusoidal spatial velocity distribution

The axial sound pressure of actuator membrane at low frequencies at a distance *r* with a spatial (sinusoidal) acceleration distribution is [41]

$$p(r) = \frac{2\rho_0 U_0 LD(-1)^{n+m} e^{-jkr}}{\pi^3 r(n+\frac{1}{2})(m+\frac{1}{2})}, m = n = 0,1,... \qquad (25)$$

where

$U_0$ is the average vibration velocity amplitude,

$L$ is the width of the actuator element,

$D$ is the length of the actuator element, and

$m$, $n$ are integers.

The sound pressure levels on the axis of the sound source at one meter from the radiating surface with sinusoidal acceleration distribution are illustrated in Figure 22. The first seven addended terms are taken into the calculation. The values are compared to the sound pressure levels emitted by a constant velocity actuator and an actuator whose vibration velocity depends on the frequency.

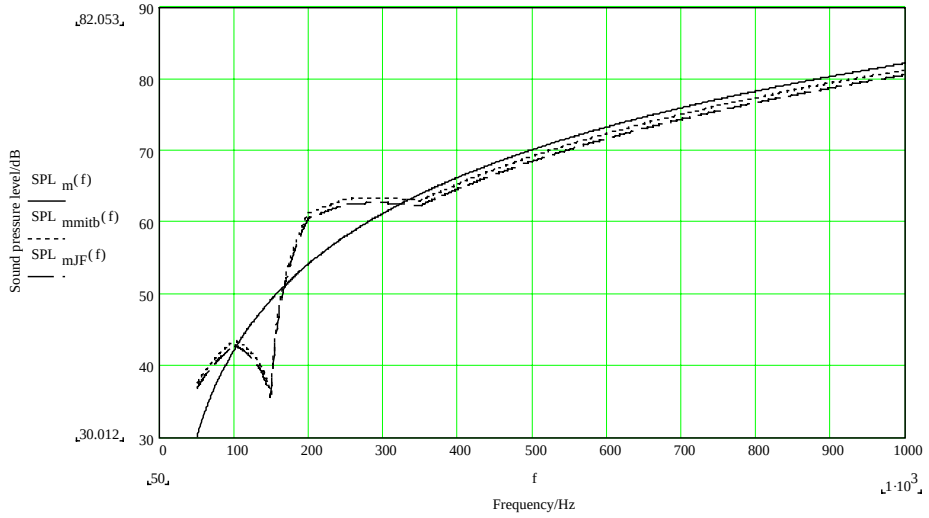


*Figure 22. Sound pressure levels of different actuator sources.*

The solid line in the figure presents the curve of Figure 19, and the dotted line that of Figure 21 for monopole sources, respectively, for comparison reasons. The arithmetic average of the vibration deflection is satisfactorily comparable to the spatially dependent vibration of the actuator film in the frequency domain when evaluating the produced sound pressure levels. This is what it should be because when the dimensions of a sound source are much smaller than the wavelength of the sound being radiated, the details of the surface motion are not important anymore.

### 4.1.4 Effect of impedance loading

The vibration velocity of the actuator film is also influenced by its external impedance in reality, especially by the flow resistance of the stator material according to equation (8) (see Figure 3). The effect of outward impedance on the

produced sound power of monopole source, compared to the situation when there is no resistive load caused by the flow resistance of the stator or the radiation resistance of the ambient fluid, is illustrated in Figure 23. The influence of impedances is minor, and they affect mainly at higher frequencies. Similar results are pertinent also to dipole source and produced sound pressure levels of both sources.

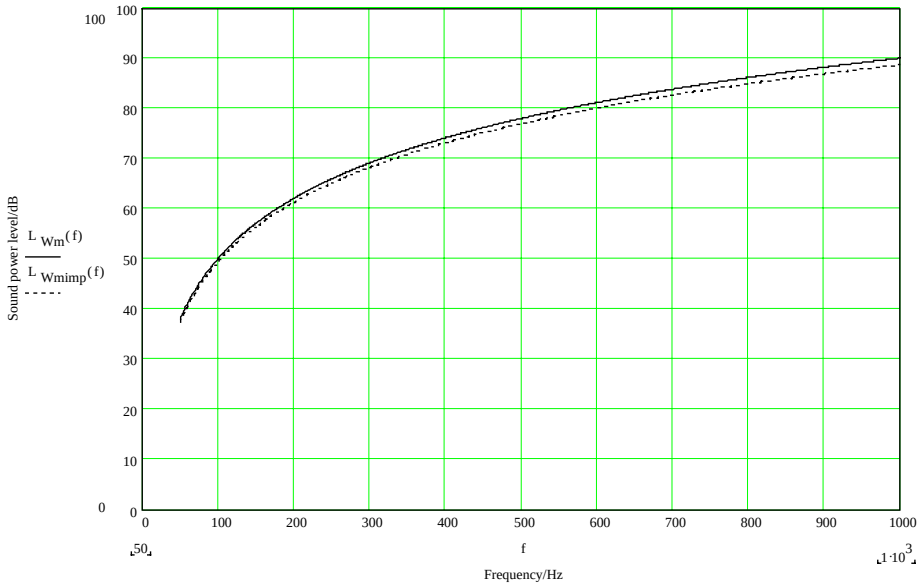


*Figure 23. Sound power levels of monopole sources.*

## 4.2 Dipole actuator near the boundary layer

The radiation of sound by a source can be strongly affected by the impedance of the surrounding space. This stands for the acoustic properties of the ambient medium, the geometry of the space occupied by this medium, and the type of boundary conditions that are imposed at the boundaries of the surrounding space. When the dipole actuator is installed on or very close to a plane boundary, its acoustical properties change. If the dimensions of the boundary are far larger than a wavelength of the radiated sound, then the boundary can be considered a plane of infinite extent [42]. If the boundary is perfectly rigid, the acoustic waves generated by the source will reflect from this plane so that $\vec{u} \cdot \hat{n} = 0$ where $\vec{u}$ is the particle velocity and $\hat{n}$ is the normal to the plane. The pressure

of the reflected wave and that of the incident wave are in phase and identical at the boundary. Sound power of a dipole source which is installed on an absorbent material (which is sited on an acoustically rigid boundary layer) in the half-space occupied by the source is [Appendixes F and G]

$$\Pi_{ddhs} = \frac{3}{2} \cdot \Pi_d \left[ \frac{1}{3}\left(1+\Gamma^2\right) - 2\Gamma\cos\varsigma\left( \frac{2\cos(kb)}{(kb)^2} + \frac{1}{kb}\left(1-\frac{2}{(kb)^2}\right)\sin(kb)\right) + 2\Gamma\sin\varsigma\left( \frac{2\sin(kb)}{(kb)^2} - \frac{1}{kb}\left(1-\frac{2}{(kb)^2}\right)\cos(kb)\right) - \frac{4\Gamma\sin\varsigma}{(kb)^3}\right] \tag{26}$$

where

$\Gamma$ is the reflection factor of the absorbent material,

$\varsigma$ is the phase between the incident and reflecting wave,

$b/2$ is the thickness of the absorbent layer,

$k$ is the wave number, and

$\Pi_d$ is the sound power of the single dipole source in the free field.

It is assumed here that the radiator is acoustically transparent for the reflecting waves from the plane surface. This assumption is justified at low frequencies where the wavelength is much longer than the dimensions of the actuator. When the value of $\Gamma$ is one and $\varsigma$ is zero (acoustically rigid boundary layer), the equation can be reduced to a case of two oppositely phased dipole sources separated at a distance $b$ from each other. The sound power levels of the dipole source on the boundary layer in function of thickness of the absorbent layer and frequency as a parameter are illustrated in Figure 24. The lossy material used in the calculations is rock wool (60 kg/m$^3$). When the thickness of the absorbent material is under 5 cm, the radiated sound power decreases strongly. When the absorbent layer is thicker than that, the power level increases slowly. The difference between the emitted sound power levels of 5 cm and 10 cm absorbent layers at 250 Hz is 7 dB. The main reason for the decrement in the radiated sound power when the thickness of the absorbent layer decreases is the destructive interference of the oppositely phased incident and reflected waves.

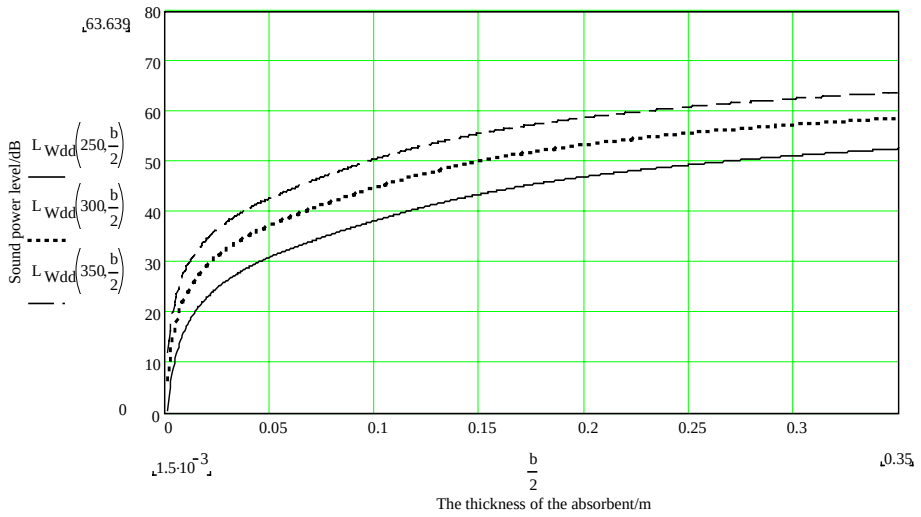


*Figure 24. Sound power level of the dipole source.*

Figure 25 illustrates the radiated sound power levels of the dipole source which is installed on a 10 cm thick rock wool layer and that of two oppositely phased dipole sources (upper curve, Appendix E) the distance between which is 20 cm. The power loss caused by the absorbent material is 5 dB at 50 Hz. The differences in the radiated power levels increase at higher frequencies. The change in the increased power loss is 0.3 dB in the frequency range of 50 - 250 Hz.

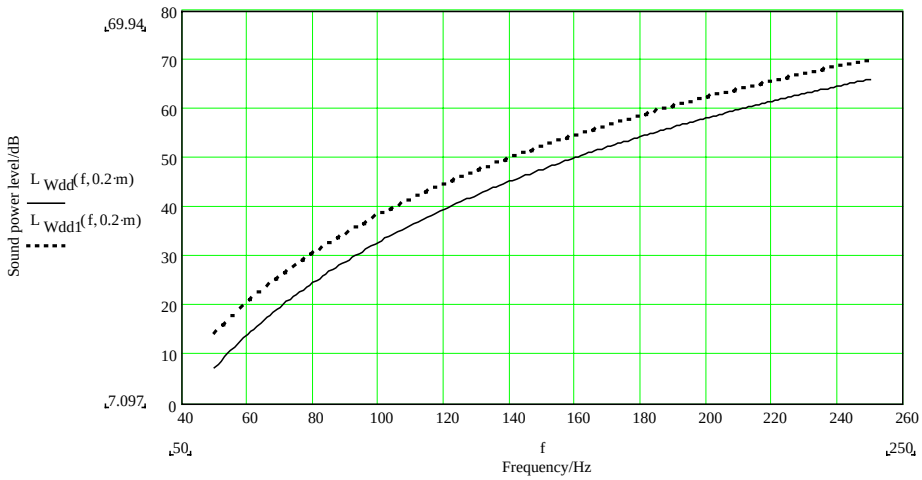


*Figure 25. Sound power levels of the dipole sources.*

The radiated sound power level of the dipole source at 100 Hz when the flow resistance of the lossy material increases (the thickness of the absorbent layer is 10 cm) is illustrated in Figure 26. The flow resistances (10 - 200)·$10^3$ Ns/$m^2$ correspond cotton or rock wool material the thickness of which varies in the density range of 20 - 100 kg/$m^3$ and 100 - 200 kg/$m^3$, respectively. The change in the radiated sound power level in the above mentioned flow resistance range is 3.5 dB.

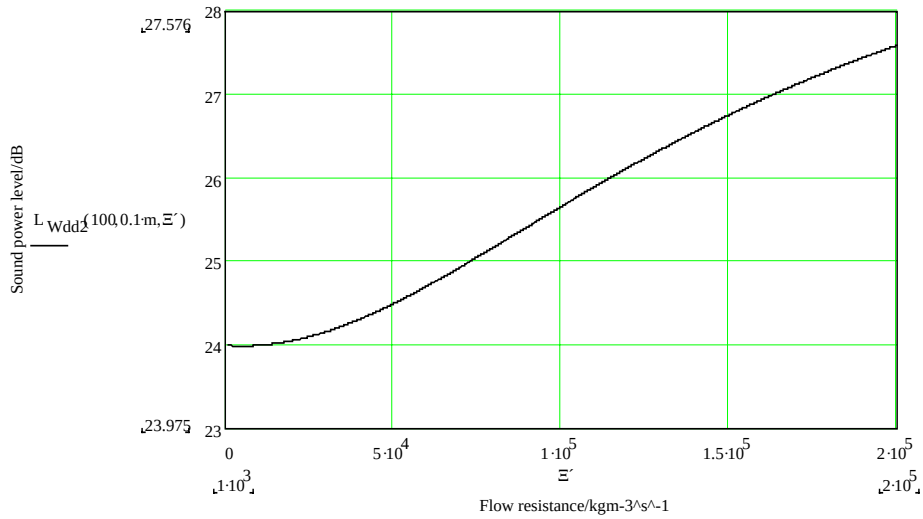


*Figure 26. The increment in the sound power level of a dipole source.*

The radiated sound power of the dipole source increases because the waves on the boundary are not totally in an opposite phase as a consequence of the increased flow resistance, and thus the influence of the acoustic short circuit is smaller.

## 4.3 Radiation pattern of the actuator

The EMFi-actuator actually consists of several membrane strips (N sections) which are located next to each other on the same plane (see Figure 1). The separate strips operate, in principle, as single line sources combined of several unit piston sources locating side by side (see Figures H1 and H2 in Appendix H).

The produced sound pressure of the actuator located in infinite baffle at a certain far field point is (Appendix H)

$$p(r,\Phi,t) = jP_{ax}H_e(\theta)H(\phi)e^{j(\omega t-kr)} \tag{27}$$

$$P_{ax}(r) = \frac{\rho_0 c_0 U_0 kL}{4\pi}\frac{d_m}{r}, \quad H_e(\theta) = \left|\frac{\sin\nu}{\nu}\right| \text{ and}$$

$$H(\phi) = \frac{\sin(\frac{N}{2}kd_m\sin\phi)}{\sin(\frac{1}{2}kd_m\sin\phi)} \text{ where } \nu = \frac{1}{2}kL\sin\theta$$

where

$P_{ax}$ is the axial pressure amplitude,

$U_0$ is the average vibration velocity amplitude,

$L$ is the width of the actuator element,

$d_m$ is the width of the actuator cell,

$r$ is the distance to the observation point, and

$N$ is the number of film strips on the actuator element.

The directional properties of the EMFi-actuator at 100 Hz, 1000 Hz and 5000 Hz are presented qualitatively in Figures 27 - 29.

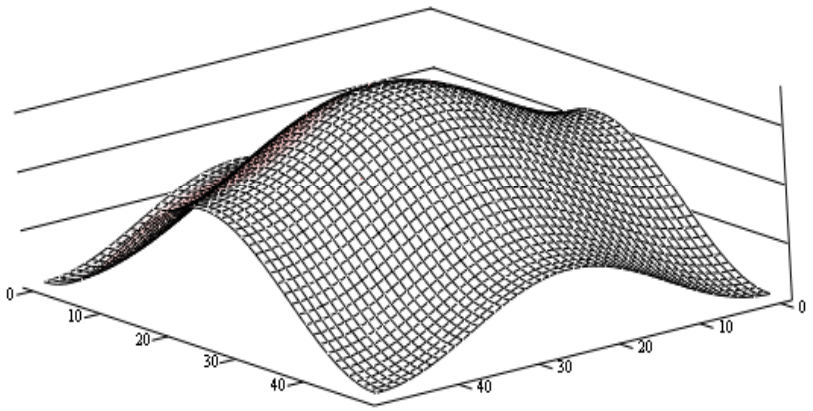


M

*Figure 27. Radiation pattern of the actuator at 100 Hz.*

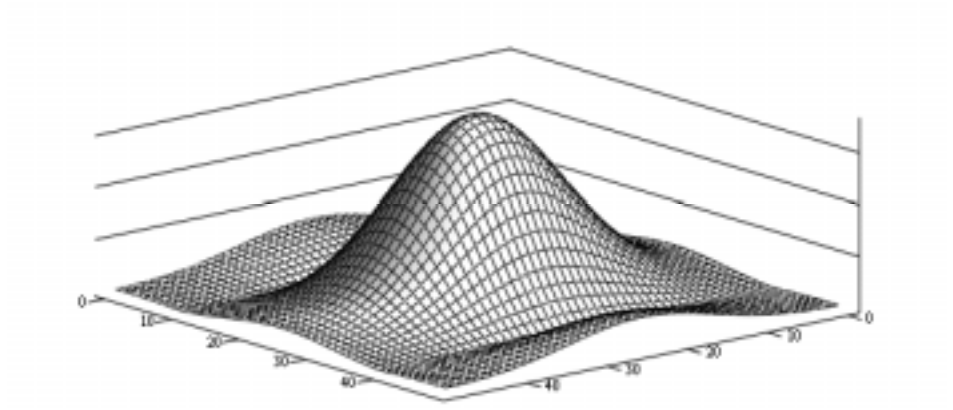

M

*Figure 28. Radiation pattern of the actuator at 1000 Hz.*

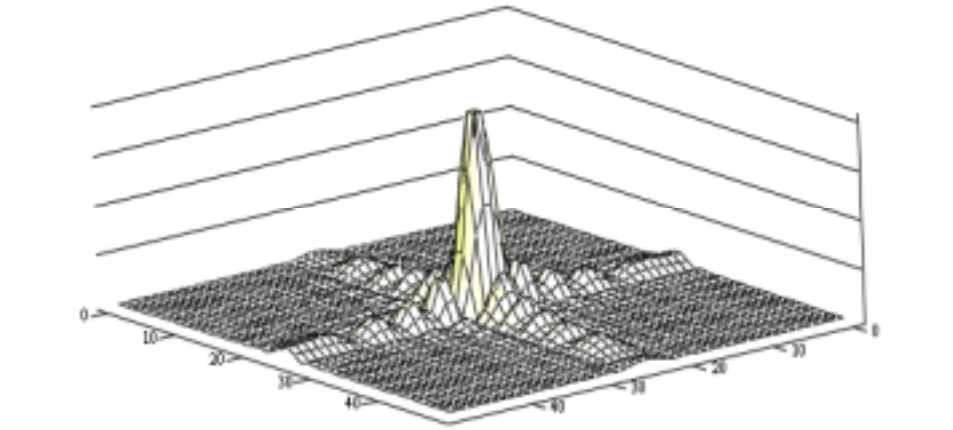

M

*Figure 29. Radiation pattern of the actuator at 5000 Hz.*

The major lobe in the radiation pattern narrows when the frequency increases. The amplitudes of the other lobes are minor compared to the major one. The major lobe corresponds to that portion of the radiation pattern with which the source elements are essentially in phase.

## 4.4 The effect of boundary condition on the sound radiation

The boundary conditions of a vibrating element influence its sound power radiation. The EMFi film is glued to the stator element so that the actuator element is composed of several single sound radiation cells (see Figure 1). The connection type of those cell strips to the boundaries of the stator is not purely rigidly neither simply supported. The consideration of the radiation properties of natural modes of simply and rigidly supported panels basically applies to plate structures. The vibration distributions of simply supported plate and membrane are, however, equal [34]. On the other hand, because the EMFi material is not totally free of bending stiffness (it does not behave like ideal membrane), the radiation properties of rigidly supported plate are studied for reference purposes. The following assumptions are made in the consideration:

- the cell strip is supposed to vibrate time harmonically in one of its eigen modes
- the cell strip is located in infinite baffle
- the load of ambient fluid is neglected
- the consideration is made in far field.

The radiated sound powers of simply and rigidly supported panels are, respectively (see Appendixes I and J)

$$\Pi_{ssp} = 4\rho_0 c_0 \left(\frac{u_m kab}{\pi^3 mn}\right)^2 \int_0^{2\pi}\int_0^{\frac{\pi}{2}} \left[\frac{\cos\left(\frac{\alpha}{2}\right)\cos\left(\frac{\beta}{2}\right)}{\sin\left(\frac{\alpha}{2}\right)\sin\left(\frac{\beta}{2}\right)}{\left[\left(\frac{\alpha}{m\pi}\right)^2 - 1\right]\left[\left(\frac{\beta}{n\pi}\right)^2 - 1\right]}\right]^2 \cdot \sin\theta d\theta d\phi \qquad (28)$$

$$\Pi_{rsp} = 4\rho_0 c_0 \left(\frac{u_m k}{\pi}\right)^2 \int_0^{2\pi} \int_0^{\frac{\pi}{2}} \left[ \frac{1}{k_{xm}^2 + \left(\frac{\alpha}{a}\right)^2} \cdot \left( k_{xm} \tanh\left(\frac{k_{xm} a}{2}\right) \cos\left(\frac{\alpha}{2}\right) \right.\right.$$

$$\left. + \frac{\alpha}{a} \sin\left(\frac{\alpha}{2}\right) \right) + \frac{1}{1 - \left(\frac{\alpha}{a k_{xm}}\right)^2} \left( \frac{\alpha}{a k_{xm}^2} \sin\left(\frac{\alpha}{2}\right) \right) \left. \right] \cdot \left[ \frac{1}{k_{yn}^2 + \left(\frac{\beta}{b}\right)^2} \left( k_{yn} \tanh\left(\frac{k_{yn} b}{2}\right) \cos\left(\frac{\beta}{2}\right) \right.\right.$$

$$\left. \left. + \frac{\beta}{b} \sin\left(\frac{\beta}{2}\right) \right) + \frac{1}{1 - \left(\frac{\beta}{b k_{yn}}\right)^2} \left( \frac{\beta}{b k_{yn}^2} \sin\left(\frac{\beta}{2}\right) \right) \right] \right]^2 \sin\theta d\theta d\phi \qquad (29)$$

where

$\Pi_{ssp}$, $\Pi_{rsp}$ are the radiated sound powers of simply and rigidly supported cell strips,

$u_m$ is the velocity amplitude of the vibrating cell strip,

$k_{xm}$, $k_{yn}$ are the structural wavenumbers to the *x*-, y- co-ordinate directions,

*a*, *b* are the dimensions of the cell strip, and

*m*, *n* are integers.

In the case of simply supported cell strip (equation 28), the odd modes are related to the cosine terms, and the even modes, correspondingly, to the sinus terms. The radiated sound power levels of some odd modes (m,n) of simply (dotted lines) and rigidly (solid lines) supported cell strips are illustrated in Figure 30.

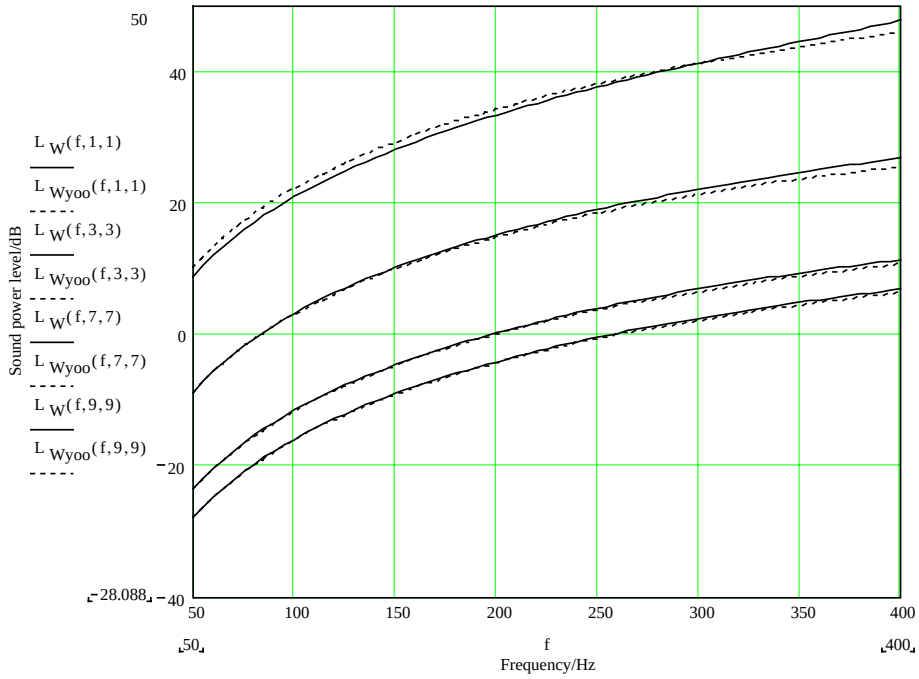


*Figure 30. The radiated sound power levels of odd modes (m,n).*

Both supporting types of the cell strips enable almost equal sound power radiation so that the vibration modes (1,1) are clearly the most efficient single radiators. The reason for the similarity of the sound radiation of the separate modes is the vibration velocity distributions of the cell strip of both boundary types. The velocity distributions of simply and rigidly supported cell strips are presented in equations 30 and 31 and for some modes in Figures 31 - 34, respectively [38, 40].

$$u_{\omega} = u_m \sin\left(\frac{m\pi x}{a}\right)\sin\left(\frac{n\pi y}{b}\right) \tag{30}$$

$$u_{\omega} = u_m\left(\frac{\cosh\left(k_{xm}x\right)}{\cosh\left(½k_{xm}a\right)} - \frac{\cos\left(k_{xm}x\right)}{\cos\left(½k_{xm}a\right)}\right)\left(\frac{\cosh\left(k_{yn}y\right)}{\cosh\left(½k_{yn}b\right)} - \frac{\cos\left(k_{yn}y\right)}{\cos\left(½k_{yn}b\right)}\right) \tag{31}$$

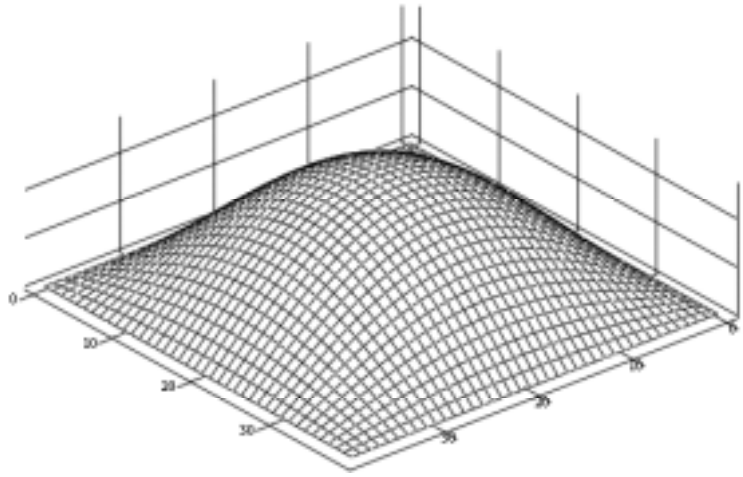


S

*Figure 31. Vibration velocity distribution of a rigidly supported cell strip of mode (1,1).*

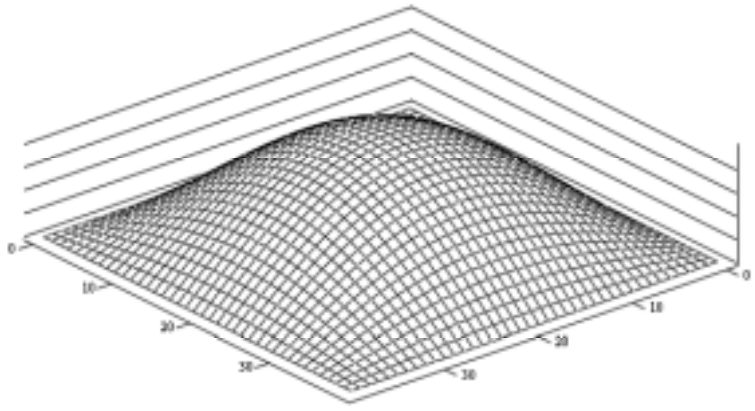


N

*Figure 32. Vibration velocity distribution of a simply supported cell strip of mode (1,1).*

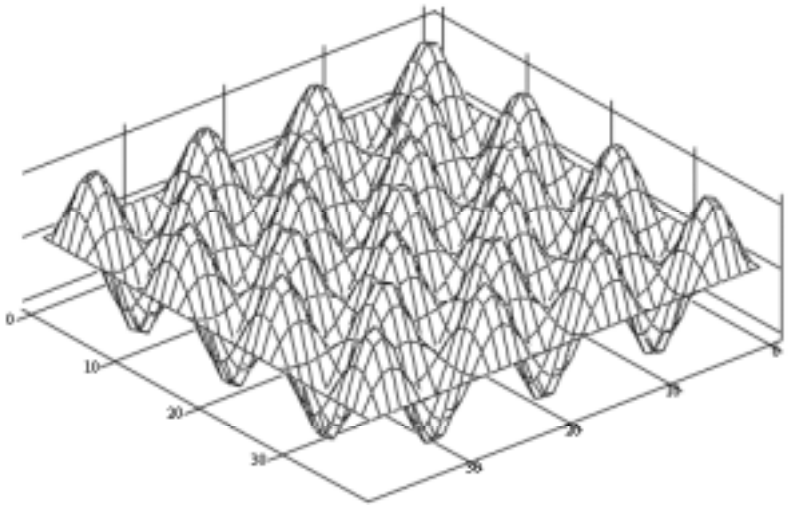


S

*Figure 33. Vibration velocity distribution of a rigidly supported cell strip of mode (7,7).*

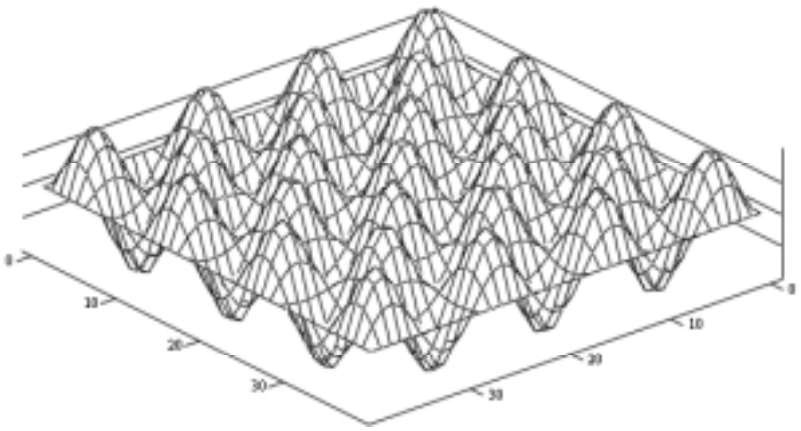


N

*Figure 34. Vibration velocity distribution of a simply supported cell strip of mode (7,7).*

The vibration velocity distributions of simply and rigidly supported cell strips of odd modes are practically equal, and thus also the radiated sound powers of the cell strips are equal. The radiated sound power levels of some even modes (m,n) of simply and rigidly supported cell strips are illustrated in Figures 35 and 36.

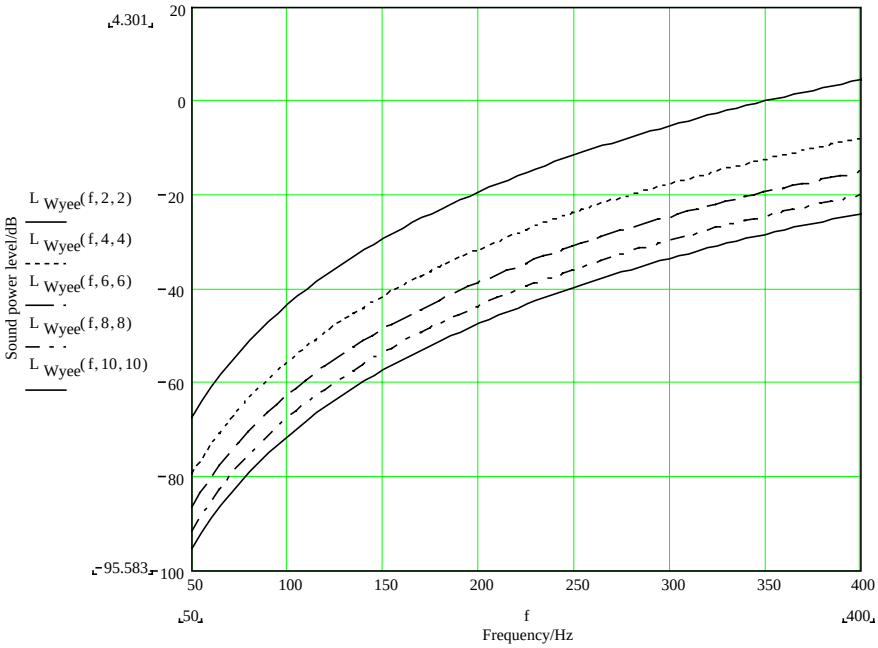


*Figure 35. The radiated sound power levels of even modes (m,n). Simple support.*

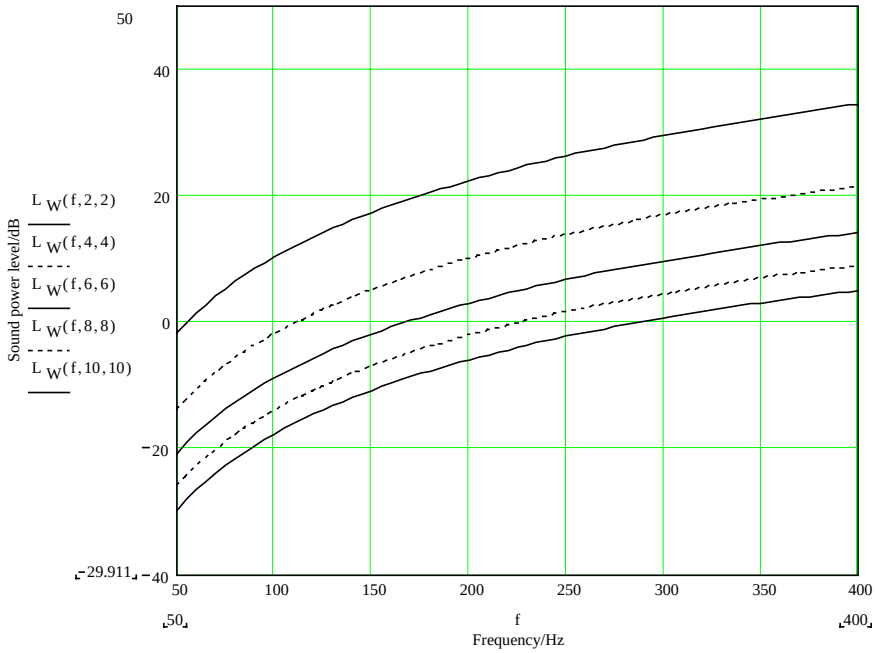


*Figure 36. The radiated sound power levels of even modes (m,n). Rigid support.*

The rigidly supported boundaries of the cell strip enable it to radiate more effectively sound power with the separate even modes compared to the simply supported boundary condition. The reason for this distinction is the vibration velocity distributions of the differently supported cell strips. The vibration velocity distributions of simply and rigidly supported cell strips of even modes (2,2) and (4,4) are presented in Figures 37 - 40.

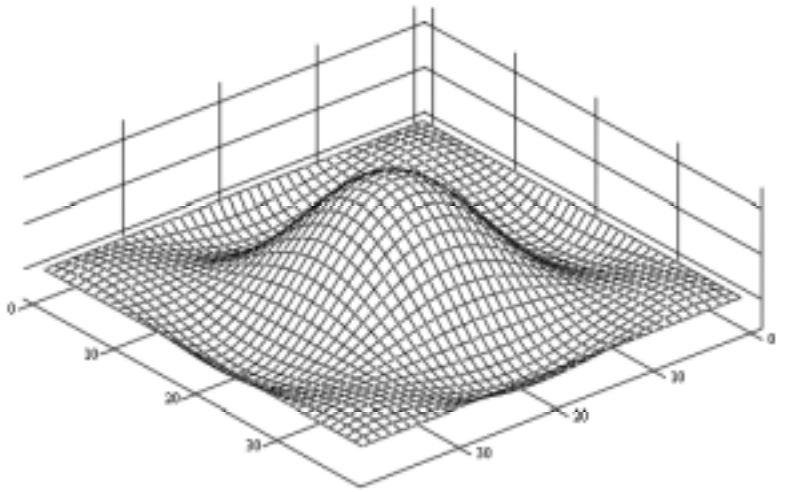

S

*Figure 37. Vibration velocity distribution of a rigidly supported cell strip of mode (2,2).*

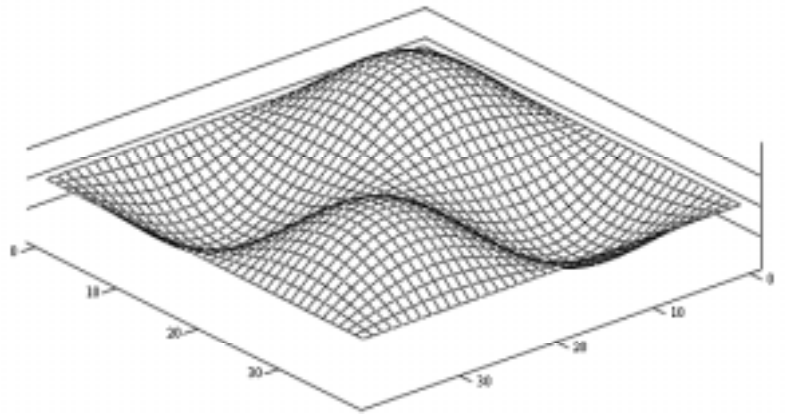

N

*Figure 38. Vibration velocity distribution of a simply supported cell strip of mode (2,2).*

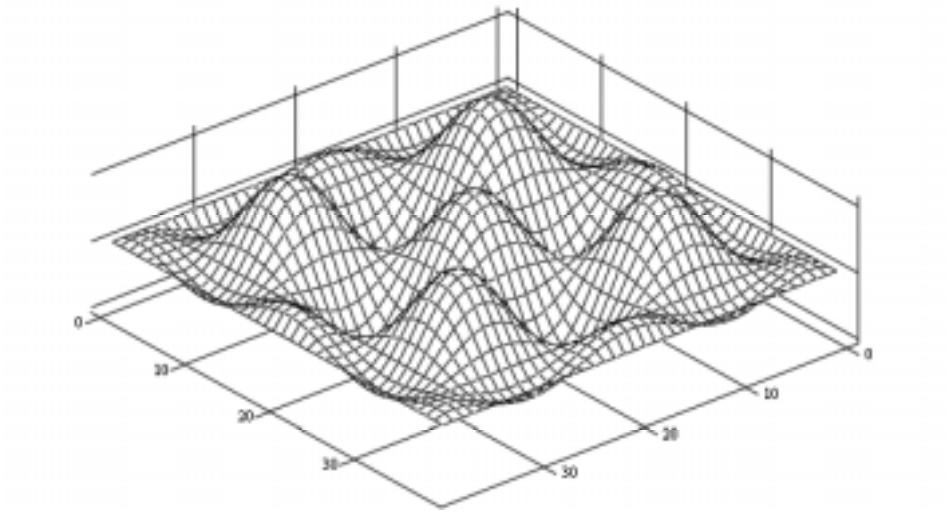


S

*Figure 39. Vibration velocity distribution of a rigidly supported cell strip of mode (4,4).*

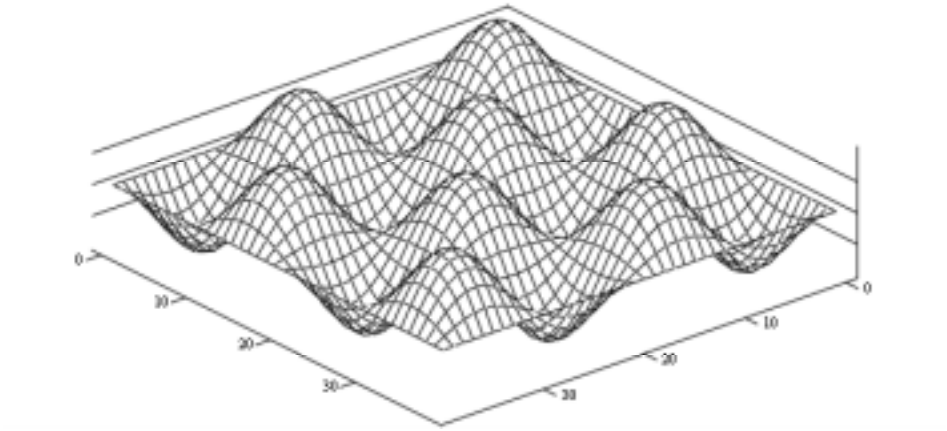


N

*Figure 40. Vibration velocity distribution of a simply supported cell strip of mode (4,4).*

The odd modes are more effective sound radiators compared to the even modes. Because the adjacent subsections of the cell strip are separated by much less than a wavelength in the surrounding air, the air displaced outward by one subsection moves to occupy the space left by the motion of the adjacent subsections, without being compressed, and very little sound power is radiated. For even modes the number of the vibrating subsections of the cell strip, which are in the opposite vibration phase, is equal, and thus the radiated net sound power decreases. On the contrary, for odd modes there always exist subsections which are out of opposite vibration phases and thus also radiate sound power. The radiation resistances and sound radiation of plates with different boundary conditions are presented in the references [43, 44, 45, 46, 47, 48].

## 4.5 The measurement vs. modelling results

Acoustical testing for a plastic panel actuator, sized 320 mm · 420 mm (see Figure 1), has been carried out in a semianechoic room by using a PC-installed MLSSA 10 measuring system [31]. The measurements cover both free and half-free acoustic fields. In half-free field measurements, the measured actuator was placed on the floor of the chamber so that either 20 mm mineral wool or only spacers were used between the floor and the panel under measurement. The sides of the actuator panel were left open and no enclosures or baffles were used in the measurements on the floor. In the free field measurements, the panel was hung from the ceiling and only anechoic part of the impulse response of the time signal (direct sound) was used in the results. The distance between the actuator and detector was 1 meter.

The constant average deflection of the film predicts quite satisfactorily the sound production properties of the actuator (see chapters 4.1.1 - 4.1.4). Thus frequency or spatial dependence of the velocity distribution of the actuator film are not taken into consideration when comparing the modelling and measurement results. Also the external impedance loading of the actuator is ignored in the examination.

### 4.5.1 The free acoustic field

Figure 41 presents the delivered sound pressure levels of the actuator element at 1 meter from the vibrating plane in the free acoustic field. The solid line with the rectangle symbols is based on the measurement results. The dashed (cross symbols) and dotted (diamond symbols) lines are based on the modelling results of the monopole and dipole type of radiation, respectively. The analytical results are calculated according to equation (24).

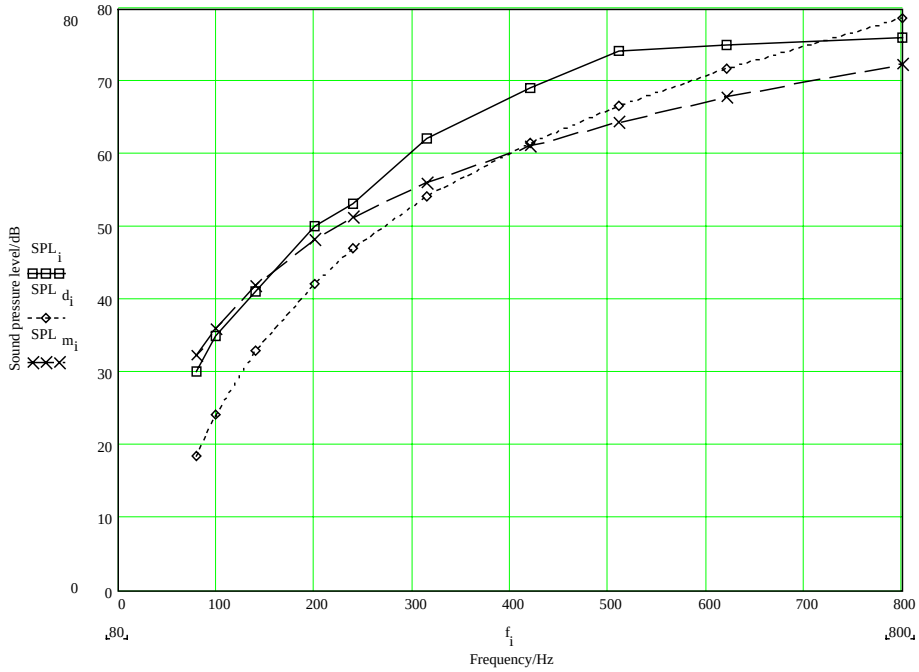


*Figure 41. Sound pressure levels in a free acoustic field.*

The calculated sound pressure level values of a monopole source are almost equal to the measured values up to 240 Hz. The shape of the sound pressure level curve of the dipole type actuator is similar compared to the measured values up to 600 Hz so that a constant 8 dB amplitude difference exists. The measured sound pressure levels are, however, normalized in such a way that the total sound pressure level is 94 dB and the amplitude values are thus not directly comparable. The monopole source type of modelling describes the delivered sound pressure output of the EMFi-actuator at low frequencies. The dipole type

of modelling describes the sound pressure production properties of the actuator in a larger frequency range when the amplitude difference, based on the normalization of the measurement results, is taken into consideration.

### 4.5.2 The half-free acoustic field

Figure 42 presents the sound pressure level values in a half-free sound field, based on the actuator element measurements, and the respective analytical results. As earlier, the analytical values are specified for a monopole and dipole type of radiation. The modelling results are calculated according to equation (24) by taking the results of Appendix G into consideration. The solid line with the rectangle symbols is based on the measurement results. The dashed (cross symbols) and dotted (diamond symbols) lines are based on the calculation results of monopole and dipole type of radiation, respectively.

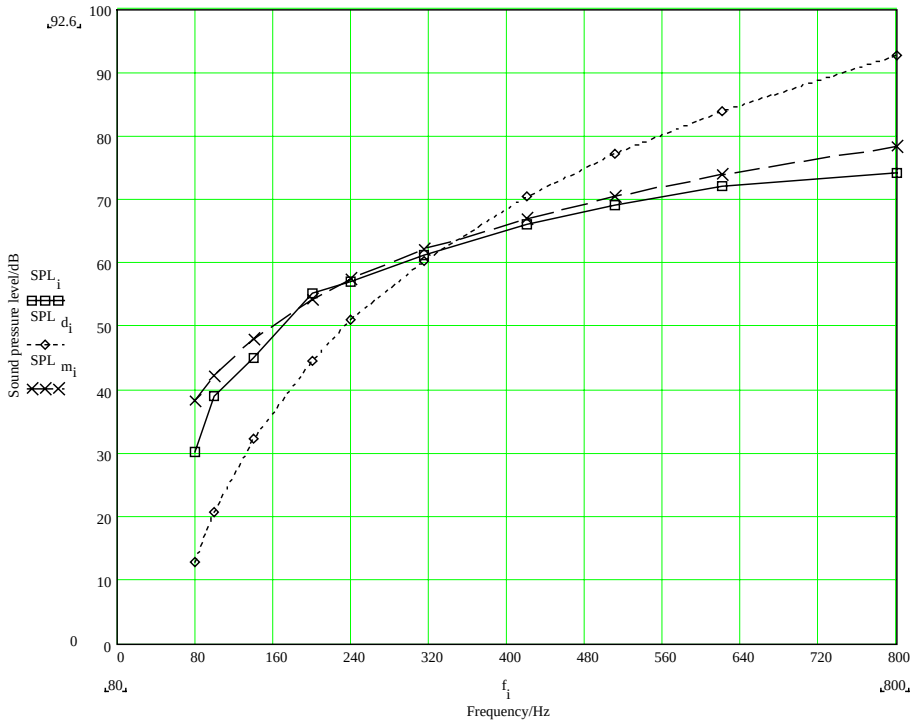


*Figure 42. Sound pressure level in a half-free acoustic field.*

The monopole source type of modelling predicts the delivered sound pressure levels of the measured actuator very accurately up to 600 Hz. The shape of the sound pressure level curve of the dipole type actuator is similar compared to the measured values up to 240 Hz. The amplitude difference between the values of the measured and dipole type modelled curves is 12 dB. The monopole type of source modelling is more realistic in half-free acoustic fields because basically in dipole type of radiation, the destructive interference of the oppositely phased incident and reflected waves do not decrease very effectively the radiated sound at low frequencies because of the absorption material under the actuator. At high frequencies, the discrepancies between the modelling and measurement results in free and half-free acoustic fields arise from the fact that the external impedance loading of the actuator has been ignored in the examination.

### 4.5.3 The directivity of the actuator

The directivity of the actuator element has been measured at 15 degree intervals in a half-free acoustic field. In measurements, a mineral wool the thickness of which is 20 mm has been inserted between the EMFi panel and the floor. The calculated (see Appendix H) and measured sound pressure levels of the EMFi-actuator at angles of 0°, 30°, 60° and 90° degrees at low frequencies are presented in Figures 43 and 44. The calculated results are based on equation (27).

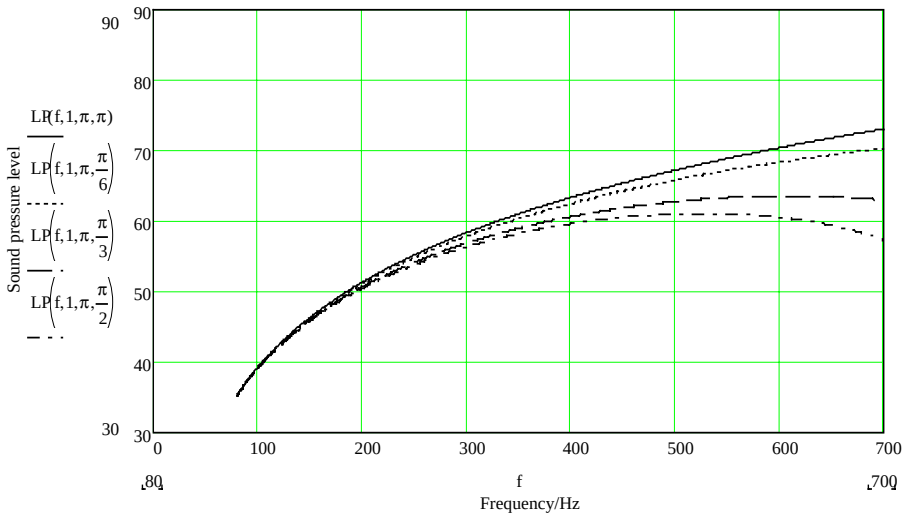


*Figure 43. Calculated sound pressure levels at different angles in a half-free acoustic field.*

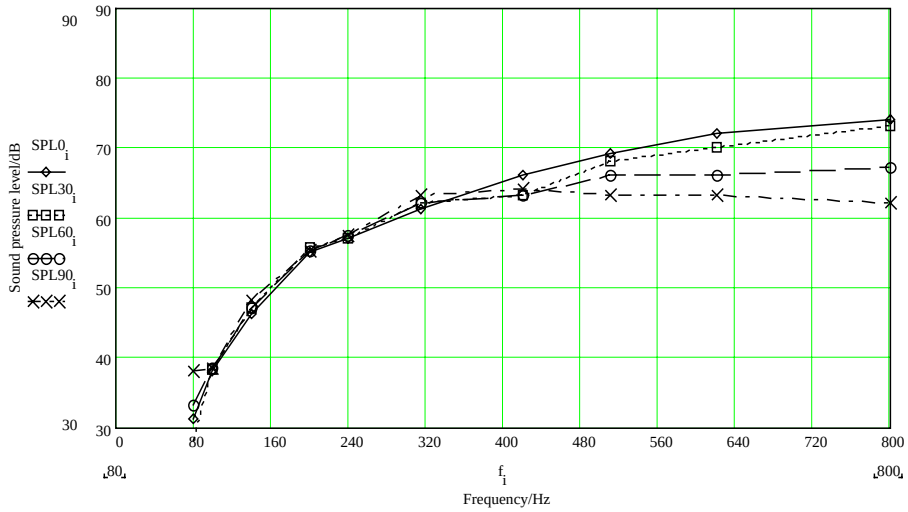


*Figure 44. Measured sound pressure levels at different angles in a half-free acoustic field.*

When the actuator panel is located near the boundary surface, radiation up to 400 Hz is very uniform in all directions. The sound pressure level curves of the measured and predicted values are very similar in every angle. The calculated and measured polarn patterns of the EMFi-actuator panel at 120 Hz, 240 Hz and 500 Hz at different angles are presented in Figures 45 and 46.

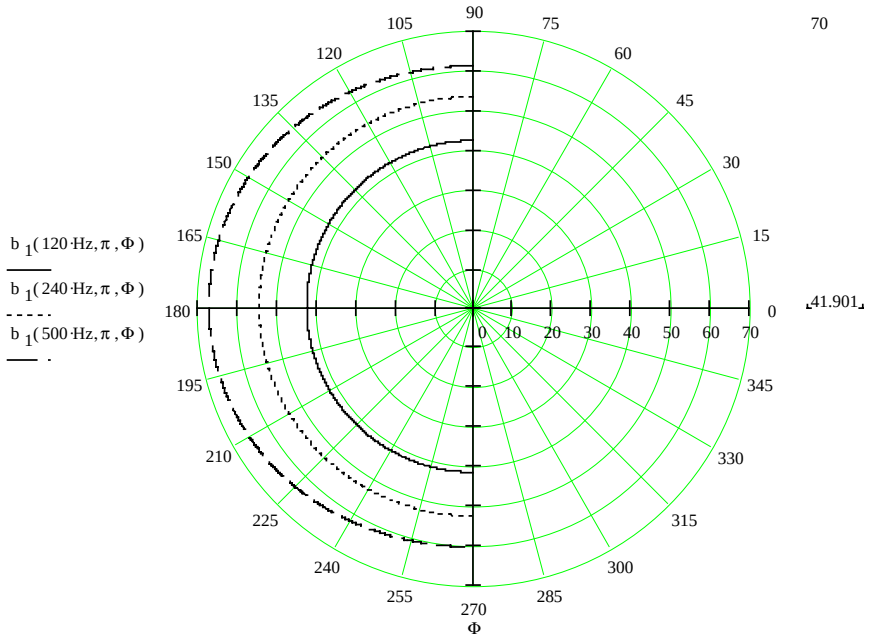


*Figure 45. Calculated polarn patterns in acoustic half-free field conditions.*

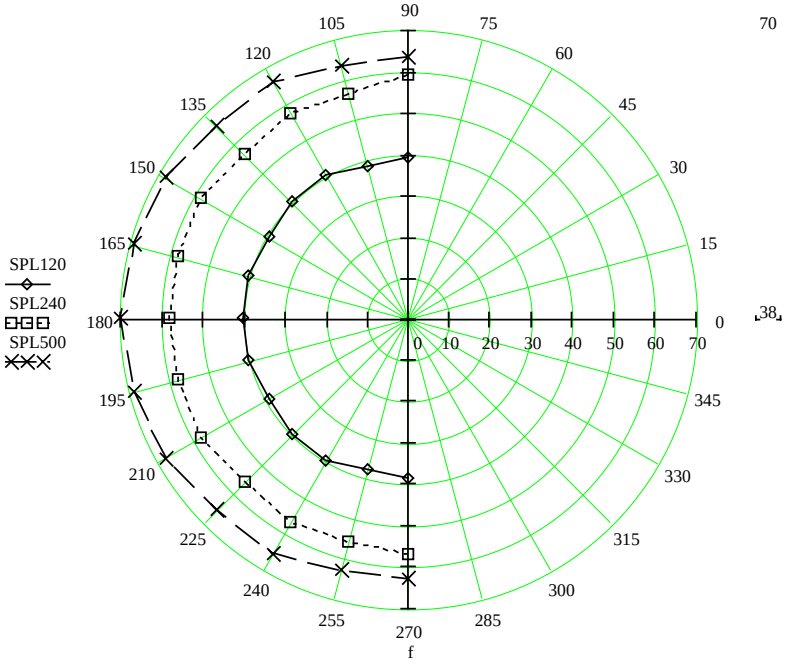


*Figure 46. Measured polarn patterns in acoustic half-free field conditions.*

The radiation patterns of the actuator element are relatively round and resemble the radiation patterns of the monopole source. The measured and predicted values are very similar in every angle. The radiation patterns produced by a piston-type actuator differ from the idealized patterns to some extent. One reason for this discrepancy is that the area of the baffle in which the actuator is mounted is necessarily finite. At high frequencies, even a baffle of small linear dimensions corresponds quite closely to an ideal infinite baffle, but at low frequencies each element of the piston will not radiate with hemispherical divergence. In addition, radiation from the back of the actuator may propagate into the region in front of the actuator so that the resulting radiation pattern approximates that of a dipole source rather than that of a piston in an infinite baffle. Another reason for discrepancy is that the material of an EMFi-actuator membrane is not perfectly rigid. Driving the actuator at its centre establishes a higher velocity amplitude in the inner parts of the film than near its rim, and at high frequencies, the film may even vibrate in normal modes. Under these circumstances, $U_0$ in equation (H3) may become a complex function of the radial distance and angle, and hence, must be considered a variable in the integration.

## 4.6 Methods to influence the sound production of the actuator

### 4.6.1 Change in the deflection of the film

The emitted sound power to the far field depends on the velocity (or the deflection) amplitude of the film according to the equations (23 and 26). The change in the deflection of the membrane depends on the membrane tension and the applied signal voltage. The sound power levels of monopole and dipole sources, related to normalized deflection and at parameter frequencies 50 Hz (solid line), 100 Hz (dotted line) and 150 Hz (dot-dashed), are illustrated in Figures 47 and 48.

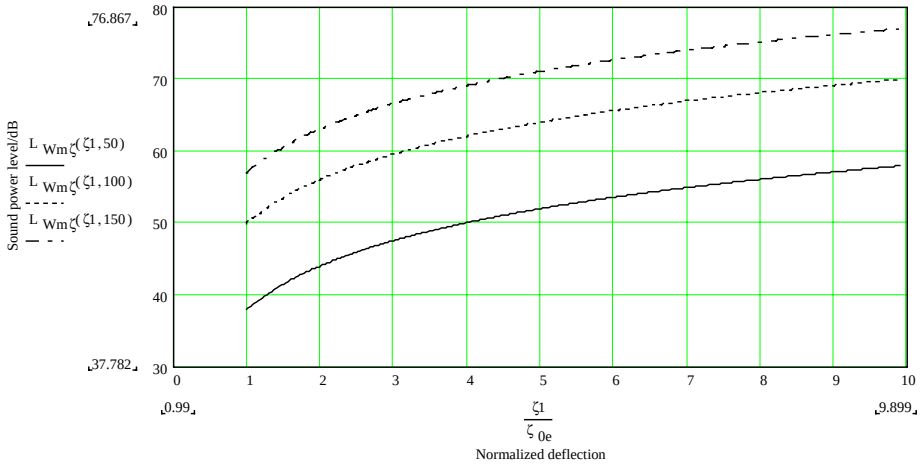


*Figure 47. Sound power levels of a monopole source as a function of film deflection.*

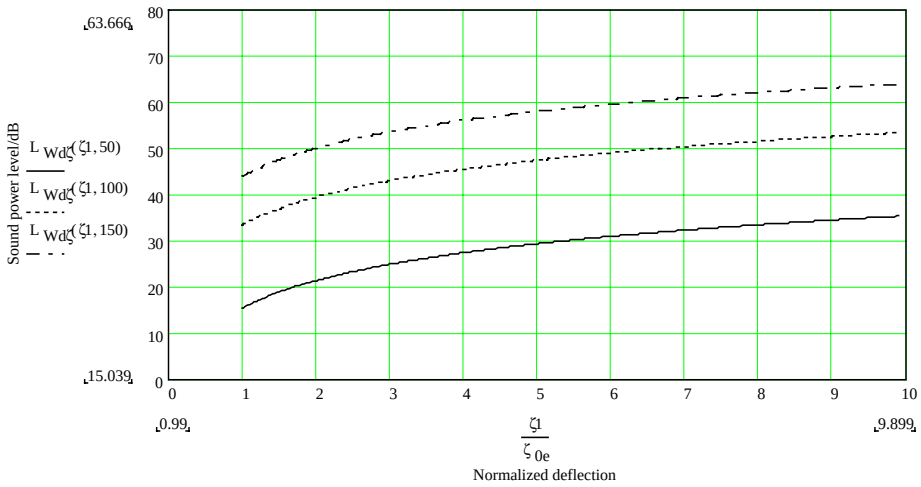


*Figure 48. Sound power levels of a dipole source as a function of film deflection.*

The radiated sound power levels of the monopole and dipole type actuators increase 6 dB when the magnitude of the deflection is doubled, and 20 dB when the magnitude of the deflection is ten times the original one. The increment does not depend on the frequency, and it is equal for both source types.

### 4.6.2 The change in the area of the radiator element

The delivered sound pressure levels of monopole and dipole type actuators related to the normalized area at frequencies 50 Hz (solid line), 100 Hz (dotted line) and 150 Hz (dot-dashed) are illustrated in Figures 49 and 50. Sound pressure levels of a monopole source increase 6 dB when the area of the actuator element is doubled. For the dipole source, the increment in the sound pressure levels is 9 dB, correspondingly. The increment does not depend on the frequency and it is not equal for the source types. When the increment of the actuator area is tenfold compared to the original area, the sound pressure levels of a monopole type source increase 20 dB and a dipole type source 30 dB, correspondingly.

It is possible to increase the delivered sound pressure of the actuator element to the acoustic far field and to lower the frequency where the source types are equal radiators by increasing the area of the actuator. Figure 51 presents the delivered sound pressure levels of monopole and dipole sources when the areas of the actuator panels are 4 $m^2$. In this case, the dipole type actuator is a more effective radiator almost in the entire examined frequency range.

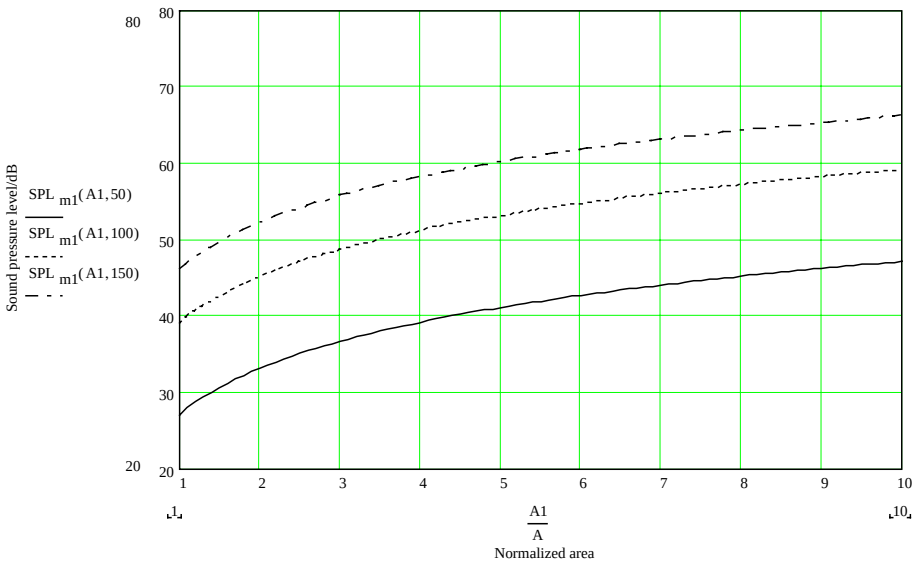


*Figure 49. Sound pressure levels of a monopole source as a function of actuator area.*

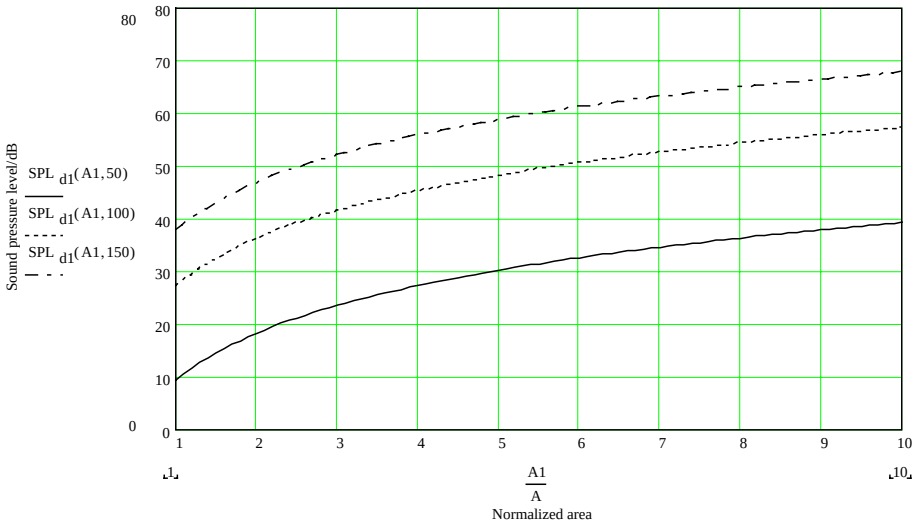


*Figure 50. Sound pressure levels of a dipole source as a function of actuator area.*

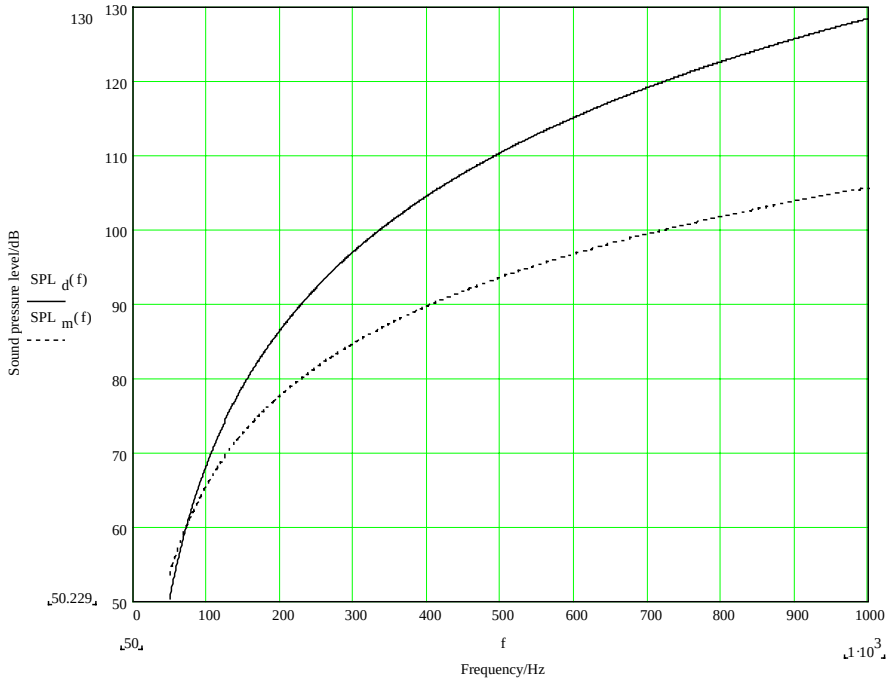


*Figure 51. Sound pressure levels of large dipole and monopole actuators.*

Increment in the emitted sound power/pressure, based on the larger actuator area, is related to the change in the radiation resistance value of the actuator element. The radiated acoustic energy is counted as losses for the vibrating element itself. Those losses increase when the larger actuator area adds to its radiation resistance. At low frequencies, the acoustic short circuit decreases the radiation efficiency of the dipole type actuator. When the area of the dipole source enlarges, the effect of the acoustic short circuit diminishes, and the actuator radiates sound more effectively.

### 4.6.3 The interaction of the sources

The sound field radiated by an actuator is often affected by neighbouring surfaces or sound sources considerably. Two sound sources interact with each other when they are close or when low frequencies are considered [38]. For a source with a characteristic dimension $a$, vibrating at an angular frequency $\omega = ck$ and located at a nominal distance $b$ from another source, the far field pressure and the net acoustic power output depend on $kb$ and $a/b$. The state of vibration of the vibrator element is assumed to be independent of $b$, and the single monopole or dipole type actuators to function like the ones discussed before. The radiated sound powers of two interacting monopole and dipole sources are, respectively ([39], Appendix F)

$$\Pi_{mm} = 2 \cdot \Pi_m \cdot \left[ 1 + \frac{\sin(kb)}{kb} \right] \tag{32}$$

$$\Pi_{dd} = 6 \cdot \Pi_d \cdot \left[ \frac{1}{3} + \frac{1}{kb}\left( 1 - \frac{2}{k^2 b^2} \right) \sin(kb) + \frac{2}{k^2 b^2} \cos(kb) \right] \tag{33}$$

In the limit $a/b << 1$, that is, when the distance between the sources is large compared to the dimensions of a single vibrator, the total acoustic field is well approximated by the superposition of those fields resulting from separate consideration of the two sources. The sound power levels of interacting monopole and dipole sources are illustrated in Figures 52 and 53. The parameters of the curves are the distance 0.1 m (thin solid line), 0.5 m (dotted line) and 1 m (dot-dashed line). The thick dashed lines present the radiated sound power levels of single monopole or dipole sources, respectively.

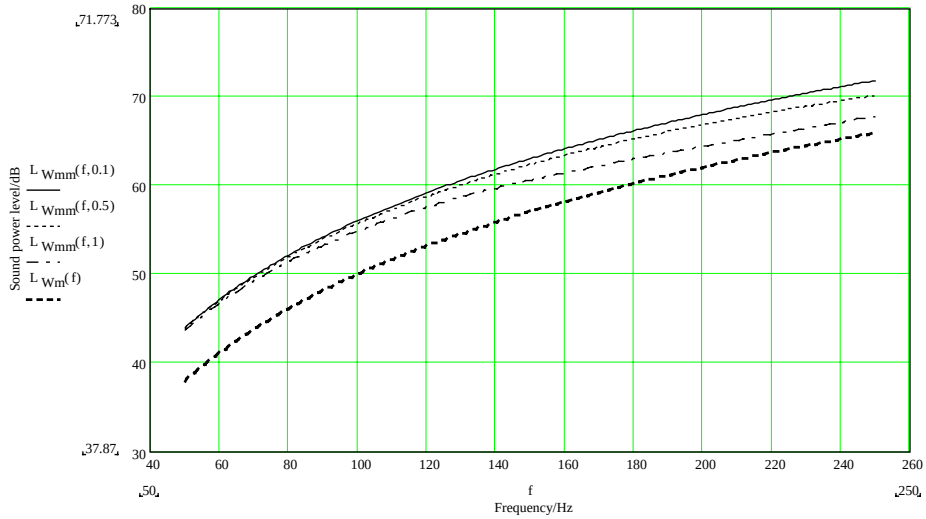


*Figure 52. Sound power levels of two interacting monopole sources at low frequencies.*

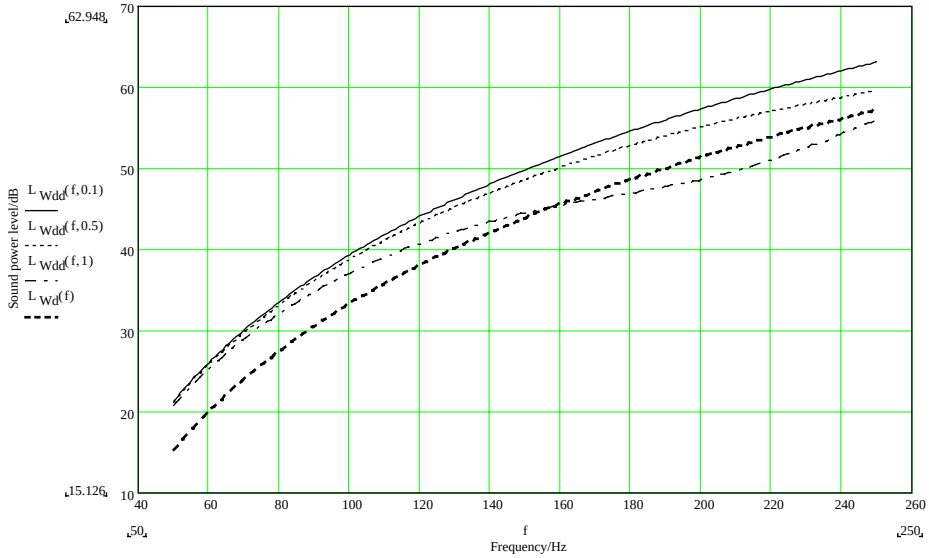


*Figure 53. Sound power levels of two interacting dipole sources at low frequencies.*

At low frequencies, or when the two actuators are located close to each other, the sound power level increases 6 dB compared to that of a single source. At high frequencies, the increment is, correspondingly, 3 dB. In the latter case, the

increment in the total sound power level equals that of two single sources without any interaction. The interaction effect of the dipole sources disappears at lower frequencies than that of the monopole sources. At low frequencies, the increment of the sound power levels of two interacting sources equals in magnitude the situation when the deflection increment of the single actuator membrane is doubled. Figure 54 illustrates the normalized sound powers of interacting monopole (solid line) and dipole (dotted line) sources. The sound power of the two interacting sources is four times as large as that of the single source at low frequencies or when the sources are located close to each other.

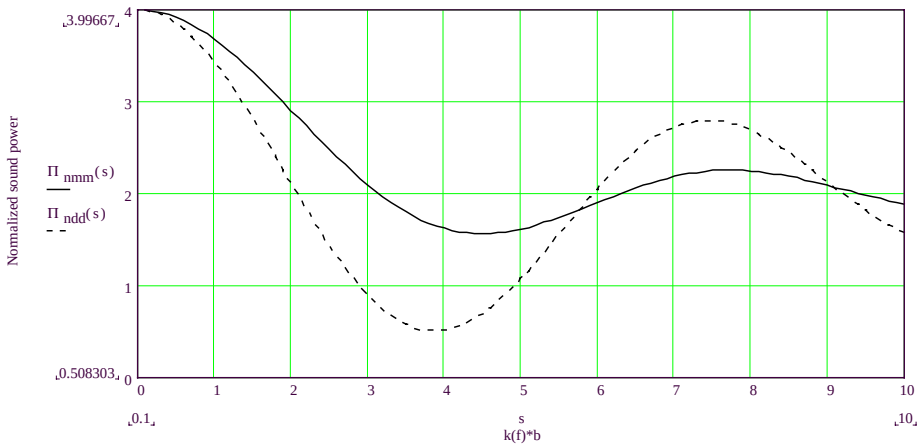


*Figure 54. The normalized sound powers of interacting monopole and dipole actuators.*

### 4.6.4 The change in the dimensions of the cell strip

The dimensions of the actuator cell affect the power the single vibration mode radiates to the acoustic far field. The radiated sound power levels of the modes (1,1) and (2,2) of the rigidly supported cell strips are illustrated in Figures 55 - 58. The actuator cell width and length are the parameters of the curves. The lengths or widths of the actuator cell are changed from 1/4 part to a fourfold of the original dimensions. The present actuator dimensions (thick dashed lines in the figures stand for the reference dimensions presented in Appendix A) seem to be acceptable. When the dimensions of the actuator cell are smaller than in the reference case, the emitted sound power decreases. When the dimensions of the

actuator cell are, correspondingly, larger, the radiated sound power does not significally increase. The sound power level values, concerning the small element lengths in Figure 56, are not pertinent at high frequencies. The same statement concerns also the radiated sound power levels of the mode (2,2) of a rigidly supported cell strip presented in Figure 58.

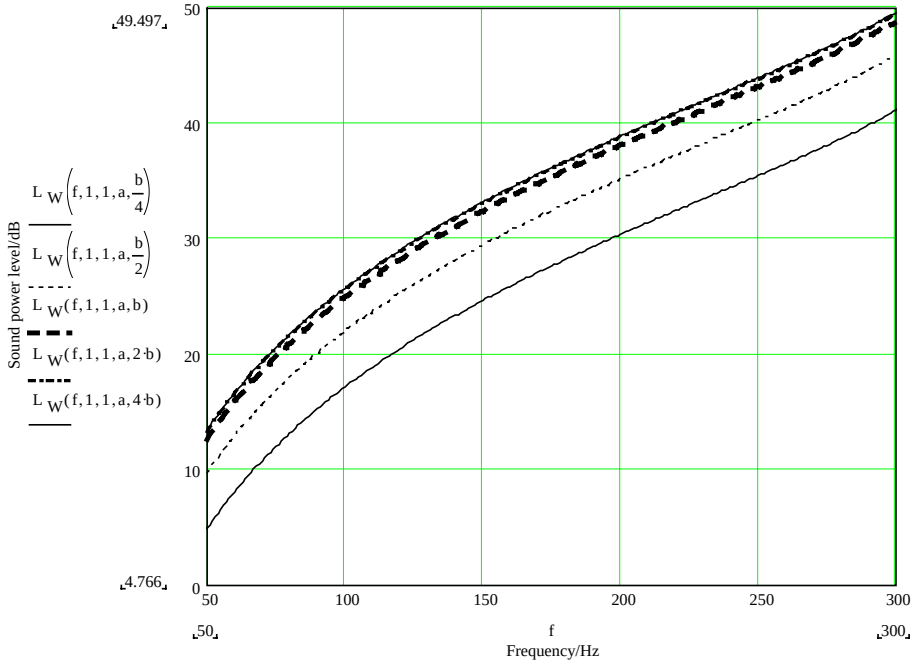


*Figure 55. The radiated sound power of mode (1,1) of a rigidly supported actuator cell having the cell width as a parameter.*

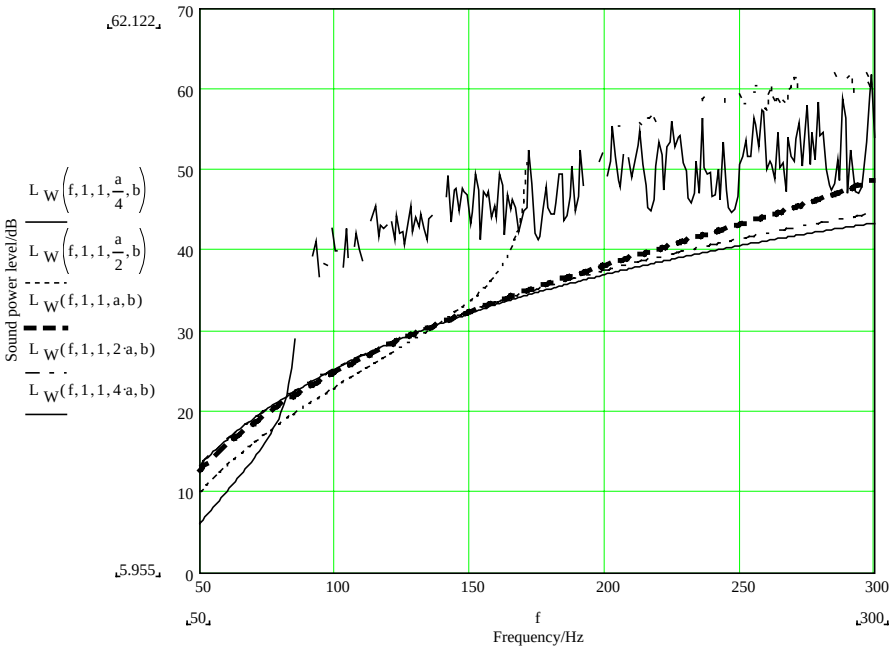


*Figure 56. The radiated sound power of mode (1,1) of a rigidly supported actuator cell having the cell length as a parameter.*

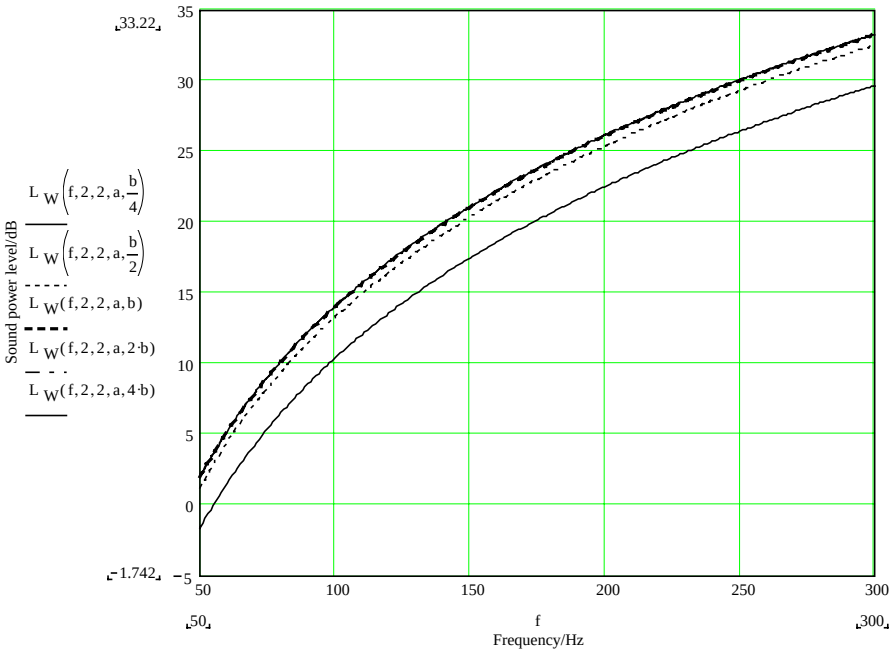


*Figure 57. The radiated sound power of mode (2,2) of a rigidly supported actuator cell having the cell width as a parameter.*

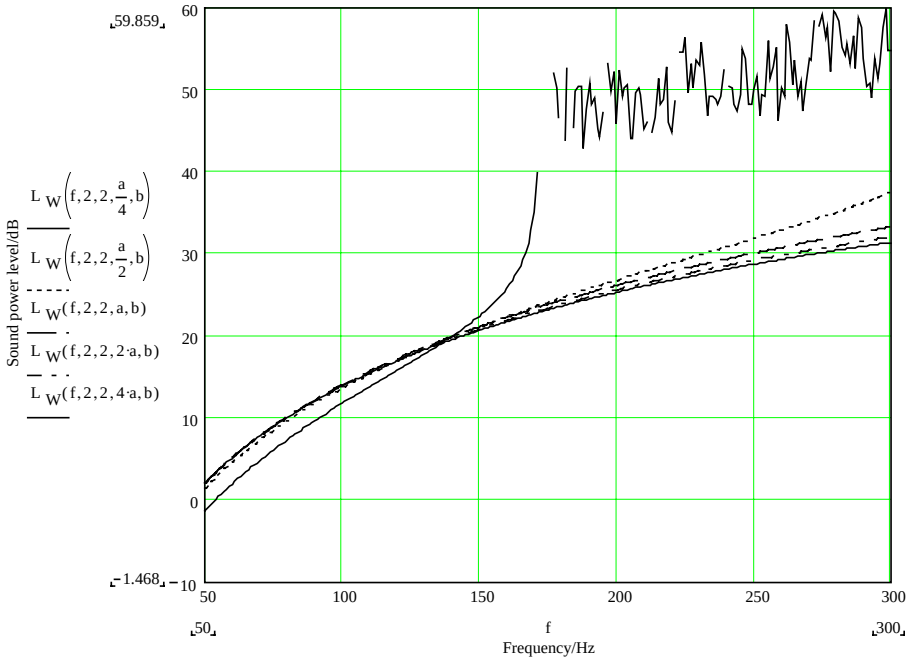


*Figure 58. The radiated sound power of mode (2,2) of a rigidly supported actuator cell having the cell length as a parameter.*

The simply supported actuator cells enable more effective sound power radiation at odd and even modes when the dimensions are larger than the original dimensions of the actuator cell (see Appendix A). The radiated sound power levels of the modes (1,1) and (2,2) of simply supported actuator cells are illustrated in Figures 59 - 62. The actuator cell width and length are the curve parameters. The even modes are very poor sound radiators. In that case, changes in the dimensions of the actuator cell have minor influence on the emitted total sound power. Doubling the element width or length increases, however, the emitted sound power of odd modes by 6 dB. Correspondingly, the fourfold increment of the width or length of the actuator cell increases the radiated sound power of odd modes by 12 dB.

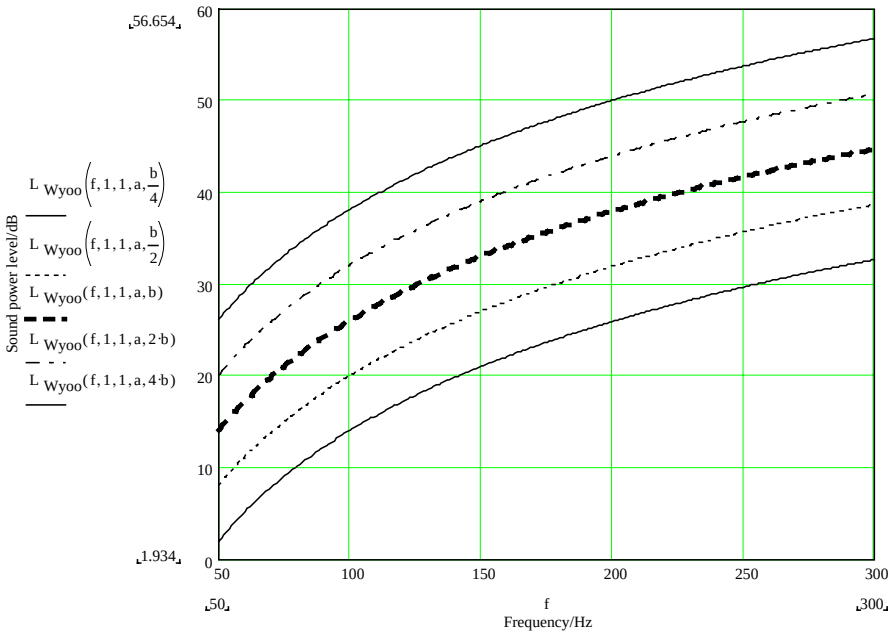


*Figure 59. The radiated sound power of mode (1,1) of a simply supported actuator cell having the cell width as a parameter.*

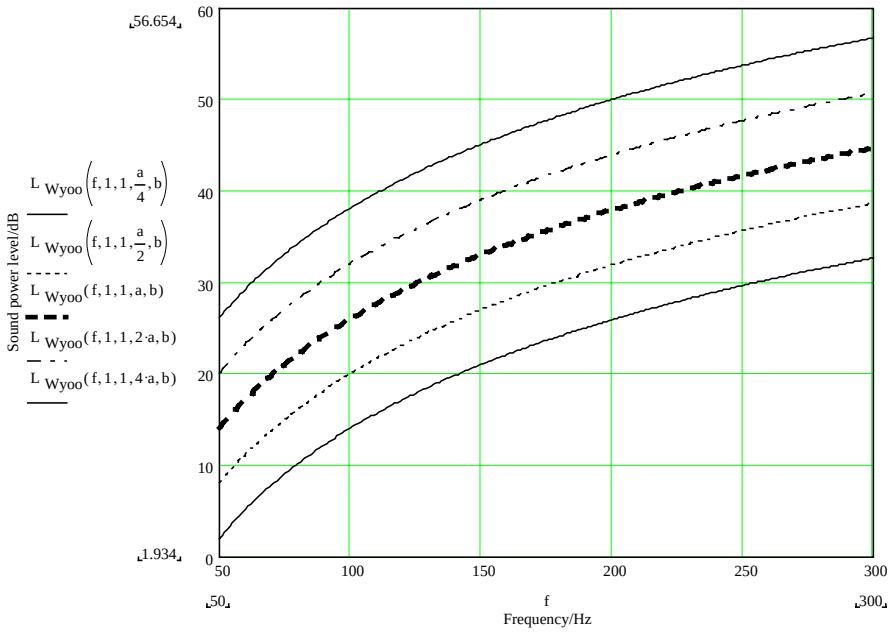


*Figure 60. The radiated sound power of mode (1,1) of a simply supported actuator cell having the cell length as a parameter.*

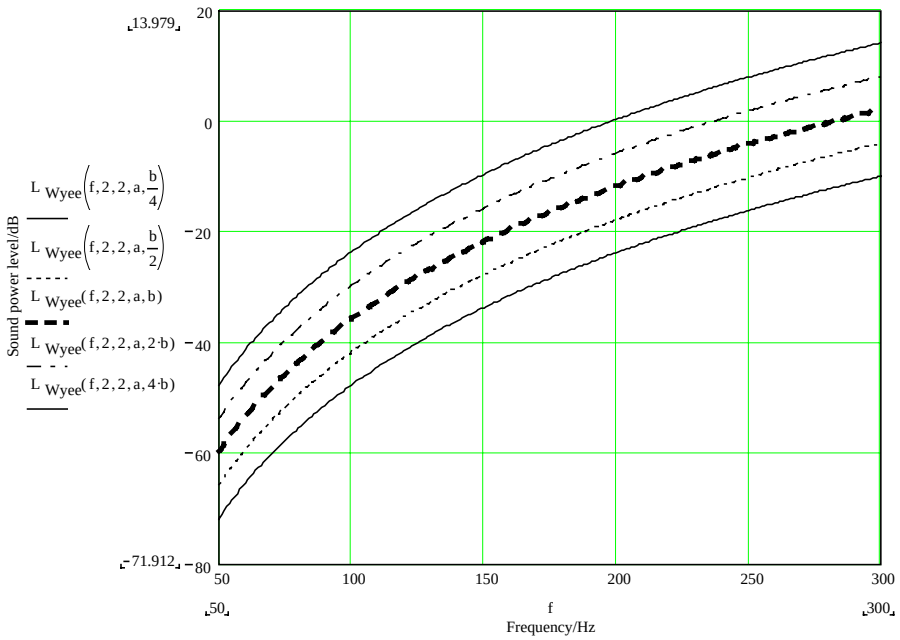


*Figure 61. The radiated sound power of mode (2,2) of a simply supported actuator cell having the cell width as a parameter.*

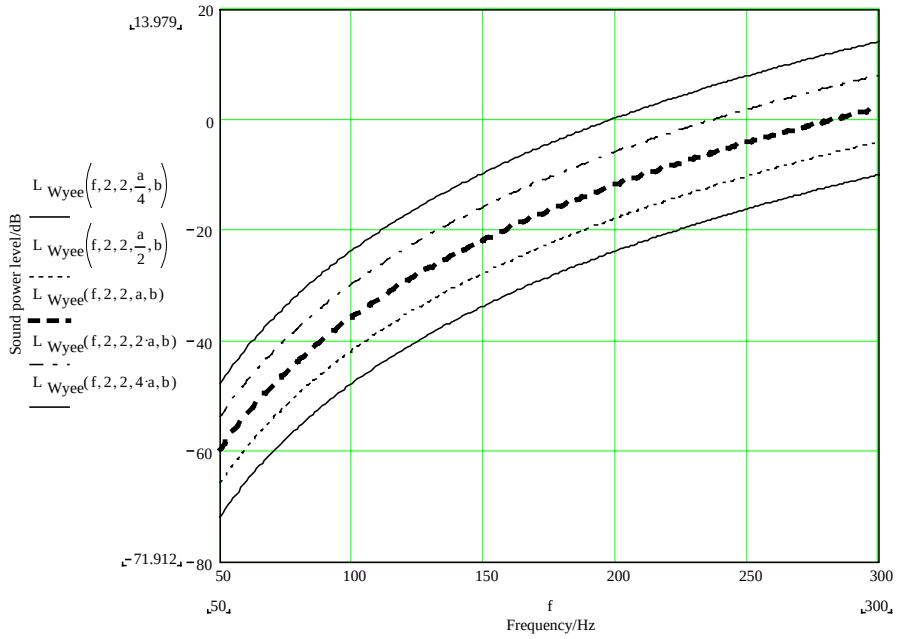


*Figure 62. The radiated sound power of mode (2,2) of a simply supported actuator cell having the cell length as a parameter.*

# 5. Sound power measurement of the actuator element

The measurement standard is applied to describe the installation, operation and environmental conditions under which the measured object must operate during the measurements. The measured value may be the average of measurements of several equipment, or a calculated value of measurements under several operating conditions of equipment, or both. The essential feature is that the measured value is the most probable sound emission value obtained when applying the given measurement standard [49]. If the manufacturer wishes the given sound emission value to have some predescribed certainty of acceptance in the possible verification, he must regard the measurements and measured values statistically. It is possible to calculate the confidence interval of the mean, using any desired probability, from the mean of the measured values and from the standard deviation of the reproducibility of the measurement method. The basic sound emission quantity used is the A-weighted sound power level.

One problem in using the basic sound power measurement standards (ISO 3740 series) for comparison and evaluation purposes of sound power production of equipment is the condition for the employment of the A-weighted standard deviation. This problem concerns also the evaluation of the declaration values of the machinery and equipment [50]. For example ISO 3743-2 states in chapter 1.3, Measurement uncertainty: “For a source which emits noise with a relatively ‘flat’ spectrum in the 100 to 10 000 Hz frequency range, the A-weighted sound power level is determined with a standard deviation of a mean value of approximately 2 dB” [51]. In present sound power measurement standards there is, however, no definition for the “relatively flat spectrum”. Thus it is impossible to know exactly in which situations one can consider equipment to emit sound “with a relatively flat spectrum” and in which situations the spectrum of the emitted sound has properties that cannot be considered to be in compliance with the standard. There are at least three reasons to avoid the use of such a concept as a “flat” spectrum:

- The uncertainties of the measurement standards in each one-third octave or octave bands in engineering methods prohibit the estimation of “flatness” of the sound spectrum of equipment because of the quite large standard

deviations. In practice, the manufacturer should use the ISO precision methods to evaluate the flatness of the spectrum before carrying out any uncertainty measurements.

- International standards already specify the character of sound allowable for the method (steady, broad band, narrow band, etc.) [52]. There should be no other determinations for the character of sound.

- The character of the sound spectrum of the equipment should not influence the manner of proceeding in general.

The A-weighted standard deviation of reproducibility for sound power measurements is currently given in standards ISO 3741 (0.5 dB), ISO 3743-1 (1.5 dB), ISO 3743-2 (2 dB), ISO 3744 (1.5 dB), ISO 3746 (3-5 dB) ), ISO 3747 (1.5 dB), ISO 9614-1 (4 dB) and ISO 9614-2 (1.5 or 4 dB) [52]. A method for determination of the A-weighted standard deviation of reproducibility for sound power measurements of equipment in a more unambiguous manner is presented in the following text.

## 5.1 Confidence interval

The confidence interval value $K$ is chosen to account for the random measurement errors occurring under reproducibility conditions. For the probability of acceptance of at least 95% in a possible subsequent verification another measurer, $K$ is equal to [53]

$$K = 1.645 \cdot \sigma_R \tag{34}$$

where $\sigma_R$ is the standard deviation of the reproducibility of the measurement method. The factor $K$ is also the confidence interval of a normal distribution having the probability of 95% in a one-sided test for checking the upper limit. When considering a batch of equipment, the differences in sound emission properties of different equipment have to be taken into account. In this case, instead of using the standard deviation of the reproducibility of the measurement method, the total standard deviation is used, which is the combination of the standard deviation of the reproducibility of the measurement method and the

standard deviation of production. The latter indicates the distribution of sound emission values of different equipment in a batch. The total standard deviation is

$$\sigma_T = \sqrt{\sigma^2{}_R + \sigma^2{}_P} \tag{35}$$

where $\sigma_R$ is the standard deviation of reproducibility and $\sigma_P$ is the standard deviation of production. $K$ is now equal to

$$K = 1.514 \cdot \sigma_T + 0.564 \cdot (\sigma_M - \sigma_T) \tag{36}$$

where $\sigma_M$ is the reference standard deviation and $K$ is the confidence interval of a normal distribution with a probability of 93.5% in a one-sided case [53].

## 5.2 Determination of the combined standard deviation

The A-weighted standard deviation values given in the measurement standards are based on the "flatness" of the spectrum emitted by the equipment. Because it is inconvenient to estimate whether or not the emitted sound is "flat", it is better to evaluate the A-weighted standard deviation of the reproducibility value from the single frequency band standard deviations given in the measurement standards and from the measured sound emission values.

The following examination is based on the assumption that the results of repeated measurements with the same equipment are normally distributed. For an arbitrary function $Y = f(X_1,X_2,...,X_N)$, the combined standard uncertainty of the estimate $y$ (where $y$ is the estimate of the measurand $Y$ and thus the result of the measurement) may be found from the accumulation law of probabilities. Because it is not possible to know exactly how the sound emission values of different frequency bands depend on each other, one must examine extreme cases in which all frequency band values are independent or totally dependent, and thus determine the upper limit for the confidence interval value $K$.

### 5.2.1 Uncorrelated vs. totally correlated data in frequency bands

The combined standard uncertainty $u_c(y)$, when all input quantities are independent of each other, is the positive square root of the combined variance $u_c^2(y)$ which is given by [54]

$$u_{c1}{}^2(y) = \sum_{i=1}^{N} \left( \frac{\partial f}{\partial x_i} \right)^2 \cdot u^2(x_i) \tag{37}$$

$$u(x_i) = \sqrt{\frac{1}{N-1} \cdot \sum_{i=1}^{N} \left( x_i - \bar{x} \right)^2} \tag{38}$$

where

$f$ is the given function,

$u(x_i)$ is a standard uncertainty determined in equation (38),

$x_i$ is the measured value, and

$\bar{x}$ is the arithmetic mean value of $N$ observations.

For a sum of A-weighted noise emission levels

$$f = 10 \cdot \lg \left( \sum_{i=1}^{N} 10^{\frac{x_i + a_i}{10}} \right) \tag{39}$$

where

$a_i$ is the A-weighting factor, and

$x_i$ is the sound emission value of the single frequency band.

The partial derivative of $f$ with respect to $x_1$ is

$$\frac{\partial f}{\partial x_i} = \frac{10^{\frac{x_1 + a_1}{10}}}{\sum_{i=1}^{N} 10^{\frac{x_i + a_i}{10}}} \tag{40}$$

Corresponding expressions can be found for the partial derivative of $f$ with respect to $x_2$, etc. When these partial derivatives of function $f$ are inserted into equation (37) the combined standard deviation is

$$u_{c1}(y) = \frac{\sqrt{\sum_{i=1}^{N} \left(u(x_i) \cdot 10^{(x_i + a_i)/10}\right)^2}}{\sum_{i=1}^{N} 10^{(x_i + a_i)/10}} \tag{41}$$

For the special case in which all the input estimates are completely correlated, the combined standard uncertainty $u_c(y)$ is the positive square root of the combined variance $u_c^2(y)$ which is given by [54]

$$u_{c2}{}^2(y) = \left[\sum_{i=1}^{N} \left(\frac{\partial f}{\partial x_i}\right) \cdot u(x_i)\right]^2 \tag{42}$$

Proceeding as before, the combined standard deviation based on the sum of the A-weighted sound emission levels is

$$u_{c2}(y) = \frac{\sum_{i=1}^{N} \left(10^{(x_i + a_i)/10} \cdot u(x_i)\right)}{\sum_{i=1}^{N} 10^{(x_i + a_i)/10}} \tag{43}$$

It is now possible to consider the characteristics of equations (41) and (43) in the following different situations:

1) The single standard deviations of reproducibility are $u(x_i) = 0$. The combined standard deviations are

$$u_{c1}(y) = u_{c2}(y) = 0 \tag{44}$$

as they should be.

2) The single standard deviations of reproducibility are similar while the sound emission levels for one-third octave or octave bands are not equal. The combined standard deviations are

$$u_{c1}(y) = u \cdot \frac{\sqrt{\sum_{i=1}^{N} \left(10^{(x_i + a_i)/10}\right)^2}}{\sum_{i=1}^{N} 10^{(x_i + a_i)/10}} \tag{45}$$

$$u_{c2}(y) = u \tag{46}$$

where $u = u(x_i)$ is constant ($\neq 0$).

3) The single standard deviations of reproducibility are similar, as well as the sound emission levels for one-third octave or octave bands. The combined standard deviations are

$$u_{c1}(y) = u \cdot \frac{\sqrt{\sum_{i=1}^{N} \left(10^{a_i/10}\right)^2}}{\sum_{i=1}^{N} 10^{a_i/10}} \tag{47}$$

$$u_{c2}(y) = u \tag{48}$$

where $u = u(x_i)$ is constant ($\neq 0$).

4) Sound emission levels for one-third octave or octave bands are similar, and the single standard deviations of the reproducibility are not equal. The combined standard deviations are

$$u_{c1}(y) = c \cdot \sqrt{\sum_{i=1}^{N} b_i \cdot u\left(x_i\right)^2} \tag{49}$$

$$u_{c2}\left(y\right) = c \cdot \sum_{i=1}^{N} \left(b_i \cdot u\left(x_i\right)\right) \tag{50}$$

where $c = \sum_{i=1}^{N} \left(10^{a_i/10}\right)^{-1}$ and $b_i = 10^{a_i/10}$ are constants.

Considering the different ISO standards for standard deviations of reproducibility of one-third octave bands, and supposing that the spectrum is flat, the combined standard deviations calculated from equations (49) and (50) are listed in Table 4. Also interlaboratory measurement results for a source which emits sound with a relatively "flat" spectrum in the 100 to 10 000 Hz frequency range are listed in the same table [52].

*Table 4. Standard deviations of reproducibility for a "flat" spectrum.*

| **ISO Standard** | **Combined standard deviation** | | **A-weighted standard deviation** | **Classification of method** |
|---|---|---|---|---|
| | $u_{c1}$ | $u_{c2}$ | | |
| 3741 | 0.46 | 1.76 | ≤ 0.5 | Precision |
| 3742 | 0.46 | 1.76 | ≤ 0.5 | Precision |
| 3743-1 | 0.75 | 1.68 | ≤ 1.5 | Engineering |
| 3743-2 | 0.98 | 2.20 | ≤ 2.0 | Engineering |
| 3744 | 0.44 | 1.73 | ≤ 1.5 | Engineering |
| 3745 | 0.29 | 1.14 | ≤ 1.0 | Precision/Semi-anechoic |
| 3745 | 0.16 | 0.64 | - | Precision/Anechoic |
| 3746 | - | - | ≤ 3 or ≤ 4 | Survey |
| 3747 | 0.80 | 1.78 | 1.5 | Engineering |
| 9614-1 | 0.32 | 1.23 | - | Precision |
| | 0.44 | 1.73 | - | Engineering |
| | - | - | 4 | Survey |
| 9614-2 | 0.44 | 1.68 | 1.5 | Engineering |
| | - | - | 4 | Survey |

In all cases $u_{c1}(y) \leq u_{c2}(y)$ (see Appendix K). The case where the input estimates are completely correlated seems to give an upper limit for the combined standard deviation. The calculated combined standard deviation values for the flat spectrum (50) are also quite congruent with the interlaboratory measurement results (A-weighted standard deviation) when the single deviation values are

large. When the single deviation values are small, the combined standard deviation value based on completely correlated input estimates seems to be more congruent with the interlaboratory measurement result. In reality, the sound emission levels of different frequency bands are not totally correlated or uncorrelated. The “true” dependence is evidently between the two.

### 5.2.2 Confidence interval values based on the combined standard deviation

The confidence interval value $K$ for single equipment based on uncorrelated or completely correlated input estimates is now equal to

$$K = 1.645 \cdot u_{c1}(y) \text{ or } K = 1.645 \cdot u_{c2}(y) \tag{51}$$

The confidence interval values for a batch of equipment can be calculated from equations (36) where

$$\sigma_T = \sqrt{{u_{c1}}^2(y) + {\sigma^2}_P} \text{ or } \sigma_T = \sqrt{{u_{c2}}^2(y) + {\sigma^2}_P} \tag{52}$$

## 5.3 Calculation examples

In order to compare the values estimated from the different combined standard deviations stated above, some calculation examples are studied. The examples are based on the spectrum of real measurements carried out according to the ISO standards.

The one-third octave band sound power levels $L_w$ of a fan (powered roof ventilator) are shown in Figure 63. Laboratory measurements were performed in compliance with ISO 3741. The sound power levels are based on measurements at 1466, 1454 and 1451 rpm speed of rotation.

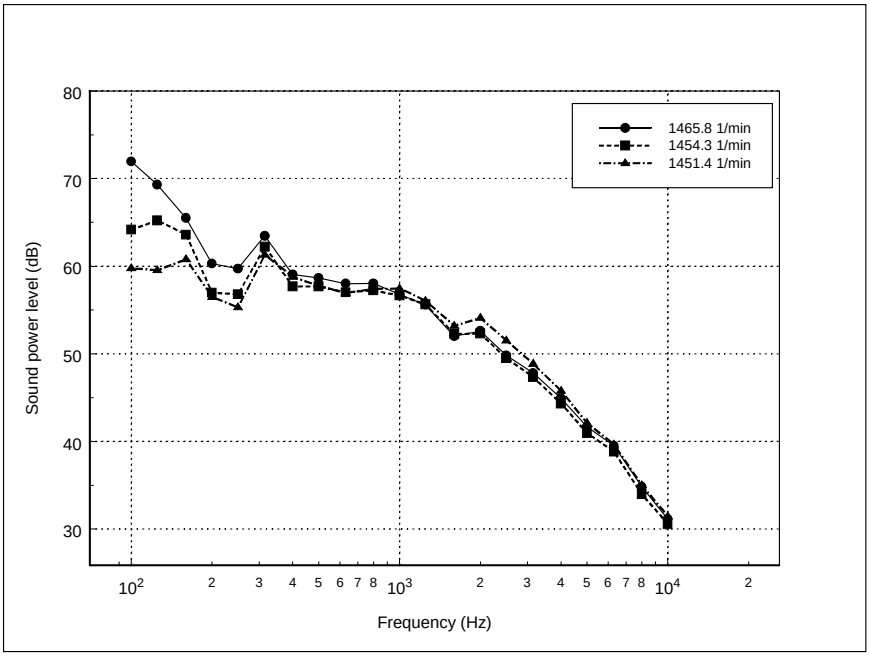


*Figure 63. One-third octave band sound power levels of a fan.*

The confidence interval values of a normal distribution $K$ are given in Table 5. The confidence intervals were calculated from equations (51), (41) and (43), and from a given A-weighted standard deviation value of reproducibility (ISO 3741) and equation (34).

*Table 5. Confidence interval values of the normal distribution.*

| | **Uncorrelated** Equation (41) $u_{c1}$/dB | **Correlated** Equation (43) $u_{c2}$/dB | **Based on "flat" spectrum** ISO 3741/dB |
|---|---|---|---|
| $K$ (1466 rpm) | 0.80 | 2.92 | 0.82 |
| $K$ (1454 rpm) | 0.79 | 2.74 | 0.82 |
| $K$ (1451 rpm) | 0.77 | 2.62 | 0.82 |

The confidence interval values of a normal distribution $K$ obtained from the combined standard deviations $u_{c1}$ (column 2 of Table 5) are quite near the measured "flat" spectrum values (column 4) obtained from the measurement standard, even when the examined spectra are not "flat" (see Figure 63).

The one-third octave band sound power levels of ventilation terminal equipment are shown in Figure 64. Laboratory measurements were performed in compliance with ISO 3741. The sound power levels are based on measurements at 1.7, 2.4 and 3.4 m/s flow velocities.

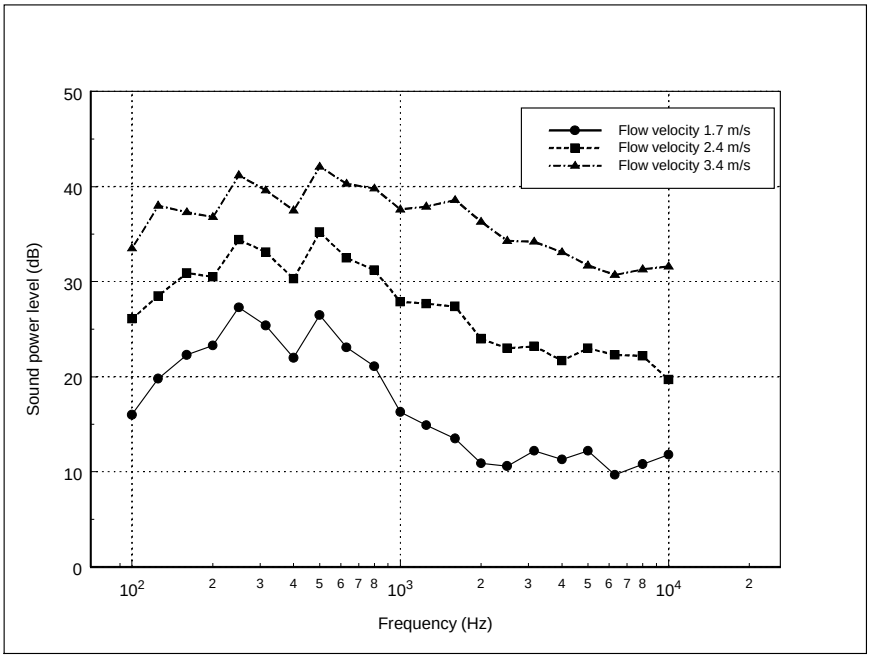


*Figure 64. One-third octave band sound power levels of ventilation terminal equipment.*

As above, the confidence interval values of the normal distribution $K$ are now given in Table 6.

*Table 6. Confidence interval values of the normal distribution.*

| | **Uncorrelated** Equation (41) $u_{c1}$/dB | **Correlated** Equation (43) $u_{c2}$/dB | **Based on "flat" spectrum** ISO 3741/dB |
|---|---|---|---|
| *K* (1.7 m/s) | 0.78 | 2.67 | 0.82 |
| *K* (2.4 m/s) | 0.88 | 2.72 | 0.82 |
| *K* (3.4 m/s) | 0.72 | 2.64 | 0.82 |

As in Table 5, the confidence interval values of a normal distribution *K* obtained from the combined standard deviations $u_{c1}$ (column 1) are again quite near the measured "flat" spectrum values (column 4), even when the examined spectra have small discrete frequency band components (see Figure 64). The equations of a combined standard deviation, based on the totally correlated input values, seem to give an upper limit for the confidence interval value *K*.

The one-third octave band sound power levels of two electric motors are shown in Figures 65 and 66. The power levels are based on intensity measurements. The engineering grade standard deviation values of reproducibility used in the calculations are from standard ISO 9614-1. The confidence interval values of a normal distribution *K* are given in Tables 7 and 8, respectively.

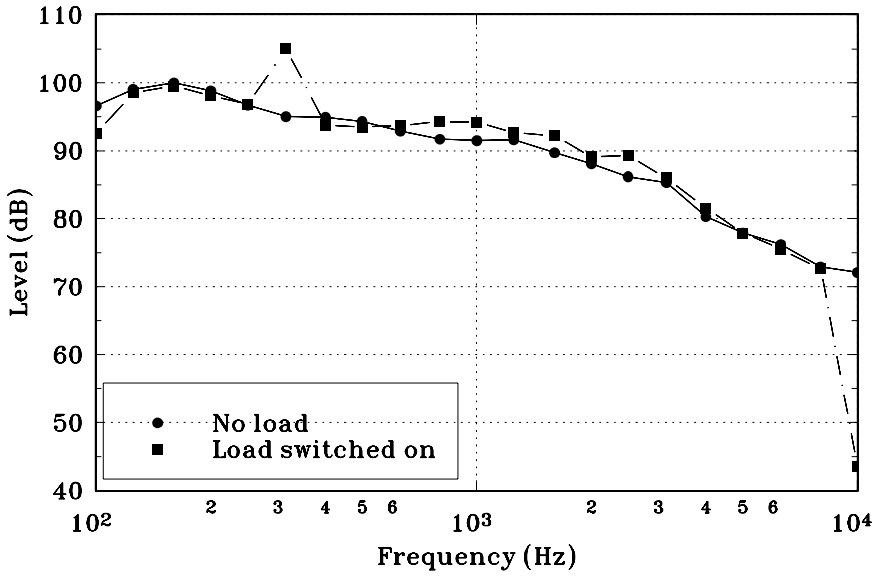


*Figure 65. One-third octave band power levels of an electric motor.*

*Table 7. Confidence interval values of the normal distribution.*

| | **Uncorrelated** Equation (41) $u_{c1}$/dB | **Correlated** Equation (43) $u_{c2}$/dB | **Based on "flat" spectrum** ISO 3744/dB |
|---|---|---|---|
| *K* (unload) | 0.79 | 2.93 | 3.29 |
| *K* (load) | 1.11 | 2.92 | 3.29 |

The low frequency content of the spectra in Figure 65 is different from that in Figures 63 and 64. The spectra are quite "flat". The "flat" spectrum values in Table 7 were calculated using an engineering grade A-weighted standard deviation taken from standard ISO 3744. The correlated values are quite congruent with values obtained with the A-weighted standard deviation value of reproducibility (ISO 3744) and equation (34).

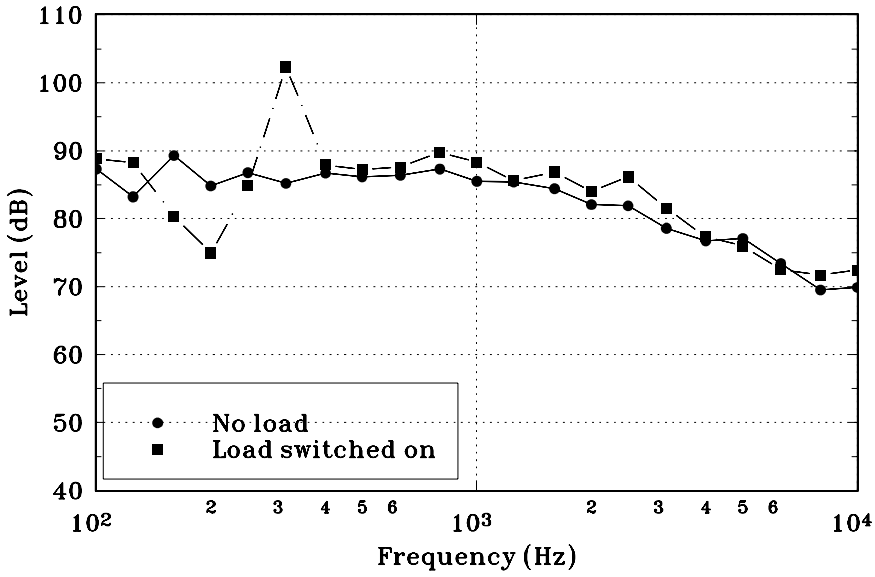


*Figure 66. One-third octave band power levels of an electric motor.*

*Table 8. Confidence interval values of the normal distribution.*

| | **Uncorrelated** Equation (41) $u_{c1}$/dB | **Correlated** Equation (43) $u_{c2}$/dB | **Based on "flat" spectrum** ISO 3744/dB |
|---|---|---|---|
| *K* (load) | 0.80 | 2.74 | 3.29 |
| *K* (unload) | 1.55 | 2.94 | 3.29 |

The low frequency content of the spectra in Figure 66 now has some discrete frequency band components. The "flat" spectrum values in Table 8 were calculated using an engineering grade A-weighted standard deviation value taken from standard ISO 3744 because, as earlier, the engineering grade value of the relevant standard (ISO 9614-1) was missing (the single frequency band deviation values are, however, almost similar to ISO 3744 and ISO 9614-1). The correlated values are again quite congruent with values obtained from the A-weighted standard deviation value of reproducibility (ISO 3744) and equation (34).

# 6. Conclusions

The general vibro-acoustical functioning of the EMFi-actuator is possible to state in the impedance oriented form by evaluating the loading impedances of the vibrating actuator film from its boundary conditions. The linear second-order ordinary differential equation with constant coefficients predicts the vibration functioning of the actuator film quite satisfactorily in the frequency domain. At low frequencies the initial tension of the film is the main factor, which affects the vibration levels. At middle and high frequencies those factors are the resistance and mass of the film, respectively. The influence of the spring force dominates the electric forces when no excitation signal exists. When the excitation voltage exists, the electric force dominates the spring force until the deflection of the film reaches a certain limiting value. The operation range of the actuator depends on the excitation voltage.

The elastic properties of the film material change when the deflection of the vibrating actuator film increases. The spring force is after some limit no more a linear function of deflection. Because of non-linear electric forces acting on the actuator film, the motion of the membrane is neither linear.

The electric forces cause vibration of, not only the actuator film, but also the stator structure of the EMFi-actuator. This recoil effect may be large enough to endanger the supporting structure of the actuator element vibrating, which may generate sound. It is possible to make the deflections of the supporting structure smaller by increasing the thickness or the dynamic stiffness of the background material of the actuator element and by increasing the damping ratios of the natural modes. It is possible to increase the response of the actuator film by decreasing the spring constant caused by the initial tension of the film. This, however, increases the deflection of the supporting structure. The response of the supporting structure may decrease about a decade without influencing the response of the actuator film. In general, the responses of the actuator system (actuator film, supporting structure and stator) are dependent on each other. The changes in the geometrical and material parameters influence straight the natural frequencies of the system. Parameters are connected to each other, and they influence the responses of the different system elements in complex ways. Basically, the situation is an optimization problem of a multi parameter case.

The use of the arithmetic average value of the vibration deflection of an EMFi-actuator in the prediction of sound power or pressure in the acoustic far field at low frequencies is satisfactorily comparable to the frequency or spatially dependent vibration of the actuator film in frequency domain most of the time. The value of the arithmetic average of vibration is valid even when the external impedance of the film is not taken into consideration.

At low frequencies, the radiated sound power of monopole and dipole type actuators diminish intensively because of small deflection of the actuator film. The decrement of the radiated power is more significant to the dipole source. At high frequencies, the dipole source produces more sound pressure into the far field than the monopole source. The change in the limiting frequency, when the dipole source is the more effective radiator, is related to the area of the actuator so that when the area increases, the limiting frequency decreases. This is natural because in the case of a dipole source, the effect of acoustical short circuit decreases also when the area increases. Large dipole actuators emit thus more sound power as well as deliver more pressure to the acoustic far field than the monopole sources. When the dipole actuator is installed on or very close to a plane boundary, its acoustical properties change. When the thickness of the absorbent material under the actuator located on a rigid structure is 5 cm, the radiated sound power decreases strongly. When the absorbent layer is thicker than that, the power level increases slowly. The main reason for the decrement of the radiated sound power when the thickness of the absorbent layer decreases is the destructive interference of the oppositely phased waves.

Comparison between the modelling and measured results is carried out by discarding the frequency or spatial dependence of the velocity distribution of the actuator film in the modelling. Also the impedance loading of the actuator was ignored in the examination. The calculated sound pressure levels of a monopole source up to 240 Hz in a free acoustic field are almost equal to measured values. The shape of the sound pressure level curve of the dipole source is similar to the measured values up to 600 Hz so that there is a constant 8 dB amplitude difference. The monopole source type of modelling describes the sound pressure output of the EMFi-actuator at low frequencies. Dipole analysis describes the behaviour of the actuator in a larger frequency range when the amplitude difference based on the normalization of the measurement results is taken into consideration. In a half-free acoustic field, the monopole source predicts the

delivered sound pressure levels very accurately up to 600 Hz. The shape of the sound pressure level curve of the dipole source is similar to the measured values up to 240 Hz. The amplitude difference between the measured and modelled curves of the dipole actuators is 12 dB.

An EMFi-actuator basically consists of several membrane strips which are located next to each other on the same plane. The different strips of the actuator element operate in principle as single line sources composed of several unit piston sources located side by side. The major lobe in the radiation pattern of the actuator narrows when the frequency increases. The amplitudes of the other lobes are minor compared to the major one. The major lobe corresponds to that portion of the radiation pattern to which the source elements are essentially in phase. The directivity measurements of the actuator element have been carried out in a half-free acoustic field. When the panel is located near the wall surface, radiation up to 400 Hz is very uniform in all directions. The sound pressure level curves of the measured and predicted results are very similar in every angle. The radiation patterns are relatively round and similar to the radiation patterns of the monopole source. The measured and predicted values of radiation patterns are very similar in every angle. The radiation patterns produced by a piston-type actuator differ from the idealized pattern to some extent. One reason for this discrepancy is that the area of the baffle in which the actuator is mounted is necessarily finite. At high frequencies, even a baffle of small linear dimensions corresponds to an ideal infinite baffle quite closely, but at low frequencies, each element of the piston does not radiate with hemispherical divergence. In addition, radiation from the back of the actuator may propagate into the region in front of the actuator so that the resulting radiation pattern approximates that of a dipole source rather than that of a piston in an infinite baffle. Another reason for discrepancy is that the material of an EMFi-actuator membrane is not perfectly rigid. Driving the actuator at its centre establishes a higher velocity amplitude in the inner parts of the film than near its rim, and at high frequencies, the film may even vibrate in normal modes. Under these circumstances, average vibration velocity amplitude of the actuator film may result in a complex function of the radial distance and angle and, hence, must be considered as a variable in the integration.

The basic problems concerning an EMFi-actuator are related to its ineffective low frequency sound production and the distortion caused by the non-linear

operation. It is possible to increase the sound power radiation properties of the monopole or dipole type sources by making the deflection of the membrane larger (using smaller tension), by using a membrane the area of which is larger, or by using two interacting actuators. The radiated sound power levels increase 6 dB when the magnitude of the deflection is doubled, and 20 dB when the magnitude of the deflection is tenfold compared to the original one. The increment does not depend on the frequency and is equal for monopole and dipole type sources. The delivered sound pressure levels of the monopole source increase 6 dB when the area of the element is doubled. The increment of the dipole source is 9 dB, correspondingly. The increment does not depend on the frequency and is not equal for source types. When the increment of the area is tenfold compared to the original area, the increment of the delivered sound pressure levels is 20 dB for a monopole source and 30 dB for a dipole source. At low frequencies or when the two sources are located close to each other, the increment of the sound power level is 6 dB compared to that of a single source. The reason for the increment is that each source has to work against its own sound pressure as well as against the sound pressure that is generated by the source near it. For the two equal sources, the work performed by each against its own pressure is equal to the work performed against the pressure at its surface that is generated by the second source. At high frequencies, the increment is 3 dB, respectively. In the latter case, the increment in the total level equals that of two single sources without any interaction. The interaction effect of the dipole sources disappears at lower frequencies than that of the monopole sources. At low frequencies, the increment in the sound power levels of two interacting sources equals in magnitude the doubled deflection increment of the single actuator membrane. The sound power of two interacting sources is four times as large as that of a single source at low frequencies or when the sources are located close to each other.

The EMFi film is glued to the stator element so that the actuator is composed of several single cell elements. The connection type of those elements to the stator boundaries is neither purely rigidly nor simply supported. In the case of odd modes, both ways to support the edges of the actuator cell produce almost equal sound power levels so that the vibration modes (1,1) are clearly the most efficient single radiators. Velocity distributions of the odd modes of differently supported film strips are practically equal, and thus, also the radiated sounds of the elements are equal. In the even mode case, the rigidly supported boundary

enables the element to radiate sound power with all the different even modes much more effectively than it is possible under a simply supported boundary condition. Odd modes are more effective sound radiators than even modes. With even modes, the number of vibrating partial surfaces of the element cell which are in the opposite vibration phase is equal, and thus the net radiated sound power decreases. Contrary to odd modes, partial surfaces which are out of opposite vibration phases always exist, and thus also sound radiation. The dimensions of the actuator cell affect the power the single vibration mode radiates to the acoustic far field. The present actuator dimensions seem to be acceptable when the film cell is rigidly supported. When the cells of the actuator panels are simply supported, larger dimensions than those of the present actuator type emit more sound power at odd and even modes. The even modes are very poor sound radiators so that changes in the dimensions of the actuator cells have minor influence on the emitted total sound power. Doubling the element width or length increases the emitted sound power of odd modes 6 dB, however. Correspondingly, the fourfold increment of the width or length of the actuator cell increases the radiated sound power 12 dB.

The confidence interval values of the normal distribution of equipment based on combined standard deviation and presented in this study are almost equal to the values based on the A-weighted standard deviation of reproducibility of the common ISO method. When the standard deviations of the single frequency bands are low, the combined standard deviation $u_{c1}(y)$ is practically identical to the A-weighted standard deviation value and, correspondingly, so is $u_{c2}(y)$ when the deviations are high. For these reasons, the combined standard deviations $u_{c1}(y)$ and $u_{c2}(y)$ seem to give as exact expressions for the calculation of the confidence interval as the A-weighted standard deviation of reproducibility when information on the frequency bands is available. It has been shown, however, that the solution for determining sound emission requires neither the definition of a “flat” spectrum nor the definition of any other spectrum shape. A case where input estimates are completely correlated gives an upper limit for the combined standard deviation value. The true sound emission value when the spectrum of the sound source is not “flat” lies probably between the ones found by using combined standard deviation values $u_{c1}(y)$ and $u_{c2}(y)$.

The main results of this work are the means to increase the radiated sound power of the actuator element without increasing concurrently the distortion of the

radiator. These resources are based on the functioning mode of the actuator (monopole, dipole), boundary conditions of the actuator element or cells of the actuator element, the larger actuator areas, interaction of actuators, and the dimensions of the actuator element cells. Another result of this study is the potentiality to evaluate the A-weighted standard deviation of the equipment on the ground of the measurement results without specifying the type of emitted sound radiated by the equipment.

# References


1. EMFi: Sound of Science. Tampere, VTT Automation and VTT Chemical Technology, VTT EMFiNFO, EMFi folder. (16.12.1999). http://www.EMFi.net

2. Latour, A. Sheet speakers may be on the wall. Finns try to wrap up new technology. The Wall Street Journal Europe, Friday - Saturday, Nov. 13 - 14, 1998.

3. Lueg, P. Process of silencing sound oscillations. U.S. Patent No. 2043416. June 9, 1936. 3 p.

4. Warnaka, G. E. Active attenuation of noise – the state of the art. Noise Control Eng. J. 1982. Vol. 18, no. 3, pp. 100 - 110.

5. Olson, H. F. and May, E. G. Electronic sound absorber. J. Acoust. Soc. Am. 1953. Vol. 25, no. 6, pp. 1130 - 1136.

6. Olson, H. F. Electronic control of noise, vibration and reverbation. J. Acoust. Soc. Am. 1956. Vol. 28, no. 5, pp. 966 - 972.

7. Nelson, P. A. and Elliott, S. J. Active control of sound. London, UK: Academic Press, 1993. 436 p. ISBN 0-12-515426-7.

8. Whetton, C. Electro-Mechanical Film. Noise & Vibration Worldwide, December 1997, pp. 13 - 16.

9. Antila, M. and Lekkala J. An exciting new sensor and actuator material. High Technology Finland 1999, pp. 120 - 121.

10. Saarinen, A. Room acoustical review – planning, evaluation and measuring. Helsinki: University of Helsinki, Department of Physics 1992. 104 p. In Finnish.

11. Uosukainen, S. JMC method applied to active control of sound. Theoretical extensions and new source configurations. Espoo, Finland: VTT, 1999. 69 p. + app. 145 p. VTT Publications 386. ISBN 951-38-5377-2

12. La Fontaine, R. F. and Shepherd, I. C. An experimental study of a broadband active attenuator for cancellation of random noise in ducts. J. Sound. Vib. 1983. Vol. 91, no. 3, pp. 351 - 362.

13. Chen, L. H. and Schweikert, D. G. Sound radiation from an arbitrary body. J. Acoust. Soc. Amer. 1963. Vol. 35, no. 10, pp. 1626 - 1632.

14. Chertock, G. Sound radiation from vibrating surfaces. J. Acoust. Soc. Amer. 1964. Vol. 36, no. 7, pp. 1305 - 1313.

15. Copley, L. Integral equation method for radiation from vibrating bodies. J. Acoust. Soc. Amer. 1967. Vol. 41, no. 4, pp. 807 - 816.

16. Copley, L. Fundamental results concerning integral representation in acoustic radiation. J. Acoust. Soc. Amer. 1968. Vol. 44, no. 1, pp. 28 - 32.

17. Schenck, H. Improved integral formulation for acoustic radiation problems. J. Acoust. Soc. Amer. 1968. Vol. 44, no. 1, pp. 41 - 58.

18. Seybert, A. F., Soenarko, B., Rizzo, F. J. and Shippy, D. J. An advanced computational method for radiation and scattering of acoustic waves in three dimensions. J. Acoust. Soc. Amer. 1985. Vol. 77, no. 2, pp. 362 - 368.

19. Fahnline, J. B. and Koopmann, G. H. A numerical solution for the general radiation problem based on the combined methods of superposition and singular-value decomposition. J. Acoust. Soc. Amer. 1991. Vol. 90, no. 5, pp. 2808 - 2819.

20. Gardner, B. K. and Bolton, J. S. Radiation efficiency calculations for verification of boundary element acoustic codes. Noise Control Eng. J. 1996. Vol. 44, no. 5, pp. 215 - 223.

21. Fahnline, J. B. and Koopmann, G. H. A lumped parameter model for the acoustic power output from a vibrating structure. J. Acoust. Soc. Amer. 1996. Vol. 100, no. 6, pp. 3539 - 3547.

22. Hwang, W. S. Boundary spectral method for acoustic radiation and scattering problems. J. Acoust. Soc. Amer. 1997. Vol. 102, no. 1, pp. 96 - 101.

23. Fahnline, J. B. and Koopmann, G. H. Numerical implementation of the lumped parameter model for the acoustic power output of a vibrating structure. J. Acoust. Soc. Amer. 1997. Vol. 102, no. 1, pp. 179 - 192.

24. Di Francescantonio, P. A new boundary integral formulation for the prediction of sound radiation. J. Sound. Vib. 1997. Vol. 202, no. 4, pp. 491 - 509.

25. Wang, W., Atalla, N. and Nicolas, J. A boundary integral approach for acoustic radiation of axisymmetric bodies with arbitrary boundary conditions for all wave numbers. J. Acoust. Soc. Amer. 1997. Vol. 101, no. 3, pp. 1468 - 1478.

26. Wu, S. F. and Hu, Q. An alternative formulation for predicting sound radiation from a vibrating object. J. Acoust. Soc. Amer. 1998. Vol. 103, no. 4, pp. 1763 - 1774.

27. Beranek, L. L. and Vér, I. L. Noise and vibration control engineering. Principles and applications. New York – Chichester – Brisbane – Toronto – Singapore: John Wiley & Sons, 1992. 804 p.

28. Allard, J. F. Propagation of sound in porous media – modelling sound absorption materials. London and New York: Elsevier Applied Science, 1993. 282 p.

29. Delany, M. E. and Bazley, E. N. Acoustical properties of fibrous materials. Applied Acoustics 1970, 3, pp. 105 - 116.

30. Uosukainen, S. Electrical forces affecting on EMF-actuators. Subtask Contribution to Report FACTS IR 2.1. Espoo, Finland 1997. 4 p.

31. Antila, M., Linjama, J. and Muurinen T. Measurements of electro-mechanical film (EMFi) actuators. Subtask Contribution to Report FACTS IR 2.1. Tampere, Finland 1997. 20 p.

32. Antila, M., Muurinen T., Linjama, J. and Nykänen H. Measurement methods of flat panel electromechanical film loudspeakers. Active 97 Budapest, Hungary, 1997, pp. 607 - 618.

33. Pennala, E. Vibration of machines and structures. Espoo, Finland 1997, Helsinki University of Technology. 254 p. In Finnish.

34. Timoshenko, S., Yong, D. H and Weaver, W. Jr. Vibration problems in engineering, fourth edition. New York - Chichester - Brisbane - Toronto - Singapore: John Wiley & Sons, 1974. 521 p.

35. Saarinen A. The optimization parameters of EMFi-actuator. Contribution to FACTS project. Espoo, Finland 1998. 10 p. In Finnish.

36. Temkin S. Elements of acoustics. New York - Chichester - Brisbane - Toronto - Singapore: John Wiley & Sons, 1981. 515 p.

37. Morse, P. M. and Ingard, K. U. Theoretical Acoustics. New York - St. Louis - San Francisco – Toronto - London - Sydney: McGraw-Hill, 1968. 927 p.

38. Skudrzyk, E. The foundations of acoustics. Wien - New York: Springler Verlag, 1971. 790 p.

39. Uosukainen, S. Lectures on acoustic field theory. Espoo, Finland: Helsinki University of Technology, Laboratory of Acoustics and Audio Signal Processing, 1989. 474 p. In Finnish.

40. Malecki, I. Physical foundations of technical acoustics. Oxford - London - Edinburgh - New York - Toronto - Sidney - Paris - Braunschweig: Pergamon Press, 1969. 743 p.

41. Junger, M. C. and Feit, D. Sound, structures, and their interaction. Cambridge - Massachusetts - London - England: The MIT Press 1986. 448 p.

42. Pierce, A. D. Acoustics. An introduction to its physical principles and applications. New York: McGraw-Hill, 1991. 678 p.

43. Fahy, F. Sound and structural vibration. Radiation, transmission and response. London - Orlando - San Diego - New York - Toronto - Montreal - Sidney - Tokyo: Academic Press, 1985. 309 p.

44. Wallace, C. E. Radiation resistance of a baffled beam. J. Acoust. Soc. Amer. 1972. Vol. 51, no. 3(II), pp. 936 - 945.

45. Wallace, C., E. Radiation resistance of a rectangular panel. J. Acoust. Soc. Amer. 1972. Vol. 51, no. 3(II), pp. 946 - 952.

46. Comperts, M. C. Sound radiation from baffled, thin, rectangular plates. Acustica 1977. Vol. 37, pp. 93 - 102.

47. Comperts, M. C. Radiation from rigid baffled, rectangular plates with general boundary conditions. Acustica 1974. Vol. 30, pp. 320 - 327.

48. Cunefare, K. A. The minimum multimodal radiation efficiency of a baffled rigid beams. J. Acoust. Soc. Amer. 1991. Vol. 90, no. 5, pp. 2521 - 2529.

49. Nykänen, H. Relationship between measured, declared and guaranteed noise emission values of machinery and equipment. Held at euro-noise '92 conference. Imperial College London, 14 - 18 September 1992. (Not in the Proceedings.)

50. Saarinen, A. Declared noise emission values of machinery and equipment based on determination of the combined standard deviation. Applied Acoustics 1999. Vol. 57, pp. 1 - 15.

51. ISO 3743-2:1994 Acoustics – Determination of sound power levels of noise sources using sound pressure – Engineering methods for small, movable sources in reverberant fields – Part 2: Methods for special reverberation test rooms. 19 p.

52. ISO/CD 3740:1996 Acoustics – Determination of sound power levels of noise sources using sound pressure – Guidelines for the use of basic standards (Revision of ISO 3740:1980). 25 p.

53. ISO 7574-4:1985 Acoustics – Statistical methods for determining and verifying stated noise emission values of machinery and equipment – Part 4: Methods for stated values for batches of machines. 20 p.

54. Guide to the expression of uncertainty in measurement. International Organization for Standardization, 1993.

# Appendix A: Calculation constants

## Material constants

The density of the actuator film material $m''_m = 550$ kg/m$^3$

Young´s constant $E_x = 4.6 \cdot 10^9$ N/m$^2$

Poisson constant $\nu = 0.4$

Surface density of the actuator element $m'_e = 4.0$ kg/m$^2$

Surface density of the actuator film $m'_m = 0.042$ kg/m$^2$

Dissipation constant of the actuator film $\varepsilon = 1 \cdot 10^{-2}$

Surface density of the stator $m'_s = 3.96$ kg/m$^2$

Dynamic stiffness of typical rock wool material (density 60 kg/m$^3$) $k_v = 0.3 \cdot 10^7$ N/m$^3$

Density of stator material $m''_s = 700$ kg/m$^3$

## Mechanical constants

Thickness of the film $h = 30 \cdot 10^{-6}$ m

Thickness of the stator $h_s = 6 \cdot 10^{-3}$ m

Length of the actuator element $D = 420 \cdot 10^{-3}$ m or $500 \cdot 10^{-3}$ m

Width of the actuator element $L = 320 \cdot 10^{-3}$ m or $600 \cdot 10^{-3}$ m

Area of the actuator element $A = 0.134$ m$^2$

Average deflection of the actuator film $\xi_0 = 0.33 \cdot 10^{-6}$ m

Width of the film strip $d_m = 30 \cdot 10^{-3}$ m

Number of film strips on the element $N = 14$

Radius of the air channel for the typical wool material $a_1 = 0.9 \cdot 10^{-3}$ m

## Acoustical constants

Density of the air $\rho_0 = 1.2$ kg/m$^3$

Velocity of sound in normal conditions $c_0 = 343$ m/s

Characteristic impedance of the air $Z_0 = 412$ kg/m$^2$s

Viscosity of the air in normal conditions $\eta = 1.8 \cdot 10^{-3}$ kg/ms

Initial tension of the actuator film $\sigma = 25 \cdot 10^6$ N/m$^2$

Flow resistance of the stator material $\Xi = 1.8 \cdot 10^4$ kg/ms

The spring constant influenced by the initial tension of the film $k'_m = 3.3 \cdot 10^6$ N/m$^3$

## Electrical constants

Permittivity of the vacuum $\varepsilon_0 = 8.854 \cdot 10^{-12}$ N$^{-1}$m$^2$C$^2$

Dielectric constant of the film material $\varepsilon_r = 1.6$

Surface charge density of the film $q = 1.6 \cdot 10^{-4}$ Cm$^2$

# Appendix B: Spring force of the film strip

The geometry of the film strip and its deflection along the symmetric line is illustrated in Figure B1. $T$ is the force caused by the initial tension $\sigma$ of the film, $T_N$ and $T_T$ are the corresponding forces in z- and x-directions, respectively, $\xi$ is the deflection of the film, $l$ is the width of the film cell, $k$ is the spring constant, and $F_k$ is the spring force.

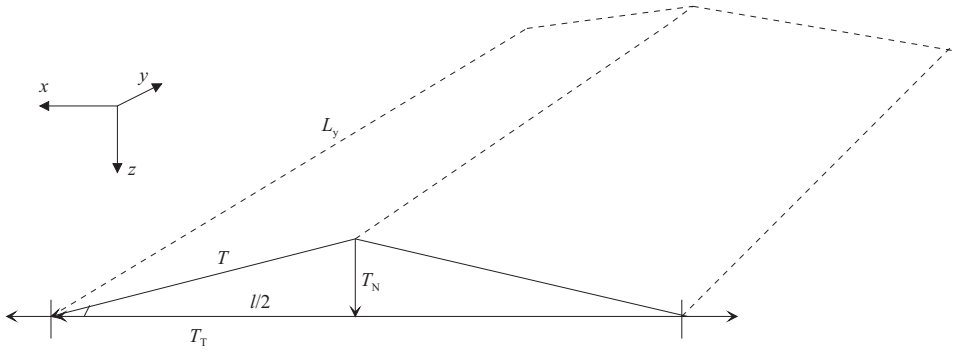


*Figure B1. Deflection of the film from its state of equilibrium.*

According to Figure B1 the normal force caused by initial tension and the spring constant are, respectively

$$T_N = T_T \cdot \tan\Theta = T_T \cdot \frac{\xi}{l/2} \tag{B1}$$

$$T_N = F_k = k\xi \;\Rightarrow\; k = \frac{2T_T}{l} \tag{B2}$$

The initial tension is evaluated per edge area of the film according to Figure B2 where $h$ is the thickness and $L_y$ the length of the film. The spring coefficient is, finally,

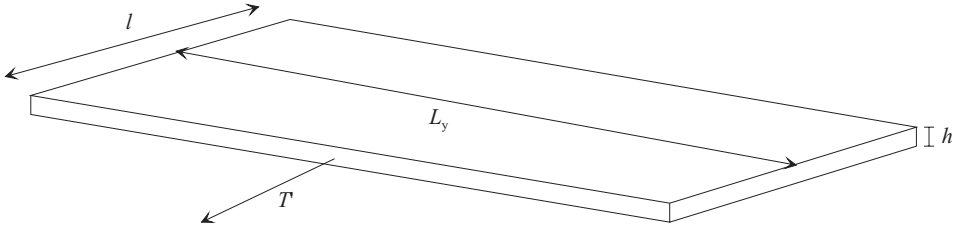


*Figure B2. Measured spring force.*

$$T_T = \sigma h L_y \;\Rightarrow\; k = \frac{2\sigma h L_y}{l} \tag{B3}$$

# Appendix C: Deflection and velocity of the actuator membrane in time domain

$$\text{deflection}(\text{steps}) := \left|\begin{array}{l}
f_s \leftarrow 0\cdot\text{newton} \\
f_d \leftarrow 0\cdot\text{newton} \\
x \leftarrow 0\cdot m \\
xt \leftarrow 0\cdot m\cdot\text{sec}^{-1} \\
xtt \leftarrow 0\cdot m\cdot\text{sec}^{-2} \\
dx \leftarrow 0\cdot m \\
\text{for } i \in 1..\text{steps} \\
\quad \left|\begin{array}{l}
t \leftarrow (i-1)\cdot\text{deg} \\
k \leftarrow k_0 \\
f_s \leftarrow f_s + k\cdot dx \\
f_d \leftarrow c\cdot xt \\
xtt \leftarrow \dfrac{\text{Re}\left(F\left(x, V_{sig}, f, t\right)\right)\cdot S - f_d - f_s}{m_f} \\
k_1 \leftarrow k + \dfrac{6\cdot m_f}{\text{deg}^2} + \dfrac{3\cdot c}{\text{deg}} \\
d_f \leftarrow \left|\begin{array}{ll}
\text{Re}\left(F\left(x, V_{sig}, f, i\cdot\text{deg}\right)\right)\cdot S & \text{if } i=1 \\
\text{Re}\left(F\left(x, V_{sig}, f, i\cdot\text{deg}\right)\right)\cdot S - \text{Re}\left[F\left[x, V_{sig}, f, (i-1)\cdot\text{deg}\right]\right]\cdot S & \text{otherwise}
\end{array}\right. \\
df1 \leftarrow d_f + m_f\cdot\left(6\cdot\dfrac{xt}{\text{deg}} + 3\cdot xtt\right) + c\cdot\left(3\cdot xt + \text{deg}\cdot\dfrac{xtt}{2}\right) \\
dx \leftarrow \dfrac{df1}{k_1} \\
dxt \leftarrow 3\cdot\dfrac{dx}{\text{deg}} - 3\cdot xt - \text{deg}\cdot\dfrac{xtt}{2} \\
x \leftarrow x + dx \\
xt \leftarrow xt + dxt
\end{array}\right. \\
xt
\end{array}\right.$$

Accuracy of the solution in the time domain is dependent on the length of the time step. The calculation is convergent if the length of the time step is shorter than one tenth of the vibration time period of the system.

# Appendix D: Sound power of the monopole source

The velocity potential of the encapsulated disk is [1]

$$\Phi_m = \frac{Q_0}{4\pi r} e^{j(\omega t - kr)} \tag{D1}$$

where the source strength

$$Q_0 = \pi\, a^2\, U_o \tag{D2}$$

and

$r$ is the distance between the source and observation points,

$\omega$ is the angular frequency,

$t$ is time,

$k$ is the wave number,

$a$ is the radius of the disk, and

$U_0$ is the average vibration velocity amplitude of the disk

Sound pressure (harmonic dependence of time is assumed)

$$p_m = \rho_0 \frac{\partial \Phi_m}{\partial t} = j\omega\rho_0 \frac{Q_0}{4\pi r} e^{j(\omega t - kr)} \tag{D3}$$

Radial component of the particle velocity for irrotational motion

$$u_{rm} = -\frac{\partial \Phi_m}{\partial r} = -Q_0 \frac{e^{j\omega t}}{4\pi}\left(\frac{-jke^{-jkr}r - e^{-jkr}}{r^2}\right) = \frac{Q_0}{4\pi r^2}\left(1 + jkr\right)e^{j(\omega t - kr)} \tag{D4}$$

Normal component of intensity

$$I_{rm} = \mathrm{Re}\left\{ p_m u_{rm}^* \right\} = \mathrm{Re}\left\{ j\omega\rho_0 \frac{Q_0}{4\pi r} e^{j(\omega t - kr)} \frac{Q_0}{4\pi r^2}(1 - jkr) e^{-j(\omega t - kr)} \right\}$$
$$= \mathrm{Re}\left\{ j\omega\rho_0 \left(\frac{Q_0}{4\pi}\right)^2 \frac{1}{r^3}(1 - jkr) \right\} = k\omega\rho_0 \left(\frac{Q_0}{4\pi r}\right)^2 \qquad \text{(D5)}$$

Sound power (integration of normal component of intensity over a sphere of radius *r*)

$$\Pi_m = \int_0^\pi 2\pi r^2 \sin\theta I_{rm} d\theta = 2\pi r^2 k\omega\rho_0 \left(\frac{Q_0}{4\pi r}\right)^2 \int_0^\pi \sin\theta \, d\theta = \frac{1}{4\pi} k\omega\rho_0 Q_0^2$$
$$= \frac{1}{4\pi} k\omega\rho_0 \left(\pi a^2 U_0\right)^2 = \frac{\pi\rho_0\omega^2 a^4 U_0^2}{4c_0} = \frac{1}{2} U_0^2 R_{rm} \qquad \text{(D6)}$$

The radiation resistance of the monopole source is

$$R_{rm} = \frac{\pi\rho_0\omega^2 a^4}{2c_0} = \frac{1}{2}\rho_0 c_0 \pi a^2 (ka)^2 \qquad \text{(D7)}$$

The pressure amplitude is inversely proportional to the distance *r* from the centre of the disk to the observation point, and the pressure disturbances at a certain point in the acoustic field are related to the amount of fluid being added or removed by the actuator. The particle velocity is entirely radial, being in phase with the pressure at distances that are large compared to the wavelength. The time-averaged intensity is also radial. The radiated sound power is proportional to the square of the frequency.

# Appendix E: Sound power of the dipole source

The velocity potential of the free vibrating disk is [1] [1]

$$\Phi_d = \frac{F_\omega}{\rho_0 c_0}\frac{e^{-jkr}}{4\pi r}\left[\frac{2J_1(ka\sin\theta)}{ka\sin\theta}\right]\cos\theta \tag{E1}$$

where the net force exerted by the disk on adjacent fluid[2]

$$\begin{aligned} F_\omega &= 2\pi a^2\rho_0 c_0 U_0 && ka >> 1 \\ &= \frac{1}{3}\pi a^2\rho_0 c_0 (j2ka + k^4a^4)U_0 && ka << 1 \end{aligned} \tag{E2}$$

The factor in brackets of equation (E1) is the same as the one entering the expression for the far field from a piston in a plane. In this case, however, there is an extra directionality factor cosθ which ensures antisymmetry about the symmetry plane. In low frequencies (for long wavelengths) the Bessel function $J_1(x) \approx x/2$ and the velocity potential becomes [2]

$$\Phi_d \approx \frac{F_\omega}{\rho_0 c_0}\frac{e^{-jkr}}{4\pi r}\cos\theta \tag{E3}$$

and [see also 3]

$$F_\omega \approx j\frac{2}{3}\pi a^3\rho_0\omega U_0 \tag{E4}$$

Sound pressure (harmonic dependence of time is assumed)

$$p_d = \rho_0\frac{\partial\Phi_d}{\partial t} = \frac{j\omega\rho_0 F_\omega}{\rho_0 c_0}\frac{e^{-jkr}}{4\pi r}\cos\theta = jkF_\omega\frac{e^{-jkr}}{4\pi r}\cos\theta \tag{E5}$$

---

[1] The symbol *j* is used here instead of *i*. They are related so that $i = -j$ and $(i)^2 = (j)^2$.
[2] The equation is incorrectly derived in reference [1] from equation 7.1.12.

Radial component of the particle velocity for irrotational motion

$$u_{rd} = -\frac{\partial \Phi_d}{\partial r} = -\frac{F_\omega \cos\theta}{4\pi\rho_0 c_0}\left(\frac{-jke^{-jkr}r - e^{-jkr}}{r^2}\right) = \frac{F_\omega}{4\pi\rho_0 c_0}\frac{e^{-jkr}}{r^2}\left(1+jkr\right)\cos\theta \tag{E6}$$

Intensity

$$I_{rd} = \mathrm{Re}\left\{p_d u_{rd}^*\right\} = \mathrm{Re}\left\{j\omega\rho_0\left(\frac{|F_\omega|\cos\theta}{4\pi\rho_0 c_0}\right)^2 \frac{1-jkr}{r^3}\right\} = \omega\rho_0\left(\frac{|F_\omega|\cos\theta}{4\pi\rho_0 c_0}\right)^2 \frac{k}{r^2} \tag{E7}$$

Sound power (integration of normal component of intensity over a sphere of radius $r$)

$$\Pi_d = \int_0^\pi 2\pi r^2 \sin\theta I_r d\theta = \frac{\omega\rho_0 k}{8\pi}\left(\frac{|F_\omega|}{\rho_0 c_0}\right)^2 \int_0^\pi \cos^2\theta \sin\theta d\theta \tag{E8}$$

By substitution $x = \cos\theta$, $dx = -\sin\theta d\theta$, $x(0) = 1$ and $x(\pi) = -1$

$$\Pi_d = \frac{\omega\rho_0 k}{8\pi}\left(\frac{|F_\omega|}{\rho_0 c_0}\right)^2 \int_{-1}^{1} x^2 dx = \frac{\omega\rho_0 k}{12\pi}\left(\frac{|F_\omega|}{\rho_0 c_0}\right)^2 = \frac{k^2}{12\pi\rho_0 c_0}\frac{4}{9}\pi^2 a^6 \rho_0^2 \omega^2 U_0^2$$
$$= \frac{\pi\rho_0\omega^4 a^6 U_0^2}{27 c_0^3} = \frac{1}{2}U_0^2 R_{rd} \tag{E9}$$

where the radiation resistance of the dipole source is

$$R_{rd} = \frac{2\pi\rho_0\omega^4 a^6}{27 c_0^3} = \frac{2}{27}\rho_0 c_0 \pi a^2 (ka)^4 \tag{E10}$$

The pressure amplitude is inversely proportional to the distance *r* from the centre of the disk to the observation point having its maximum along the dipole axis. The particle velocity is entirely radial, being in phase with the pressure at distances large compared to the wavelength. The time-averaged intensity is also radial. The radiated sound power is more strongly dependent on the frequency than the sound power of the monopole source.

# Appendix F: The interaction of two dipole sources

When two dipole sources of the same phase are close to each other, according to Figure F1, the velocity potential is

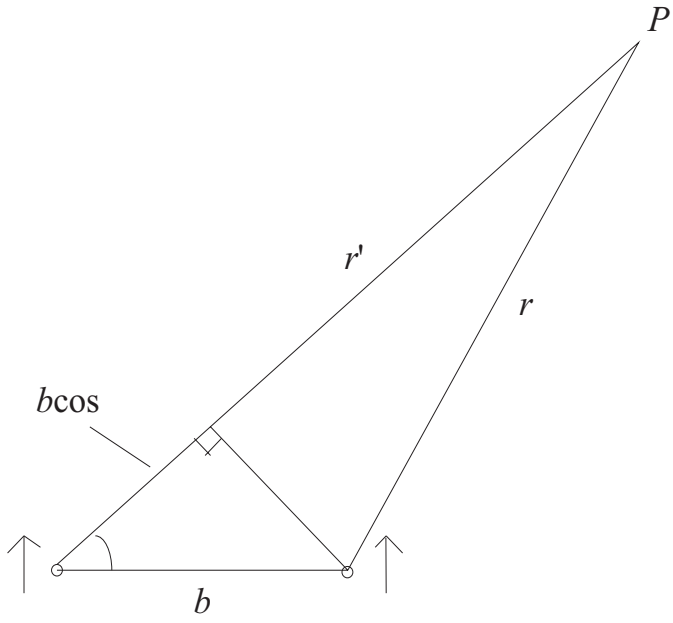


*Figure F1. Two closely situated dipole sources.*

$$\Phi_{dd} = \frac{F_\omega \cos\theta}{4\pi\rho_0 c_0}\left(\frac{e^{-jkr}}{r} + \frac{e^{-jk(r+b\cos\theta)}}{r+b\cos\theta}\right) = \frac{F_\omega \cos\theta}{4\pi r\rho_0 c_0} e^{-jk\left(r+\frac{1}{2}b\cos\theta\right)}\left[e^{j\frac{1}{2}kb\cos\theta} + e^{-j\frac{1}{2}kb\cos\theta}\right]$$
$$= \frac{F_\omega \cos\theta}{2\pi r\rho_0 c_0}\cos\left(\tfrac{1}{2}kb\cos\theta\right)e^{-jk\left(r+\frac{1}{2}b\cos\theta\right)} \qquad \text{(F1)}$$

The corresponding sound pressure and the normal component of the particle velocity are, respectively

$$p_{dd} = \rho_0 \frac{\partial \Phi_{dd}}{\partial t} = j \frac{F_\omega k \cos\theta}{2\pi r} \cos\left(\tfrac{1}{2} kb \cos\theta\right) e^{-jk\left(r + \frac{1}{2} b \cos\theta\right)} \tag{F2}$$

$$u_{rdd} = -\frac{\partial \Phi_{dd}}{\partial r} = \frac{F_\omega \cos\theta}{2\pi r \rho_0 c_0} \cos\left(\tfrac{1}{2} kb \cos\theta\right) \left( jk + \frac{1}{r} \right) e^{-jk\left(r + \frac{1}{2} b \cos\theta\right)} \tag{F3}$$

The intensity is the product of the sound pressure and the complex conjugate of particle velocity

$$\begin{aligned} I_{rdd} &= \mathrm{Re}\left[ p_{dd} u_{rdd}^{*} \right] = \mathrm{Re}\left[ j \frac{\left|F_\omega\right|^2 k \cos^2\theta}{(2\pi r)^2 \rho_0 c_0} \cos^2\left(\tfrac{1}{2} kb \cos\theta\right) \left( - jk + \frac{1}{r} \right) \right] \\ &= \frac{\left|F_\omega\right|^2 k^2 \cos^2\theta}{(2\pi r)^2 \rho_0 c_0} \cos^2\left(\tfrac{1}{2} kb \cos\theta\right) \end{aligned} \tag{F4}$$

Integrating the normal component of the intensity over a sphere of radius *r* results in the sound power the two dipole sources emits

$$\Pi_{dd} = \int_0^\pi 2\pi r^2 \sin(\theta)\, I_{rdd}\, d\theta = 2\pi r^2 \frac{\left|F_\omega\right|^2 k^2}{(2\pi r)^2 \rho_0 c_0} \int_0^\pi \cos^2\theta \cos^2\left(\tfrac{1}{2} kb \cos\theta\right) \sin\theta d\theta \tag{F5}$$

By substitution $x = \cos\theta$ and $dx = -\sin\theta d\theta$, $x(0) = 1$ and $x(\pi) = -1$ then

$$\Pi_{dd} = \frac{\left|F_\omega\right|^2 k^2}{2\pi \rho_0 c_0} \int_{-1}^{1} x^2 \cos^2\left(\tfrac{1}{2} kbx\right) dx \tag{F6}$$

Making use of the integral table [2]

$$\int x^2 \cos^2(ax) dx = \frac{x^3}{6} + \left( \frac{x^2}{4a} - \frac{1}{8a^3} \right) \sin(2ax) + \frac{x \cos(2ax)}{4a^2} \tag{F7}$$

$$\Pi_{dd} = \Pi_d \cdot 6 \cdot \left[ \frac{1}{3} + \frac{1}{kb}\left(1 - \frac{2}{k^2 b^2}\right)\sin(kb) + \frac{2}{k^2 b^2}\cos(kb) \right] \qquad \text{(F8)}$$

If the two dipole sources are in opposite phases, the emitted sound power is accordingly

$$\Pi_{dd-} = \Pi_d \cdot 6 \cdot \left[ \frac{1}{3} - \frac{1}{kb}\left(1 - \frac{2}{k^2 b^2}\right)\sin(kb) - \frac{2}{k^2 b^2}\cos(kb) \right] \qquad \text{(F9)}$$

# Appendix G: Dipole actuator locating on an absorbent layer

The situation where the dipole source is located on an absorbent material is illustrated graphically in Figures G1 and G2. The absorbent material is located on an acoustically rigid layer. A mirror dipole source the phase of which is opposite compared to the real source is created on the other side of the layer.

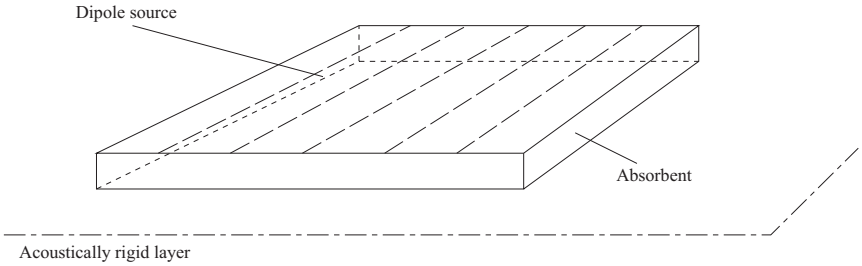


*Figure G1. Dipole source on an absorbent layer.*

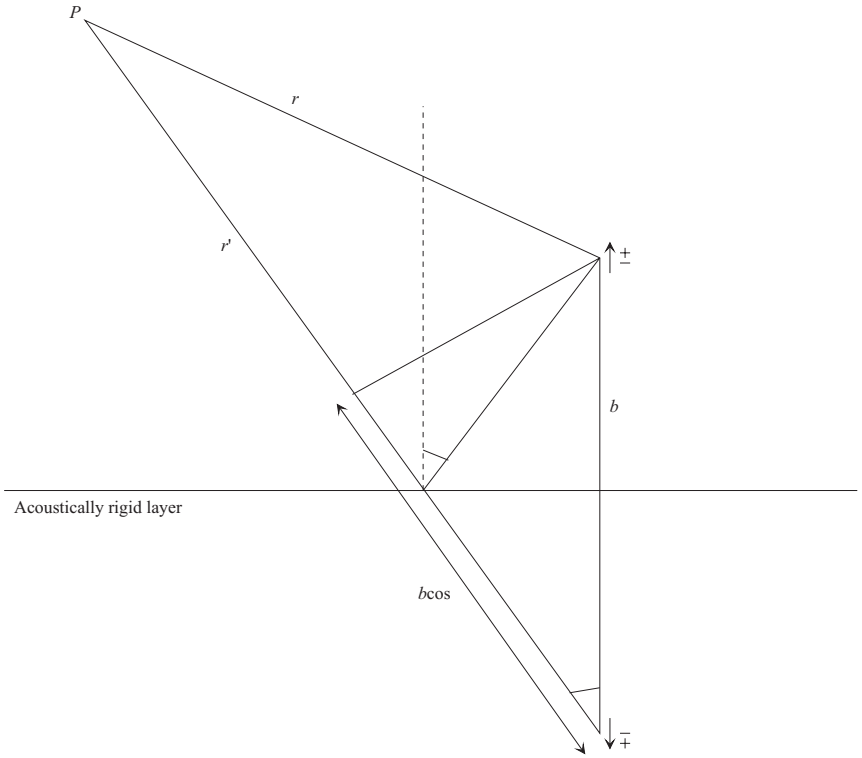


*Figure G2. Dipole source and its mirror dipole source.*

By applying the image source principle, the velocity potential of the two dipole sources is

$$\begin{aligned}\Phi_{ddhs} &= \frac{F_\omega \cos\theta}{4\pi\rho_0 c_0}\left(\frac{e^{-jkr}}{r} - \frac{\Gamma(\alpha,\omega)}{r'}e^{-jkr'}e^{-j\varsigma(\alpha,\omega)}\right)\\ &= \frac{F_\omega \cos\theta}{4\pi\rho_0 c_0}\left(\frac{e^{-jkr}}{r} - \frac{\Gamma(\alpha,\omega)}{r+b\cos\theta}e^{-jk(r+b\cos\theta)}e^{-j\varsigma(\alpha,\omega)}\right)\\ &= \frac{F_\omega \cos\theta}{4\pi r\rho_0 c_0}\left[e^{-jkr} - \Gamma(\alpha,\omega)e^{-jk(r+b\cos\theta)}e^{-j\varsigma(\alpha,\omega)}\right]\\ &= \frac{F_\omega}{\rho_0 c_0}\frac{e^{-jkr}}{4\pi r}\cos\theta\left(1-\Gamma e^{-jkb\cos\theta}e^{-j\varsigma}\right) = \Phi_d\left(1-\Gamma e^{-jkb\cos\theta}e^{-j\varsigma}\right)\end{aligned} \tag{G1}$$

where

$T(\alpha,\omega)$ is the reflection coefficient related to the absorbent surface

$\varsigma(\alpha,\omega)$ describes the phase between the incident and reflecting wave, and

$\alpha$ is the angle between the reflected wave and the normal to the plane where the sources are located.

The corresponding sound pressure and the normal component of the particle velocity are, respectively

$$\begin{aligned}p_{ddhs} &= \rho_0\frac{\partial\Phi_{ddhs}}{\partial t} = j\omega\rho_0\frac{F_\omega}{\rho_0 c_0}\frac{e^{-jkr}}{4\pi r}\cos\theta\left(1-\Gamma e^{-jkb\cos\theta}e^{-j\varsigma}\right)\\ &= p_d\left(1-\Gamma e^{-jkb\cos\theta}e^{-j\varsigma}\right)\end{aligned} \tag{G2}$$

$$\begin{aligned}u_{rddhs} &= -\frac{\partial\Phi_{ddhs}}{\partial r} = -\frac{F_\omega}{4\pi\rho_0 c_0}\cos\theta\left(1-\Gamma e^{-jkb\cos\theta}e^{-j\varsigma}\right)\left(\frac{-jke^{-jkr}r - e^{-jkr}}{r^2}\right)\\ &= \frac{F_\omega}{4\pi\rho_0 c_0}\frac{e^{-jkr}}{r^2}\left(1+jkr\right)\cos\theta\left(1-\Gamma e^{-jkb\cos\theta}e^{-j\varsigma}\right) = u_{rd}\left(1-\Gamma e^{-jkb\cos\theta}e^{-j\varsigma}\right)\end{aligned} \tag{G3}$$

The intensity is the product of sound pressure and complex conjugate of particle velocity

$$
\begin{aligned}
I_{rddhs} &= \mathrm{Re}\left[p_{ddhs} u^{*}_{rddhs}\right] \\
&= \mathrm{Re}\left[ j\omega\rho_0 \left(\frac{F_\omega \cos\theta}{4\pi\rho_0 c}\right)^2 \frac{1}{r^3} e^{-jkr}\left(1-\Gamma e^{-jkb\cos\theta} e^{-j\varsigma}\right) e^{jkr}\left(1-jkr\right)\left(1-\Gamma e^{jkb\cos\theta} e^{j\varsigma}\right)\right] \\
&= \omega\rho_0 \left(\frac{F_\omega \cos\theta}{4\pi\rho_0 c}\right)^2 \frac{1}{r^3} \mathrm{Re}\left[(kr+j)\left(1-\Gamma e^{jkb\cos\theta} e^{j\varsigma} - \Gamma e^{-jkb\cos\theta} e^{-j\varsigma} + \Gamma^2\right)\right] \\
&= \frac{k\omega\rho_0 |F_\omega|^2 \cos^2\theta}{(4\pi r\rho_0 c)^2}\left(1+\Gamma^2 - 2\Gamma\cos(kb\cos\theta+\varsigma)\right) \\
&= I_r\left(1+\Gamma^2 - 2\Gamma\cos(kb\cos\theta+\varsigma)\right)
\end{aligned}
\tag{G4}
$$

Integrating the normal component of the intensity over half sphere of radius $r$ results in the sound power the dipole sources emits

$$
\begin{aligned}
\Pi_{ddhs} &= \int_0^{\pi/2} 2\pi r^2 \sin\theta I_{rddhs} d\theta \\
&= 2\pi r^2 \frac{k\omega\rho_0 |F_\omega|^2}{(4\pi r Z_0)^2} \int_0^{\pi/2} \left(1+\Gamma^2 - 2\Gamma\cos\left(kb\cos\theta+\varsigma\right)\right)\cos^2\theta\sin\theta d\theta \\
&= \frac{k\omega\rho_0 |F_\omega|^2}{8\pi {Z_0}^2} \int_0^{\pi/2} \left(1+\Gamma^2 - 2\Gamma\cos\left(kb\cos\theta+\varsigma\right)\right)\cos^2\theta\sin\theta\, d\theta
\end{aligned}
\tag{G5}
$$

By substitution $x = \cos\theta$ and $dx = -\sin\theta d\theta$, $x(0) = 1$ and $x(\pi/2) = 0$ then

$$
\begin{aligned}
\Pi_{ddhs} &= \frac{k\omega\rho_0 |F_\omega|^2}{8\pi {Z_0}^2} \int_0^1 \left(1+\Gamma^2 - 2\Gamma\cos\left(kbx+\varsigma\right)\right)x^2\, dx \\
&= \frac{k\omega\rho_0 |F_\omega|^2}{8\pi {Z_0}^2} \int_0^1 \left(x^2 + \Gamma^2 x^2 - 2\Gamma x^2\cos\left(kbx+\varsigma\right)\right) dx
\end{aligned}
\tag{G6}
$$

Making use of the integral table [2]

$$
\int x^2\cos(ax)dx = \frac{2x\cos(ax)}{a^2} + \frac{a^2x^2-2}{a^3}\sin(ax) \tag{G7}
$$

$$\int x^2 \sin(ax)dx = \frac{2x}{a^2}\sin(ax) - \frac{a^2x^2 - 2}{a^3}\cos(ax) \tag{G8}$$

$$\begin{aligned}
\Pi_{ddhs} &= \frac{k\omega\rho_0|F_\omega|^2}{8\pi {Z_0}^2}\int_0^1 \left(x^2 + \Gamma^2 x^2 - 2\Gamma x^2\cos(kbx)\cos(\varsigma) + 2\Gamma x^2\sin(kbx)\sin(\varsigma)\right)dx \\
&= \frac{k\omega\rho_0|F_\omega|^2}{8\pi {Z_0}^2}\left[\int_0^1 \frac{1}{3}x^3 + \frac{1}{3}\Gamma^2 x^3 - 2\Gamma\cos(\varsigma)\left(\frac{2x\cos(kbx)}{(kb)^2} + \frac{(kb)^2x^2 - 2}{(kb)^3}\right)\sin(kbx)\right. \\
&\quad \left. + 2\Gamma\sin(\varsigma)\left(\frac{2x\sin(kbx)}{(kb)^2} - \frac{(kb)^2x^2 - 2}{(kb)^3}\right)\cos(kbx)\right] \\
&= \frac{k\omega\rho_0|F_\omega|^2}{8\pi {Z_0}^2}\left[\frac{1}{3} + \frac{1}{3}\Gamma^2 - 2\Gamma\cos(\varsigma)\left(\frac{2\cos(kb)}{(kb)^2} + \frac{(kb)^2 - 2}{(kb)^3}\sin(kb)\right)\right. \\
&\quad \left. + 2\Gamma\sin(\varsigma)\left(\frac{2\sin(kb)}{(kb)^2} - \frac{(kb)^2 - 2}{(kb)^3}\right)\cos(kb) - \frac{4\Gamma\sin(\varsigma)}{(kb)^3}\right] \\
&= \frac{3}{2}\cdot\Pi_d\cdot\left[\frac{1}{3}(1+\Gamma^2) - 2\Gamma\cos(\varsigma)\left(\frac{2\cos(kb)}{(kb)^2} + \frac{1}{kb}\left(1 - \frac{2}{(kb)^2}\right)\sin(kb)\right)\right. \\
&\quad \left. + 2\Gamma\sin(\varsigma)\left(\frac{2\sin(kb)}{(kb)^2} - \frac{1}{kb}\left(1 - \frac{2}{(kb)^2}\right)\cos(kb)\right) - \frac{4\Gamma\sin(\varsigma)}{(kb)^3}\right]
\end{aligned} \tag{G9}$$

If the reflecting surface is acoustically hard $\Rightarrow$ T = 1 and $\varsigma = 0$

$$\begin{aligned}
\Pi_{ddhs} &= \frac{3}{2}\cdot\Pi_d\cdot\left[\frac{2}{3} - 2\left(\frac{2\cos(kb)}{(kb)^2} + \frac{1}{kb}\left(1 - \frac{2}{(kb)^2}\right)\sin(kb)\right)\right] \\
&= 3\cdot\Pi_d\cdot\left[\frac{1}{3} - \frac{1}{kb}\left(1 - \frac{2}{(kb)^2}\right)\sin(kb) - \frac{2}{(kb)^2}\cos(kb)\right]
\end{aligned} \tag{G10}$$

The result equals half of the sound power of two oppositely phased dipole sources which are located at a distance *b* from each other (Appendix E). If the distance *b* between the sources approaches infinity, the radiated sound power is the same as the radiated power of a single dipole source.

# Appendix H: Radiation pattern of the actuator element

An EMFi actuator element is combined of several membrane strips which are located next to each other on the same plane. The different cells of the actuator element can be considered to operate as single line sources. The elementary source is a part of a line source of length *dx* (see Figure H1)

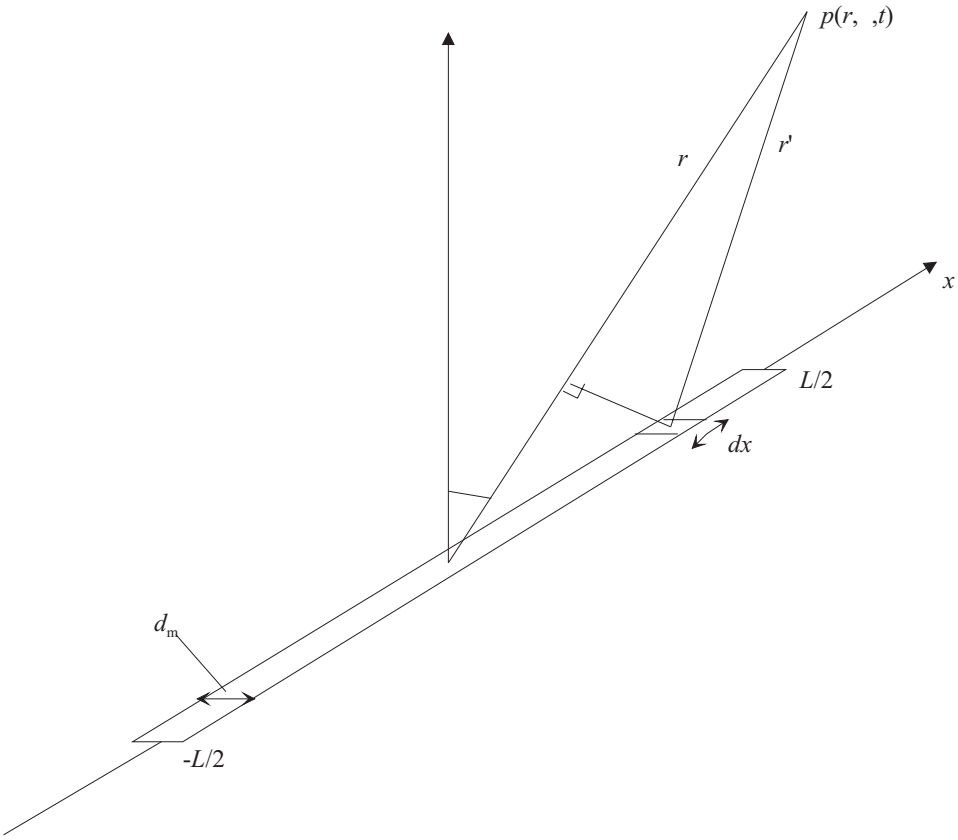


*Figure H1. Elementary source on the line source.*

The source strength of an elementary source segment is

$$dQ = U_0 d_m dx \tag{H1}$$

where $d_m$ is the width of the line source and $U_0$ is the radial vibration velocity. Each of the elementary source segments generates a pressure increment to the half space in the far field point ($r$, θ) (see Appendix D, equation D3)

$$dp = j\frac{\rho_0 c_0 k}{4\pi r'} U_0 d_m e^{j(\omega t - kr')} dx \tag{H2}$$

The distance from the source point to the field point is $r' = r - x\sin\theta$, $r >> L$ (see Figure H1). The resultant sound pressure is

$$\begin{aligned} p(r,\theta,t) &= j\frac{\rho_0 c_0 U_0 k d_m}{4\pi r} e^{j(\omega t - kr)} \int_{-L/2}^{L/2} e^{jkx\sin\theta} dx \\ &= j\frac{\rho_0 c_0 U_0 kL}{4\pi}\frac{d_m}{r} e^{j(\omega t - kr)} \left[\frac{\sin(\frac{1}{2}kL\sin\theta)}{\frac{1}{2}kL\sin\theta}\right] \\ &= jP_{ax}(r)H_e(\theta)e^{j(\omega t - kr)} \end{aligned} \tag{H3}$$

where

$$P_{ax}(r) = \frac{\rho_0 c_0 U_0 kL}{4\pi}\frac{d_m}{r} \quad \text{and} \quad H_e(\theta) = \left|\frac{\sin\nu}{\nu}\right| \quad \text{where} \quad \nu = \tfrac{1}{2}kL\sin\theta \tag{H4}$$

The function $H_e(\theta)$ is the zeroth order spherical Bessel function of the first kind, $j_o(\nu)$. An EMFi actuator is built of $N$ adjacent strip elements which are separated by a distance $d_m$ from each other. They have the same source strength and they radiate with the same phase according to Figure H2.

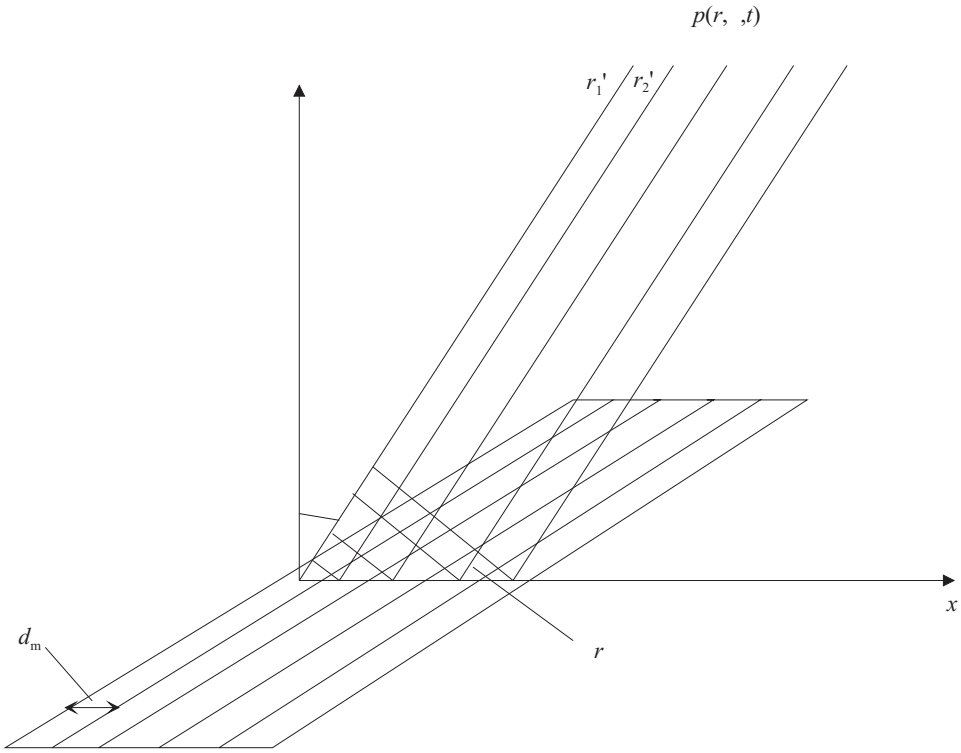


*Figure H2. The line source elements.*

In the acoustic far field all the rays from the array of line sources to the field point can be considered parallel (see Figure H2). Source *i* produces sound pressure

$$p_i(r,\Phi,t) = j\frac{\rho_0 c_0 U_0 kL}{4\pi}\frac{d_m}{r_i'}H(\theta)e^{j(\omega t - kr_i')} \qquad \text{(H5)}$$

The resultant pressure at the field point is the summation

$$p_{TOT}(r,\Phi,t) = j\frac{\rho_0 c_0 U_0 kLd_m}{4\pi}H(\theta)\sum_{i=1}^{N}\frac{e^{j(\omega t - kr_i')}}{r_i'} \qquad \text{(H6)}$$

The distance between the element source and the field point is $r_i' = r_1 - (i\text{-}1)\Delta r$ where $\Delta r = d_m \sin\phi$. The distance to the centre of the array of line sources is $r = r_1 - \frac{1}{2} P/d_m \Delta r$ where the length of the array is $P = (N\text{-}1)\, d_m$.

$$p_{TOT}(r,\Phi,t) = j\frac{\rho_0 c_0 U_0 kLd_m}{4\pi r} H(\theta) e^{-j\frac{1}{2}\frac{P}{d_m}k\Delta r} e^{j(\omega t - kr)} \sum_{i=1}^{N} e^{j(i-1)k\Delta r} \quad \text{(H7)}$$

$$\begin{aligned}
\sum_{i=1}^{N} e^{j(i-1)k\Delta r} &= \sum_{i=0}^{N-1} e^{jik\Delta r} = \sum_{i=0}^{N-1} \left[\cos(ik\Delta r) + j\sin(ik\Delta r)\right] \\
&= \frac{\sin\left(\frac{N}{2}k\Delta r\right)\cos\left(\frac{N-1}{2}k\Delta r\right)}{\sin\left(\frac{k\Delta r}{2}\right)} + j\frac{\sin\left(\frac{N}{2}k\Delta r\right)\sin\left(\frac{N-1}{2}k\Delta r\right)}{\sin\left(\frac{k\Delta r}{2}\right)} \\
&= \frac{\sin\left(\frac{N}{2}k\Delta r\right)}{\sin\left(\frac{k\Delta r}{2}\right)} e^{j\left(\frac{N-1}{2}k\Delta r\right)} = \frac{\sin\left(\frac{N}{2}k\Delta r\right)}{\sin\left(\frac{k\Delta r}{2}\right)} e^{j\frac{1}{2}\frac{P}{d_m}k\Delta r}
\end{aligned}$$

$$\begin{aligned}
p_{TOT}(r,\Phi,t) &= j\frac{\rho_0 c_0 U_0 kLd_m}{4\pi r} H_e(\theta) \frac{\sin\left(\frac{N}{2}k\Delta r\right)}{\sin\left(\frac{1}{2}k\Delta r\right)} e^{j(\omega t - kr)} \\
&= j\frac{\rho_0 c_0 U_0 kLd_m}{4\pi r} H_e(\theta) \frac{\sin\left(\frac{N}{2}kd_m \sin\phi\right)}{\sin\left(\frac{1}{2}kd_m \sin\phi\right)} e^{j(\omega t - kr)} \qquad \text{(H8)} \\
&= jP_{ax} H_e(\theta) H(\phi) e^{j(\omega t - kr)}
\end{aligned}$$

where $H(\Phi) = \frac{\sin\left(\frac{N}{2}kd_m \sin\phi\right)}{\sin\left(\frac{1}{2}kd_m \sin\phi\right)}$

# Appendix I: Sound power of natural mode of a simply supported plate

Surface velocity distribution of a (m,n) mode of a simply supported plate with an infinite baffle is [4]

$$u_{\omega} = u_m \sin\left(\frac{m\pi x}{a}\right) \sin\left(\frac{n\pi y}{b}\right) \tag{I1}$$

where $0 \le x \le a \quad ; \; 0 \le y \le b$

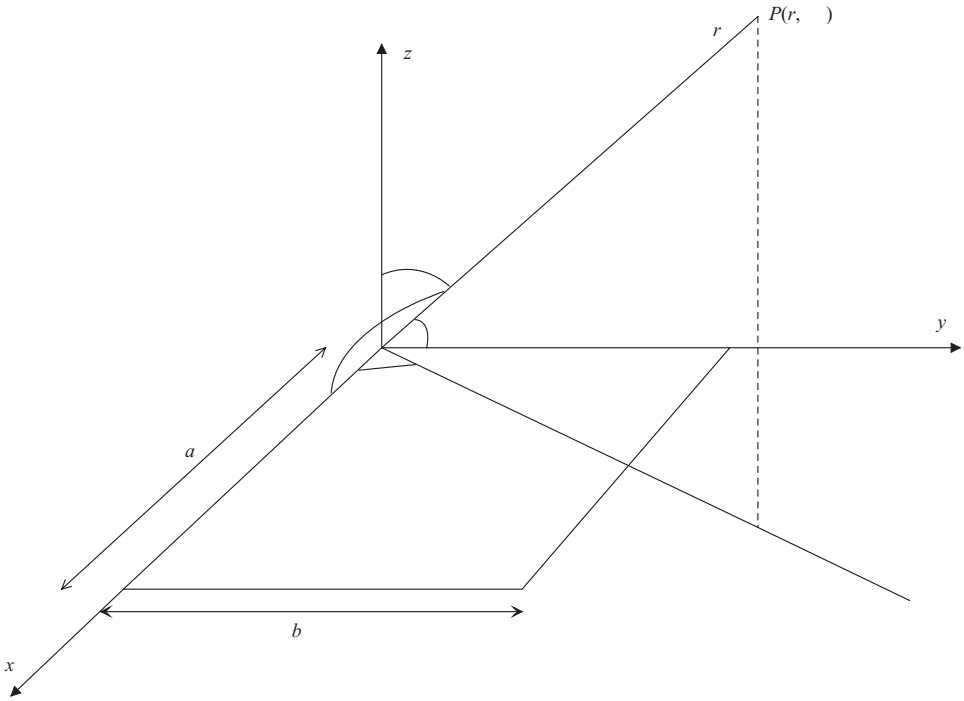


*Figure I1. Simply supported plate with infinite baffle.*

Sound pressure in the acoustic far field according to Rayleigh integral is [3]

$$\begin{aligned} p_\omega &= jk\rho_0 c_0 \frac{e^{-jkr}}{2\pi r}\int_{-b/2}^{b/2}\int_{-a/2}^{a/2} u_\omega(x,y)e^{j\frac{\alpha}{a}x}e^{j\frac{\beta}{b}y}dxdy \\ &= jk\rho_0 c_0 \frac{e^{-jkr}}{2\pi r}\int_{-b/2}^{b/2}\int_{-a/2}^{a/2} u_m \sin(\frac{m\pi x}{a})\sin\left(\frac{n\pi y}{b}\right)e^{j\frac{\alpha}{a}x}e^{j\frac{\beta}{b}y}dxdy \end{aligned} \qquad \text{(I2)}$$

where $\alpha = ka\sin\theta\cos\phi$ and $\beta = kb\sin\theta\sin\phi$

By integration

$$\int_0^a \sin\left(\frac{m\pi x}{a}\right)e^{j\frac{\alpha}{a}x}dx = \frac{\frac{a}{m\pi}\left[(-1)^m e^{j\alpha}-1\right]}{\left(\frac{\alpha}{m\pi}\right)^2-1}$$

$$\int_0^b \sin\left(\frac{n\pi y}{b}\right)e^{j\frac{\beta}{b}y}dy = \frac{\frac{b}{n\pi}\left[(-1)^n e^{j\beta}-1\right]}{\left(\frac{\beta}{n\pi}\right)^2-1}$$

Sound pressure in the acoustic far field is

$$p_\omega = ju_m k\rho_0 c_0 \frac{e^{-jkr}}{2\pi r}\ \frac{ab}{mn\pi^2}\left[\frac{(-1)^m e^{j\alpha}-1}{\left(\frac{\alpha}{m\pi}\right)^2-1}\right]\left[\frac{(-1)^n e^{j\beta}-1}{\left(\frac{\beta}{n\pi}\right)^2-1}\right] \qquad \text{(I3)}$$

The average sound power on the one side of the plate radiates to the acoustic far field

$$\Pi_{ssp} = \int_0^{2\pi}\int_0^{\frac{\pi}{2}}\frac{\left|p_\omega\right|^2}{\rho_0 c_0}r^2\sin\theta d\theta d\phi = 4\rho_0 c_0\left(\frac{u_m kab}{\pi^3 mn}\right)^2\int_0^{2\pi}\int_0^{\frac{\pi}{2}}\left[\frac{\cos\left(\frac{\alpha}{2}\right)\cos\left(\frac{\beta}{2}\right)}{\sin\left(\frac{\alpha}{2}\right)\sin\left(\frac{\beta}{2}\right)}{\left[\left(\frac{\alpha}{m\pi}\right)^2-1\right]\left[\left(\frac{\beta}{n\pi}\right)^2-1\right]}\right]^2\cdot\sin\theta d\theta d\phi \qquad \text{(I4)}$$

The odd modes of the equation (I4) are related to the cosine terms and the even modes correspondingly to the sinus terms.

# Appendix J: Sound power of natural mode of a rigidly supported plate

Surface velocity distribution of mode (m,n) of a rigidly supported plate with an infinite baffle is [5]

$$u_{\omega} = u_m \left( \frac{\cosh\left(k_{xm}x\right)}{\cosh\left(½k_{xm}a\right)} - \frac{\cos\left(k_{xm}x\right)}{\cos\left(½k_{xm}a\right)} \right) \left( \frac{\cosh\left(k_{yn}y\right)}{\cosh\left(½k_{yn}b\right)} - \frac{\cos\left(k_{yn}y\right)}{\cos\left(½k_{yn}b\right)} \right) \qquad \text{(J1)}$$

where

$-a/2 \le x \le a/2 \;\; ; \;\; -b/2 \le y \le b/2 \;\; ; \; k_{xm} = m\pi/a \;\; ; \; k_{yn} = n\pi/b$

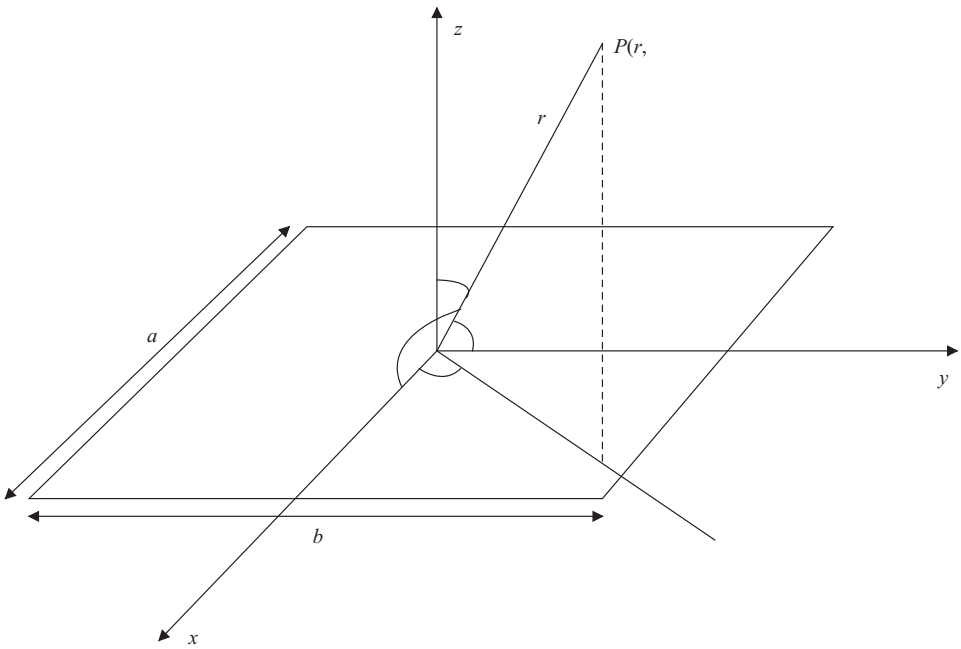


*Figure J1. Rigidly supported plate with infinite baffle.*

Sound pressure in the acoustic far field according to Rayleigh integral is [3]

$$p_\omega = jk\rho_0 c_0 \frac{e^{-jkr}}{2\pi r}\int_{-b/2}^{b/2}\int_{-a/2}^{a/2} u_\omega(x,y)e^{j\frac{\alpha}{a}x}e^{j\frac{\beta}{b}y}dxdy$$

$$= jk\rho_0 c_0 u_m \frac{e^{-jkr}}{2\pi r}\int_{-b/2}^{b/2}\int_{-a/2}^{a/2}\left(\frac{\cosh(k_{xm}x)}{\cosh(½k_{xm}a)}-\frac{\cos(k_{xm}x)}{\cos(½k_{xm}a)}\right) \qquad \text{(J2)}$$

$$\cdot\left(\frac{\cosh(k_{yn}y)}{\cosh(½k_{yn}b)}-\frac{\cos(k_{yn}y)}{\cos(½k_{yn}b)}\right)e^{j\frac{\alpha}{a}x}e^{j\frac{\beta}{b}y}dxdy$$

where $\alpha = ka\sin\theta\cos\phi$ and $\beta = kb\sin\theta\sin\phi$

By integration

$$\int_{-a/2}^{a/2}\cosh(k_{xm}x)e^{j\frac{\alpha}{a}x}dx = \frac{k_{xm}-j\frac{\alpha}{a}}{k_{xm}^2+\left(\frac{\alpha}{a}\right)^2}\sinh\left[½\left(k_{xm}a+j\alpha\right)\right]+\frac{k_{xm}+j\frac{\alpha}{a}}{k_{xm}^2+\left(\frac{\alpha}{a}\right)^2}\sinh\left[½\left(k_{xm}a-j\alpha\right)\right]$$

where $\sinh\left[½\left(k_{xm}a+j\alpha\right)\right] = \sinh\left(\frac{k_{xm}a}{2}\right)\cos\left(\frac{\alpha}{2}\right)+j\cosh\left(\frac{k_{xm}a}{2}\right)\sin\left(\frac{\alpha}{2}\right)$

Thus the integral above is

$$\int_{-a/2}^{a/2}\cosh(k_{xm}x)e^{j\frac{\alpha}{a}x}dx = \frac{k_{xm}-j\frac{\alpha}{a}}{k_{xm}^2+\left(\frac{\alpha}{a}\right)^2}\left[\sinh\left(\frac{k_{xm}a}{2}\right)\cos\left(\frac{\alpha}{2}\right)+j\cosh\left(\frac{k_{xm}a}{2}\right)\sin\left(\frac{\alpha}{2}\right)\right]+$$

$$\frac{k_{xm}+j\frac{\alpha}{a}}{k_{xm}^2+\left(\frac{\alpha}{a}\right)^2}\left[\sinh\left(\frac{k_{xm}a}{2}\right)\cos\left(\frac{\alpha}{2}\right)-j\cosh\left(\frac{k_{xm}a}{2}\right)\sin\left(\frac{\alpha}{2}\right)\right]$$

$$= \frac{2}{k_{xm}^2+\left(\frac{\alpha}{a}\right)^2}\left[k_{xm}\sinh\left(\frac{k_{xm}a}{2}\right)\cos\left(\frac{\alpha}{2}\right)+\frac{\alpha}{a}\cosh\left(\frac{k_{xm}a}{2}\right)\sin\left(\frac{\alpha}{2}\right)\right]$$

Correspondingly, the other integrals are

$$\int_{-b/2}^{b/2} \cosh\left(k_{yn} y\right) e^{j\frac{\beta}{b}y} dy = \frac{2}{k_{yn}^2 + \left(\frac{\beta}{b}\right)^2} \left[ k_{yn} \sinh\left(\frac{k_{yn} b}{2}\right) \cos\left(\frac{\beta}{2}\right) + \frac{\beta}{b} \cosh\left(\frac{k_{yn} b}{2}\right) \sin\left(\frac{\beta}{2}\right) \right]$$

$$\int_{-a/2}^{a/2} \cos\left(k_{xm} x\right) e^{j\frac{\alpha}{a}y} dx = \frac{\frac{-2\alpha}{a k_{xm}^2} \cos\left(\frac{k_{xm} a}{2}\right) \sin\left(\frac{\alpha}{2}\right)}{1 - \left(\frac{\alpha}{a k_{xm}}\right)^2}$$

$$\int_{-b/2}^{b/2} \cos\left(k_{yn} y\right) e^{j\frac{\beta}{b}y} dy = \frac{\frac{-2\beta}{b k_{yn}^2} \cos\left(\frac{k_{yn} b}{2}\right) \sin\left(\frac{\beta}{2}\right)}{1 - \left(\frac{\beta}{b k_{yn}}\right)^2}$$

The sound pressure is

$$p_\omega = jk\rho_0 c_0 u_m \frac{e^{-jkr}}{2\pi r} \left\{ \left[ \frac{2}{k_{xm}^2 + \left(\frac{\alpha}{a}\right)^2} \left( k_{xm} \tanh\left(\frac{k_{xm} a}{2}\right) \cos\left(\frac{\alpha}{2}\right) + \frac{\alpha}{a} \sin\left(\frac{\alpha}{2}\right) \right) + \frac{1}{1 - \left(\frac{\alpha}{a k_{xm}}\right)^2} \left( \frac{2\alpha}{a k_{xm}^2} \sin\left(\frac{\alpha}{2}\right) \right) \right] \cdot \left[ \frac{2}{k_{yn}^2 + \left(\frac{\beta}{b}\right)^2} \left( k_{yn} \tanh\left(\frac{k_{yn} b}{2}\right) \cos\left(\frac{\beta}{2}\right) + \frac{\beta}{b} \sin\left(\frac{\beta}{2}\right) \right) + \frac{1}{1 - \left(\frac{\beta}{b k_{yn}}\right)^2} \left( \frac{2\beta}{b k_{yn}^2} \sin\left(\frac{\beta}{2}\right) \right) \right] \right\}$$

(J3)

The average sound power radiating on one side of the plate to the acoustic far field is

$$\Pi_{rsp} = \int_0^{2\pi}\int_0^{\frac{\pi}{2}} \frac{\left|p_\omega\right|^2}{\rho_0 c_0} r^2 \sin\theta d\theta d\phi = 4\rho_0 c_0 \left(\frac{u_m k}{\pi}\right)^2 \int_0^{2\pi}\int_0^{\frac{\pi}{2}} \left[ \frac{1}{k_{xm}^2 + \left(\frac{\alpha}{a}\right)^2} \cdot \left( k_{xm} \tanh\left(\frac{k_{xm} a}{2}\right) \cos\left(\frac{\alpha}{2}\right) \right.\right.$$

$$\left. + \frac{\alpha}{a} \sin\left(\frac{\alpha}{2}\right)\right) + \frac{1}{1 - \left(\frac{\alpha}{a k_{xm}}\right)^2} \left( \frac{\alpha}{a k_{xm}^2} \sin\left(\frac{\alpha}{2}\right)\right) \Bigg] \cdot \Bigg[ \frac{1}{k_{yn}^2 + \left(\frac{\beta}{b}\right)^2} \left( k_{yn} \tanh\left(\frac{k_{yn} b}{2}\right) \cos\left(\frac{\beta}{2}\right) \right.$$

$$\left. \left. + \frac{\beta}{b} \sin\left(\frac{\beta}{2}\right)\right) + \frac{1}{1 - \left(\frac{\beta}{b k_{yn}}\right)^2} \left( \frac{\beta}{b k_{yn}^2} \sin\left(\frac{\beta}{2}\right)\right) \Bigg] \right|^2 \sin\theta d\theta d\phi \qquad \text{(J4)}$$

# Appendix K: Inequality condition for a combined standard deviation

From equations (45) and (46) the inequality condition $u_{c1}(y) \leq u_{c2}(y)$ reduces to equation

$$\sqrt{\sum_{i=1}^{N}\left(10^{(x_i+a_i)/10}\right)^2} \leq \sum_{i=1}^{N} 10^{(x_i+a_i)/10} \tag{K1}$$

Because

$$\sqrt{\sum_{i=1}^{N}\left(10^{(x_i+a_i)/10}\right)^2} \leq \sqrt{\left(\sum_{i=1}^{N} 10^{(x_i+a_i)/10}\right)^2} = \sum_{i=1}^{N} 10^{(x_i+a_i)/10} \tag{K2}$$

the condition is valid. In a similar way it is possible to show for equations (47), (48) and (49), (50) that $u_{c1}(y) \leq u_{c2}(y)$.

# References for Appendices


1. Morse, P. M. and Ingard, K. U. Theoretical Acoustics. New York - St. Louis - San Francisco - Toronto - London - Sydney: McGraw-Hill, 1968. 927 p.

2. Abramowitch, M. and Stegun, I. A. Handbook of mathematical functions. New York: Dover publications, 1970. 1046 p.

3. Pierce, A. D. Acoustics. An introduction to its physical principles and applications. New York: McGraw-Hill, 1991. 678 p.

4. Skudrzyk, E. The foundations of acoustics. Wien - New York: Springler Verlag, 1971. 790 p.

5. Malecki, I. Physical foundations of technical acoustics. Oxford - London - Edinburgh - New York - Toronto - Sidney - Paris - Braunschweig: Pergamon Press, 1969. 743 p.

Published by

Vuorimiehentie 5, P.O.Box 2000, FIN-02044 VTT, Finland
Phone internat. +358 9 4561
Fax +358 9 456 4374

Series title, number and report code of publication

VTT Publications 405
VTT–PUBS–405

Author(s)
Saarinen, Ari

Title

# EMFi-actuator: vibro-acoustical consideration

Abstract

In this paper the vibro-acoustical properties of the EMFi-actuator are studied. The examination is carried out by modelling the operation of the actuator and by comparing the modelling results to the corresponding measured values in case they are available. The modelling is based on an analytical approach. The equations used are derived in the Appendices. Consideration on the properties of the vibration is divided into three parts: the basic vibration of the film, vibration of the film in the time domain and vibration of the functional elements of the actuator. The sound production properties of the actuator have been examined in the free acoustic field and in cases with boundaries near the source. The effect of the different vibration distributions of the actuator film and impedance loading for the emitted sound has been studied. Also the radiation pattern of the actuator is modelled and compared to the measured results.

The general vibro-acoustical functioning of the EMFi-actuator is stated in the impedance-oriented form by evaluating the loading impedance of the vibrating film from its boundary conditions. The basic vibration functioning of the actuator film in the frequency domain is predicted by using a linear second-order ordinary differential equation with constant coefficients. In the time domain the non-linear effects of the spring force and electric forces acting on the actuator film are considered. The recoil effect of the actuator is studied with a normal-mode method of dynamic analysis. It is found that the response of the supporting structure may decrease with about a decade without influencing the response of the actuator film.

The use of the arithmetic average value of the vibration deflection of the EMFi-actuator in the prediction of sound power or sound pressure in the acoustic far field at low frequencies is compared to the frequency or spatially dependent vibration of the actuator film. The value of the arithmetic average of vibration is valid even when the outward impedance of the film is not taken into consideration. The large dipole type actuators are more effective sound radiators than monopole sources. The effect of the thickness of the absorbent material under the dipole actuator, the radiation pattern and the effect of the boundary conditions of the vibrating cell on the radiating sound power are considered. The measured and predicted values of radiation patterns are very similar in every angle. The rigidly supported boundary of the actuator cell enables the actuator panel to radiate much more sound power with all the different even modes than it is possible with a simply supported boundary condition. The basic problems concerning the operation of an EMFi-actuator are related to its ineffective low frequency sound production and the distortion caused by non-linear vibration. It is possible to increase the sound power radiation properties of the monopole or dipole type functional modes of the actuator by making the deflection of the membrane larger (using smaller tension), by using larger membrane areas or by using two interacting actuators. The dimensions of the actuator element cell affect the power the single vibration mode is able to radiate into the acoustic far field. When the film cells of the actuator panels are simply supported, the larger dimensions compared to those of the present actuator type, produce more sound power at odd and even modes.

The confidence intervals of a normal distribution used in the evaluation of the reliability of the sound power measurements have been obtained by calculating combined standard deviation values from standard deviation values of single frequency bands given in the standards. It is shown that it is possible to find an upper limit for the confidence interval.

The main results of this work are the means to increase the radiated sound power of the actuator element without increasing concurrently the distortion of the radiator. These resources are based on the functioning mode of the actuator (monopole, dipole), boundary conditions of the actuator element or cells of the actuator element, the larger actuator areas, interaction of actuators and the dimensions of the actuator element cells. Another result of this study is the potentiality to evaluate the A-weighted standard deviation of the sound power of the equipment to be measured from the measurement results without specifying the type of emitted sound radiated by the equipment.

Keywords
EMFi-actuator, actuators, vibration, acoustic properties, modelling, evaluation, vibro-acoustical properties, sound production, measurement

Activity unit
VTT Building Technology, Building Physics, Building Services and Fire Technology,
Lämpömiehenkuja 3, P.O.Box 1804, FIN–02044 VTT, Finland

| ISBN | | | Project number |
|---|---|---|---|
| 951–38–5554–6 (soft back ed.)<br>951–38–5555–4 (URL: http://www.inf.vtt.fi/pdf/) | | | R9SU00394 |
| Date | Language | Pages | Price |
| December 1999 | English | 109 p. + app. 30 p. | C |
| Name of project | | Commissioned by | |
| ACTIVA, FACTS | | Tekes, EU | |
| Series title and ISSN | | Sold by | |
| VTT Publications<br>1235–0621 (soft back ed.)<br>1455–0849 (URL: http://www.inf.vtt.fi/pdf/) | | VTT Information Service<br>P.O.Box 2000, FIN-02044 VTT, Finland<br>Phone internat. +358 9 456 4404<br>Fax +358 9 456 4374 | |